UNIVERSITÀ DEGLI STUDI DI PADOVA

UNIVERSITÀ DEGLI STUDI DI PADOVA

Dipartimento di Costruzioni e Trasporti

SCUOLA DI DOTTORATO DI RICERCA IN SCIENZE
DELL'INGEGNERIA CIVILE ED AMBIENTALE

CICLO XXII

SENSITIVITY ANALYSIS APPLIED TO FEM MODELS FOR COUPLED MULTIPHASE SYSTEMS

Direttore della Scuola: Ch.mo Prof. Stefano Lanzoni

Supervisori: Ch.mo Prof. Bernhard Schrefler, Dr. Francesco Pesavento

Correlatore: Ch.mo Prof. Olivier Pironneau

Dottoranda: Ronel Ngaradoumbe Nanhornguè

Luglio 2010

A Piero

Indice

Summary

Coupled multiphysics problems are very actual research topics in civil engineering. In this work we focus on multiphase models for concrete exposed to high temperature, applicable to the evaluation of fire resistance in industrial and civil concrete structures.

Many non-linear phenomena and interactions are involved in concrete behaviour when temperatures higher than the standard ones are considered. Such phenomena involve not only heat conduction and vapour diffusion, but also liquid water flow caused by pressure gradients, capillary effects, adsorbed water content gradients, as well as latent heat transfer due to water phase change inside the pores. Moreover, high temperatures induce severe micro-structural changes and several interacting physical and chemical phenomena, resulting in significant changes of the material inner structure and properties.

During modelling of hygro-thermal-mechanical behaviour of concrete, one should use models considering possibly the whole complexity and mutual interactions of the analysed physical processes. The use of fully coupled multiphase models, based on mechanics of multiphase porous media, is therefore necessary to correctly predict the hygro, thermal, chemical and mechanical behaviour of this material, including damage effects.

These models are nevertheless very complex and sophisticated because they are dealing with several fields strongly coupled, they are characterized by sets of coupled, nonlinear, differential equations and they require a large number of material parameters. Moreover, as it is well known, the computer solution of such large set of equations needs rather long computer times when applied to real life problems and can be therefore quite expensive.

From this stems the necessity to reduce both the number of parameters to be determined accurately by experiments, and the computing time.

Hence, a sensitivity analysis of the model with respect to variations of its parameters is needed, to be able to distinguish how sensitive is the solution to variations of the

parameters of the equation set. Such an analysis reveals which are the main control parameters in the model and which are the effects of parameter changes, suggesting which parameters should be determined in an accurate way and which can simply be found from literature. The identification of parameters influence should also allows to proceed to a simplification of the mathematical model (model reduction).

The aim of this thesis is the sensitivity analysis of a finite element model (Comes-HTC) for the analysis of the behaviour of concrete exposed to high temperature; the sensitivity analysis has been performed with the automatic differentiation (AD) technique.

The application of AD to the fem code Comes-HTC has allowed to develop an efficient tool for the computation of the sensitivity coefficients, which has enabled to quantify the effect and relative importance of the material parameters with regards to the different model outputs. The results obtained allow for a better understanding of physical phenomena described by the Comes-HTC; they also highlight the full coupling between the hygral, thermal and mechanical field that impacts on the link between model variables and material parameters.

Summario

I problemi che accoppiano vari campi della fisica sono temi molto attuali nell'ambito dell'ingegneria civile. Il presente lavoro prende in esame modelli multifase per lo studio di calcestruzzi sottoposti ad alte temperature, applicabili per la valutazione della resistenza al fuoco di strutture civili o industriali.

Numerosi fenomeni non lineari interessano il comportamento del calcestruzzo quando si considerano temperature elevate; tali fenomeni riguardano non solo la conduzione di calore e la diffusione di vapore, ma anche il trasferimento di calore latente provocato dal cambiamento di fase dell'acqua all'interno dei pori ed il flusso d'acqua causato da gradienti di pressione, da effetti capillari, da gradienti del contenuto di acqua adsorbita. Inoltre le alte temperature causano forti cambiamenti microstrutturali e fanno sì che si sviluppino diversi fenomeni fisici e chimici interagenti fra di loro, che provocano variazioni significative della struttura interna e delle proprietà del materiale.

Nella modellazione del comportamento igro-termo-meccanico del calcestruzzo, si dovrebbero utilizzare modelli che considerano la complessità e le interazioni dei processi fisici descritti in precedenza. L'utilizzo di modelli accoppiati multifase, basati sulla meccanica dei mezzi porosi, si dimostra pertanto uno strumento necessario per una corretta previsione del comportamento igrometrico, termico, chimico e meccanico di tale materiale.

Questi modelli sono tuttavia molto complessi e sofisticati, perché hanno a che fare con parecchi campi fortemente accoppiati, sono caratterizzati da sistemi accoppiati di equazioni differenziali non lineari e richiedono un gran numero di parametri del materiale. Inoltre, nelle applicazioni di interesse pratico, la soluzione numerica di tali sistemi di equazioni richiede notevoli tempi di calcolo risultando quindi piuttosto costosa.

Nasce quindi l'esigenza di ridurre sia l'onere richiesto dalla determinazione sperimentale dei parametri necessari, sia i tempi computazionali.

Per poter procedere in questo senso serve quindi un'analisi della sensitività del modello rispetto alla variazione dei suoi parametri, per poter individuare in che modo

la soluzione venga influenzata dalla variazione dei parametri che compaiono nei sistemi di equazioni. Tale analisi rivela quali sono i parametri che controllano il modello e quali sono gli effetti delle loro variazioni, permettendo quindi di individuare i parametri la cui determinazione precisa è essenziale per l'accuratezza dei risultati e distinguerli da quelli la cui determinazione può essere meno precisa o che possono essere reperiti in letteratura. Dopo aver eseguito tale analisi, si potrà procedere ad una semplificazione del modello matematico, con effetti benefici anche sui tempi di calcolo, ed avviare in questo modo un processo di "model reduction".

Lo scopo di questa tesi è l'analisi di sensitività di un modello agli elementi finiti (Comes-HTC) per l'analisi del comportamento del calcestruzzo esposto ad alte temperature; l'analisi di sensitività è stata effettuata attraverso la differenziazione automatica (AD). L'applicazione di questa tecnica al codice fem Comes-HTC ha permesso di sviluppare uno strumento efficiente per il calcolo dei coefficienti di sensitività, attraverso il quale è stato possibile quantificare gli effetti e l'importanza relativa dei parametri del materiale sull'insieme di soluzioni calcolate dal modello. I risultati ottenuti hanno consentito una migliore comprensione dei fenomeni fisici descritti dal codice Comes-HTC, evidenziando anche il forte accoppiamento tra il campo igrometrico, termico e meccanico che influisce sul legame tra le variabili del modello e i parametri del materiale.

Chapter 1

Introduction

Coupled multiphysics problems are very actual research topics in civil engineering. In this work we focus on multiphase models for concrete exposed to high temperature, applicable to the evaluation of fire resistance in industrial and civil concrete structures [1, 2]; another possible application is the analysis of concrete structures of nuclear reactors in hypotetical core-distruptive accidents or in operative conditions [3].

Many non-linear phenomena and interactions are involved in concrete behaviour when temperatures higher than the standard ones are considered. Such phenomena involve not only heat conduction and vapour diffusion, but also liquid water flow caused by pressure gradients, capillary effects (due to interface curvature inside pores induced by surface tension), adsorbed water content gradients, as well as latent heat transfer due to water phase change (evaporation or desorption) inside the pores.

Moreover, high temperatures induce severe micro-structural changes and several interacting physical and chemical phenomena, resulting in significant changes of the material inner structure and properties [4]. The pore structure of concrete and hence also its physical properties change with time, following the hydration and aging processes, and are strongly influenced not only by the mechanical load, but also by the thermal-hygrometric state of concrete and their time history [5]. The permeability, which varies with moisture content and temperature changes, exhibits a sharp increase above 100°C. Physical properties of fluids (liquid water and moist air) filling up the pores of the material are also strongly temperature dependent. During hydration (below 95°C) or dehydration process (under about 120°C) considerable amounts of heat are released or adsorbed [6].

During modelling of hygro-thermal-mechanical behaviour of concrete, one should use models considering possibly the whole complexity and mutual interactions of the

analysed physical processes. The use of fully coupled multiphase models [7] is therefore necessary to correctly predict the hygro, thermal, chemical and mechanical behaviour of this material, including damage effects.

Consequently, a proper choice may be models based on mechanics of multiphase porous media, taking into account chemical reactions (hydration-dehydration), phase changes, cracking and thermo-chemical material degradation, as well as their mutual couplings and influence on the hygro, thermal, chemical and mechanical properties of concrete [8].

These models are nevertheless very complex and sophisticated because they are dealing with several fields strongly coupled, they are characterized by sets of coupled, nonlinear, differential equations and they require a large number of material parameters. Moreover, as it is well known, the computer solution of such large set of equations needs rather long computer times when applied to real life problems and can be therefore quite expensive. From this stems the necessity to reduce both the number of parameters to be determined accurately by experiments, and the computing time.

Hence, a sensitivity analysis of the model with respect to variations of its parameters is needed to be able to distinguish how sensitive is the solution to variations of, or inherent uncertainties in, the parameters of the equation set. Such an analysis reveals which are the main control parameters in the model and which are the effects of parameter changes, suggesting which parameters should be determined in an accurate way and which can simply be found from literature. The identification of parameters influence should also allows to proceed to a simplification of the mathematical model (model reduction).

The problem of sensitivity of model systems to variation of its parameters is one of the most important aspects necessary for a proper understanding of the behaviour of systems, and of the models representing such systems, because it leads to gain deeper insight into the effect and relative importance of material parameters with regards to the structural response behaviour. It is now widely acknowledged that any reliable approach to practical engineering problems should provide the researcher with an assessment of parameter sensitivity, in order to know how sensitive the output variables are to changes of, or uncertainties in, the parameters and which of the output variables are sensitive (or not sensitive) to which of the parameters.

The essential ideas of design sensitivity can be traced back to a few basic concepts of a general theory called the theory of sensitivity. This theory originates from purely mathematical studies of the influence of coefficient variations on several differential

equations [9]. It was much later that the theory of sensitivity became the subject of thorough studies in the field of engineering. Analytic design sensitivity analysis formulations for linear systems are well established [10, 11]. However, the development of analytic design sensitivity analysis formulations for nonlinear systems is an area of on-going research. Several works formulate sensitivity expressions for steady-state uncoupled nonlinear systems [12, 13, 14, 15]. Design sensitivity analysis for transient uncoupled systems are addressed in [16, 17, 18]. Sensitivity analysis for steady-state and transient coupled systems are investigated in [19, 20, 21, 22].

The theory of sensitivity can be generally divided into two categories: sensitivity analysis and sensitivity synthesis. The latter is defined as the structural system design according to sensitivity analysis directives, in order to obtain minimal or maximal sensitivity with respect to parameter variations. Thus, sensitivity analysis is the foundation of sensitivity synthesis. The main purpose of sensitivity analysis of models is the derivation of the so-called sensitivity gradients of objective functions with respect to the material and/or shape characteristics of the analysed structure (material and shape sensitivity analysis). Furthermore, the numerical values of these gradients can reveal the effects of different design parameters on the model response and point out the most crucial design parameters, being the purpose of this work.

Researchers have developed a number of different methods for performing sensitivity analysis which can be collect in two categories: global and local sensitivity analysis. In local methods, sensitivity coefficients are computed at some nominal values considered for the parameters and the behaviour of the response function is described only locally in the input space. In contrast, global sensitivity analysis methods evaluate the effect of a parameter while all other parameters are varied simultaneously, thus accounting for interactions between parameters without depending on the stipulation of a nominal point (they explore the entire range of each parameter). Focusing on the local methods, three different approaches can be used to determine the sensitivity coefficients: (i) analytical differentiation, (ii) numerical differentiation of the solution by finite differences and (iii) automatic differentiation [23] of the governing equations.

In the arena of modern sensitivity techniques, analytic differentiation of the governing equations is generally very difficult. Finite differencing, is the simplest, most common and most computationally expensive strategy of obtaining sensitivity coefficients. It requires the "brute force" solution of the governing system for every design variable, using first or second-order differentiating formula. The third method involves the automatic differentiation of the equations at the system level. It consists in modi-

fying the initial mathematical system by the introduction of an additional differential system, which is obtained differentiating the original system with respect to the variables involved in the sensitivity analysis. Considerable effort has been applied to develop this technique which have been found to be more accurate and less expensive than finite differences.

The object of this work is the sensitivity analysis of a finite element model for the analysis of the behaviour of concrete exposed to high temperature; it has been performed with the automatic differentiation technique. Next chapter includes a review of different techniques to perform the sensitivity analysis of mathematical models. Three different approaches to compute the sensitivity coefficients are presented, highlighting the main advantages and drawbacks of each method. In chapter 3 the mathematical model for the coupled hygro-thermal-chemical-mechanical processes taking place in partially saturated deforming porous media is described. A brief description of the discretization in space and in time domain of the governing equations used for the solution of the boundary-initial problem is also given. An analysis of mechanical and hygro-thermal behaviour of concrete at high temperature, treated as a multiphase porous material, is presented in chapters 4 and 5. Chapter 6 describes the procedure adopted to perform the sensitivity analysis of a finite element code for the analysis of concrete behaviour at high temperature. In chapter 7 the results of this study are presented and discussed.

Bibliography

[1] Schrefler B.A, Brunello P., Gawin D., Majorana C., Pesavento F., Concrete at high temperature with application to tunnel fire, Comput. Mech. 29, 43-51, 2002.

[2] Luccioni B.M., Figueroa M.I, Danesi R.F., Thermo-mechanic model for concrete exposed to elevated temperatures, Engineering Structures 25: 729-742, 2003.

[3] Ranc G., Sercombe J., Rodrigues S., Gatabin C., Structural and local behaviour of reinforced high strength mock-up subjected to high temperatures, In Fracture Mechanics of Concrete Structures: Proceedings of the Fourth International Conference FRAMCOS 4, Cachan, France, 28 May–1 June 2001.

[4] Bazant Z.P., Kaplan M.F., Concrete at high temperatures: material properties and mathematical models, London: Longman Group Limited, 1996.

[5] Maso J.C. (Ed.), Pore Structure and Construction Materials Properties, Chapman & Hall, London, 1987.

[6] Gawin D., Majorana C.E., Schrefler B.A., Numerical analysis of hygro-thermal behaviour and damage of concrete at high temperature, Int. J. Mech. Cohes.-Frict. Mater., 4: 37-74, 1999.

[7] Lewis R.W, Schrefler B.A., The finite element method in the static and dynamic deformation and consolidation of porous media, 2nd ed., John Wiley & Sons, Chichester, 1998.

[8] Gawin G., Pesavento F., Schrefler B.A., Towards prediction of the thermal spalling risk through a multi-phase porous media model of concrete, Comput. Methods Appl. Mech. Engrg. 195: 5707-5729, 2006.

[9] Frank P.M., Introduction to System Sensitivity Theory, New York: Academic Press, 1978.

[10] Haug E.J., Choi K.K., Komkov V., Design Sensitivity Analysis of Structural Systems, Academic Press, New York, 1986.

[11] Tortorelli D.A., Lu S.C.Y., Haber R.B., Design Sensitivity Analysis for Elastodynamic Systems, Mechanics of Structures and Machines, 18(1): 77-105, 1990.

[12] Mroz Z., Kamat M.P., Plaut R.H., Sensitivity Analysis and Optimal Design of Nonlinear Beams an Plates, Journal of Structural Mechanics, 13(3): 245-266, 1985.

[13] Choi K.K., Santos J.L.T., Design Sensitivity Analysis of Nonlinear Structural Systems: Part I, Theory, Int. J. Num. Meths in Engineering, 24(11): 2039-2055, 1987.

[14] Santos J.L.T., Choi K.K., Sizing Design Sensitivity Analysis of Nonlinear Structural Systems: Part-II, Numerical Method, Int. J. Num. Meths in Engineering, 26(9): 2097-2114, 1988.

[15] Phelan D.G., Vidal C., Haber R.B., An Adjoint Variable Method for Sensitivity Analysis of Nonlinear Elastic Systems, Int. J. Num. Meths in Engineering, 31: 1649-1667, 1991.

[16] Dems K., Sensitivity in Thermal Problems I: Variation of Material Parameters within a Fixed Domain, Journal of Thermal Stresses, 9: 303-324, 1986.

[17] Dems K., Sensitivity in Thermal Problems II: Structural Shape Variation, Journal of Thermal Stress, 10: 1-16, 1986.

[18] Haftka R.T., Techniques for Thermal Sensitivity Analysis, Int. J. Num. Meths in Engineering, 17: 71-80, 1981.

[19] Ryu Y.S., Haririan M., Wu C.C., Arora J.S., Structural Design Sensitivity Analysis of Nonlinear Response, Computers and Structures, 21(1/2): 245-255, 1985.

[20] Tsay J.J., Arora J.S., Nonlinear Structural Design Sensitivity Analysis for Path Dependent Problems. Part 1: General Theory, Comput. Methods Appl. Mech. Engrg., 81: 183-208, 1990.

[21] Tortorelli D.A., Haber R.B., Lu S.C.Y., Adjoint Sensitivity Analysis For Nonlinear Dynamic Thermoelastic Systems, AIAA Journal, 29(2): 253-263, 1991.

[22] Vidal C.A., Lee H.S., Haber R.B., The Consistent Tangent Operator for Design Sensitivity Analysis of History-Dependent Response, Computing Systems in Engineering, 2(5-6): 509-523, 1991.

[23] Griewank A., Evaluating Derivatives: Principles and Techniques of Algorithmic Differentiation, Frontiers in Applied Mathematics, Siam, 2000.

Chapter 2

Sensitivity Analysis

2.1 Introduction

Sensitivity analysis is the study of how the variation (numerical or otherwise) in the output of a model can be apportioned to different sources of variation in the model input[1]: in other words sensitivity analysis characterizes the change in model output due to the variation in model input parameters.

In this chapter we focus on parameter sensitivity that is generally performed through a series of test in which the user sets different parameter values to understand how a change in the parameter causes a change in the behaviour of the considered problem. Sensitivity analysis is therefore a useful tool which not only allows to understand how the model behaviour depends on certain parameters in the model formulation, but also indicate which parameters values are reasonable to use in the model. It is possible to conduct sensitivity analysis for a number of reason including the need to determine: which parameters are most highly associated with the output variability; what level of accuracy is necessary for a parameter in order to obtain acceptable results; which parameters are less significant and can be obtained from literature, considered constant or even eliminated from the final model.

Sensitivity analysis can be divided into two categories: global and local sensitivity analysis; the difference between these consists in the magnitude of the parameter changes to be studied. While global sensitivity analysis techniques are better appropriated to measure the effect of large changes in the parameters, in local sensitivity analysis parameter changes are constrained to be small.

Global sensitivity methods analyze in a random or systematic way the whole range of possible parameter sets and of input parameter values that are of interest; this technique

provides an overall view on the influence of parameter variations on model outcomes. There are several different methods that belong to the class of global sensitivity analysis as for example Monte Carlo and Latin Hypercube Sampling methods, Sobol's method, Fourier amplitude sensitivity test technique, etc.

Local sensitivity analysis attends to evaluate the impact of each parameter variation, in the vicinity of a sample point, on the model output: this type of analysis focuses hence on the effect caused by changes in a certain parameter value (mean, default or optimum). The term local refers to the fact that this analysis describes the system around a given set of values for the input parameters and not for the entire parameters distribution. Local analysis generally relies on the estimation of the partial derivatives of the output function with respect to input parameters.

In the following we will focus on local sensitivity analysis and we will describe three different methods to compute the local sensitivity coefficients: the first one is analytical, the second one is numerical and the third way is by means of automatic differentiation [2]. Conceptually all three are equivalent because they are based on the fact that a small perturbation of a certain input is propagated through the system and the corresponding deviation of one, many or all outputs is estimated.

2.2 Analytical sensitivity analysis

It is possible to compute analytical sensitivity by hand or using one of the symbolic differentiation packages.

Hand coding is a powerful technique because it develops highly-optimized implementation, but it is also error-prone and very laborious, especially when the problem complexity increases; moreover this method has the big disadvantage that any modification of the original model will require manual re-differentiation [3].

Symbolic differentiation is provided by symbolic manipulation packages as for example Maple or Mathematica. Given a string describing the definition of a function, symbolic manipulation packages provide exact derivatives, expressing all them in terms of intermediate variables. Whereas accurate, this approach is limited by the fact that the representation of the differentiated expression grows fast with the number of input variables: consequently it may run into resource limitations when the function description is complicated. Functions involving branches or loops cannot readily handled by symbolic differentiation. Furthermore, symbolic differentiation is inherently inefficient in terms of computing time due to the rapid growth of the underlying expressions [3].

2.3 Numerical sensitivity analysis

Numerical sensitivity analysis is performed through finite difference approximation. This technique is also called the brute force method or indirect method: it is easy to implement because it makes use directly and solely of the original model and therefore does not require the development of a specific differentiated code.

This method consists in solving a given system repeatedly, while varying one or more input parameters at a time and keeping the others fixed. In this way the sensitivity coefficients are approximated by finite difference. Finite difference method is a straightforward way of performing numerical sensitivity analysis but, in addition to the problem of precision due to the numerical approximations implicit in the method, it suffers from high computational costs in the case of long-running models, since at least two program runs are request to calculate each sensitivity [4]; this method becomes less viable as the model become more comprehensive.

We consider a differentiable function f which depends on some input parameters that can be summarized in the vector $\boldsymbol{x}$; the numerical computation of the sensitivity requires the evaluation of the difference quotient $df(\boldsymbol{x})/d\boldsymbol{x}$. This is realized by the calculation of function values of $f(\boldsymbol{x})$ in a small neighborhood $d\boldsymbol{x}$ of the observed value $\boldsymbol{x}$. The estimation of the first derivatives, therefore, is represented by the forward, the backward as well as the central difference method, which all can be derived from a forward or backward Taylor series, respectively:

$$\begin{aligned} f(\boldsymbol{x}+d\boldsymbol{x}) &= f(\boldsymbol{x}) + \frac{df}{d\boldsymbol{x}}\Big|_{\boldsymbol{x}} d\boldsymbol{x} + \frac{1}{2!}\frac{d^2 f}{d\boldsymbol{x}^2}\Big|_{\boldsymbol{x}} (d\boldsymbol{x})^2 + ... \\ f(\boldsymbol{x}-d\boldsymbol{x}) &= f(\boldsymbol{x}) - \frac{df}{d\boldsymbol{x}}\Big|_{\boldsymbol{x}} d\boldsymbol{x} + \frac{1}{2!}\frac{d^2 f}{d\boldsymbol{x}^2}\Big|_{\boldsymbol{x}} (d\boldsymbol{x})^2 - ... \end{aligned} \tag{2.1}$$

Truncating the first equation $(2.1)_1$ after the linear term, one obtains the forward difference method. Thus, the i-th component of the sensitivity vector $df(\boldsymbol{x})/d\boldsymbol{x}$ is given by

$$\frac{\partial f(\boldsymbol{x})}{\partial x_i}\Big|_{x_i} \approx \frac{f(x_i + dx_i) - f(x_i)}{dx_i} \tag{2.2}$$

Similarly, the second equation $(2.1)_2$ truncated after the linear term leads to the backward difference method:

$$\frac{\partial f(\boldsymbol{x})}{\partial x_i}\Big|_{x_i} \approx \frac{f(x_i) - f(x_i - dx_i)}{dx_i} \tag{2.3}$$

The central difference method is obtained by the subtraction of $(2.1)_2$ from $(2.1)_1$ by neglecting terms of third and higher order:

$$\frac{\partial f(\boldsymbol{x})}{\partial x_i}\Big|_{x_i} \approx \frac{f(x_i + dx_i) - f(x_i - dx_i)}{2dx_i} \tag{2.4}$$

It is therefore easily evident that the central difference method is a second order approximation, whereas the forward as well as the backward difference method are only a first approximation. But it is also clear that for the central difference method two additional computations of the variable $f(\boldsymbol{x})$ are required, which denotes that the numerical effort is twice than using the forward or backward difference method.

The accuracy of this method depends on the step size used in the finite difference approximation, i.e. on the choice of the increment dx_i . Hence, if dx_i is too small, rounding errors in consequence of the machine accuracy occur. Otherwise, if dx_i is too large, the errors due to the neglecting higher order terms in the Taylor series increase (truncation errors). This is a serious drawback of finite differences: some trade off must be found between truncation errors and approximation errors. Moreover the optimal choice of dx_i is not known *a priori*, and may vary not only from a function to another, but also from an input parameter to another: finding the best dx_i requires numerous executions of the program, and anyway then the computed derivatives are just approximations. However, with a reasonable choice of increments dx_i, the numerical sensitivity analysis yields suitable results, for the most cases [5].

Another method to approximate derivatives of real functions is based on complex calculus. If in equation $(2.1)_1$ we replace $d\boldsymbol{x}$ with $id\boldsymbol{x}$ ($i = \sqrt{-1}$, imaginary step size) it is possible to make use of the following Taylor series expansion:

$$f(\boldsymbol{x} + id\boldsymbol{x}) = f(\boldsymbol{x}) + i\frac{df}{d\boldsymbol{x}}\Big|_{\boldsymbol{x}} d\boldsymbol{x} - \frac{1}{2!}\frac{d^2 f}{d\boldsymbol{x}^2}\Big|_{\boldsymbol{x}} (d\boldsymbol{x})^2 - \frac{1}{3!}\frac{d^3 f}{d\boldsymbol{x}^3}\Big|_{\boldsymbol{x}} (d\boldsymbol{x})^3 + ... \tag{2.5}$$

Equating the imaginary part of the complex function with its expansion results:

$$\Im\left[f(\boldsymbol{x}+id\boldsymbol{x})\right] = \frac{df}{d\boldsymbol{x}}\Big|_{\boldsymbol{x}} d\boldsymbol{x} - \frac{1}{3!}\frac{d^3 f}{d\boldsymbol{x}^3}\Big|_{\boldsymbol{x}} (d\boldsymbol{x})^3 + O\left[(d\boldsymbol{x})^4\right]$$

$$\frac{\mathrm{d}f(\boldsymbol{x})}{d\boldsymbol{x}} \approx \frac{\Im\left[f(\boldsymbol{x}+id\boldsymbol{x})\right]}{d\boldsymbol{x}} + O\left[(d\boldsymbol{x})^2\right] \tag{2.6}$$

The complex method allows to achieve a second order approximation with just one function evaluation. Moreover the first derivatives are obtained without the subtraction of two similarly valued functions: it follows that complex variable method does not suffer from subtractive cancellation errors and so the choice of step size is based upon accuracy requirements alone [6].

In order to implement the sensitivity analysis with the complex method it is necessary to modify the source code that computes the value of the function f. The implementation procedure can be summarized in three steps: at first all real type variable declarations must be substituted with complex declarations (it is not strictly necessary to declare all variables complex, but it is much easier to do so); then it is necessary to define all functions and operators that are not defined for complex arguments; finally a complex-step can then be added to the desired x_i and $\partial f(\boldsymbol{x})/\partial x_i$ can be estimated using equation $(2.6)_2$. This step of the implementation, adding the complex-step to the variable of interest and using the complex-step approximation must be done manually [7].

The disadvantage of the complex variable approximation is the increased run-time required by the program when runs with complex arguments. With current compiler options, this run time is on the order of three times the cost of the original solver [8].

2.4 Automatic differentiation

Automatic differentiation (AD) is an automated procedure for calculating derivatives of mathematical functions and it is used in the following areas: sensitivity analysis, numerical methods, design optimization, data assimilation and inverse problem.

Automatic differentiation consists of a set of techniques based on the application of the chain rule to obtain derivatives of a function given as a computer program. AD exploits the fact that every computer program, no matter how complicated, executes a sequence of elementary arithmetic operations (addition, multiplication, etc.) or elementary functions (sin, cos, etc.). By applying the chain rule of derivative calculus over and over to the composition of these elementary operations, derivatives of arbi-

trary order can be computed automatically. Unlike numerical methods that give an estimation of derivatives by finite difference, AD is a procedure that allows to obtain exact derivatives, accurate to working precision. Furthermore, it avoids the tedious and error-prone analytical derivation work done by hand.

Automatic differentiation tools take as input a source program P that, given a vector argument $X \in \mathbb{R}^n$, computes some vector function $Y = F(X) \in \mathbb{R}^m$.

AD tools behave largely like pre-compilers that analyze the code written for evaluating functions of several variables (input parameters, X) and automatically evaluate their first or higher order partial derivatives with respect to the inputs: the values of partial derivatives are a measure of local sensitivity analysis (figure 2.1).

The differentiated program ideally should never be modified or post-processed by hand; in reality AD approach requires to know the source of the program P and needs a certain amount of work by the final user to perform a correct differentiation. This is considered a weakness and AD tools are attempting to progressively eliminate these hand modification stages [9].

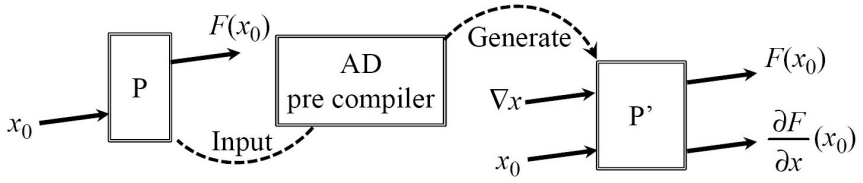

Figure 2.1: Automatic differentiation technique [10]

The fundamental principles of AD are discussed in [11] and an overview of the primary mechanisms of code generation is given in [12].

Implementation of AD can be generally classified into two categories: operator overloading and source transformation [13].

AD tools based on operator overloading exploit the fact that several programming languages offer the possibility to redefine the semantics of elementary operators, according to the type of their arguments. Overloading consists in replacing each variable used to compute a derivative, with a new variable which holds two values, the first value is the original variable value, and the second value holds the differential information. Also each elementary operation is treated in the same way, thus internally replaced by a new operation, which holds the computed value and its derivative. This procedure is carried out at compiling time: this means that the changes in the original code are just the necessary to inform where to apply the replacements (this is usually done by

changing the variables and operations types and names). The advantage of overloading is that it requires very little code transformation. The drawbacks are that not all languages support overloading and that overloaded programs are poorly optimized by the compiler [14].

AD tools based on source transformation change the semantics by explicitly rewriting the code and generating a new program. Source transformation strategies rely on compiler technology to transform source code for computing functions into source code for computing both the derivatives of the functions and the functions themselves. This technique consists in adding into the program the new variables, arrays, and data structures that will hold the derivatives, and in adding the new instructions that compute these derivatives. The advantages of the source transformation strategy is that the resulting program can be compiled into an efficient code; the drawback is that this is an enormous transformation, that cannot be done by hand on large programs.

The aim of automatic differentiation is, either with operator overloading or with source transformation, to compute derivatives without going back to the underlying mathematical equations, considering only the source program P: this source transformation is possible because AD assumes that P represents all its possible run-time sequences of instructions, and it in fact differentiate these sequences [9].

Since programs are identified with sequence of instructions, it is possible to identify any sequence of instructions with a composition of vector functions, each of which is assumed to be differentiable. Thus we can write:

$$\begin{array}{lcl} P & \text{is} & \{I_1; I_2; ...; I_p\} \\ F(X) & = & f_p \circ f_{p-1} \circ ... \circ f_1 \end{array} \tag{2.7}$$

where each f_k is the elementary function implemented by instruction I_k.

Among the outputs of P, we detect a subset Y of variables that we want to differentiate; symmetrically, among the inputs of P, we identify a subset X of variables with respect to which we want to differentiate Y. Both X and Y are in general multi-dimensional, and must consist of variables of a continuous type. The X are often called the "independent variables" and Y the "dependents variables". We are looking for the derivatives of $Y = F(X)$ at the current input point $X = X_0$. We can then simply apply the chain rule to write the derivative of the program for a given input vector X. Note that the chain rule of calculus can be applied only if the involved functions are differentiable. If we write for short X_k as the value of all variables after instruction I_k,

i.e. $X_0 = X$ and $X_k = f_k(X_{k-1})$, the chain rule gives the Jacobian F' of F:

$$\begin{array}{rcl} Y' & = & f'_p(X_{p-1}) \times f'_{p-1}(X_{p-2}) \times ... \times f'_1(X_0) \\ F' & : & X \in \mathbb{R}^n \rightarrow Y' \in \mathbb{R}^m \end{array} \tag{2.8}$$

At least in theory automatic differentiation can yield the complete Jacobian matrix $J = \nabla F$, i.e. the partial derivatives of each output with respect to each input. In practice, these mathematical objects are often too large or expensive to compute and store because their computation involves matrix-by-matrix multiplications; moreover for most applications the full Jacobian matrix is not really necessary. Therefore, AD can also return smaller objects at a cheaper cost (e.g. directional derivatives, gradients, directional higher-order derivatives, or Taylor series expansions) computing the derivatives only along some directions using matrix-by-vector multiplications [15].

In general, given a matrix A $\in \mathbb{R}^{m,n}$ and two vectors, $X \in \mathbb{R}^n$ and $Y \in \mathbb{R}^m$, it is possible to perform the matrix by vector multiplication in a twofold manner: by right, i.e. computing $b = AX$, $b \in \mathbb{R}^m$; or by left, i.e. computing $c^T = Y^T A$, $c \in \mathbb{R}^n$ (and the multiplication can be viewed as the right multiplication using the transpose matrix A^T, namely $c = A^T Y$). In order to use the two multiplications, many automatic differentiation packages have two different approaches to compute derivatives: they are distinguished by how the chain rule is used to propagate derivatives through the computation. The first method is the forward (or tangent) mode that computes first-order directional derivatives and is the most straightforward. The second one is the reverse (or adjoint) mode that computes the gradient of functions [13]. This latter method is very efficient in execution time, but is a great consumer of memory and should therefore be optimized whenever possible. In the following we'll briefly summarize the theoretical background that we need for these two particular modes.

2.4.1 Forward mode

Computing the product of all the elementary Jacobian matrices returns the complete Jacobian matrix J of $F(X)$, i.e. equation $(2.8)_1$. This is certainly expensive in time and space: often, resolution of many problems requires only some projection of $F'(X)$. For example, for a given small variation dX in the input space, one may just needs the corresponding first-order variation of the output, that is the sensitivity, also known as directional derivative. By definition of the Jacobian matrix this sensitivity is represented by $dY = F'(X) \times dX$ [16]. Historically this is the first application of AD. Using

equation $(2.8)_1$, we get the expression of sensitivity:

$$\begin{aligned} &dY = F'(X) \times dX = f'_p(X_{p-1}) \times f'_{p-1}(X_{p-2}) \times ... \times f'_1(X_0) \times dX \\ &F' \times dX \ : \ X, dX \in \mathbb{R}^n \rightarrow dY \in \mathbb{R}^m \end{aligned} \tag{2.9}$$

which is efficiently computed from right to left, because this involves the multiplication of a matrix by a vector instead of the multiplication of a matrix by a matrix. This is not difficult to implement, because it requires X_0 first, and then X_1, and so on until X_{p-1}. In other words, at each computational stage, derivatives of the intermediate variables with respect to the input variables are computed and are propagated forward, through the computational stages. Differentiated instructions, that compute the Jacobian matrices and multiply them, can be done along with the initial program; it is only necessary to interleave the original instructions and the derivative ones.

In the tangent mode, the new program $\dot{\mathrm{P}}$ is just a copy of the given program P because the differentiated instructions are inserted just before each instruction. The control structures of the program are unchanged, i.e. the call graph and the flow graph have the same shape in P and $\dot{\mathrm{P}}$.

In figure 2.2 is illustrated an example of AD in tangent mode. On the left column is an example subroutine, that measures the difference between two given array `T` and `U`. The right column shows the tangent differentiate subroutine, which computes tangent derivatives, conventionally shown with a dot above. For example, the differentiated instruction that precedes instruction `e = SQRT(e2)`, implements the following vector assignment that multiplies the instruction's elementary Jacobian by the vector of tangent derivatives.

original: T,U ↦ e	**tangent mode:** T,Ṫ,U,U̇ ↦ e,ė
	ė2 = 0.0
e2 = 0.0	e2 = 0.0
do i=1,n	do i=1,n
	ė1 = Ṫ(i)-U̇(i)
e1 = T(i)-U(i)	e1 = T(i)-U(i)
	ė2 = ė2 + 2.0*e1*ė1
e2 = e2 + e1*e1	e2 = e2 + e1*e1
end do	end do
	ė = 0.5*ė2/SQRT(e2)
e = SQRT(e2)	e = SQRT(e2)

Figure 2.2: Automatic differentiation in tangent mode [15]

The tangent mode of automatic differentiation is quite straightforward. However,

it can be improved through some specific optimizations based on static analysis of the program. In particular activity analysis (see section 2.4.5) can simplify the tangent differentiated program, by statically detecting derivatives that are always zero.

2.4.2 Reverse mode

The main goal of the revers mode is to compute linear combinations of the columns of the Jacobian, that is to compute gradients. The gradients are important because they are used in optimization, data assimilation, inverse problem or adjoint problems [9]. The interest on the gradient lies on the information regarding the directions in the input space, which show the largest ratio of change in the output space.

For a scalar-valued function the gradient is defined like the column vector whose components are the weighed partial derivatives of the function. In the general case where Y is a vector, we need to build a vector $\bar{Y}$ that defines the weights of each component of the original output $Y = F(X)$. The composition of this vector with the original output vector Y defines a scalar output:

$$\bar{Y}^T \times Y = Y^T \times \bar{Y} \tag{2.10}$$

Replacing $Y = F(X)$ in (2.10) we obtain

$$\bar{Y}^T \times Y = F^T(X) \times \bar{Y} \tag{2.11}$$

and applying the chain rule we get the gradient:

$$\begin{aligned} &\bar{X} = F'^T(X) \times \bar{Y} = f_1'^T(X_0) \times f_2'^T(X_1) \times ... \times f_{p-1}'^T(X_{p-2}) \times f_p'^T(X_{p-1}) \times \bar{Y} \\ &F' \times \bar{Y} \ : \ \bar{Y} \in \mathbb{R}^m, \ X \in \mathbb{R}^n \rightarrow \bar{X} \in \mathbb{R}^n \end{aligned} \tag{2.12}$$

where every $f_k'^T$ and $F'^T(X)$ are transposed Jacobians. Again equation $(2.12)_1$ is efficiently computed from right to left, because this involves the multiplication of a matrix by a vector, that is cheaper than the multiplication of a matrix by a matrix [14].

This is the principle of the reverse mode of AD; the program differentiated in reverse mode is often called the adjoint program of P, and is indicated with $\bar{P}$.

There is a difficulty with the reverse mode because in $(2.12)_1$ the order of computation is inverted compared to the one of P: the intermediate values X_{p-1}, in fact, are

used first, and then X_{p-2}, and so on until X_0; the intermediate values may have been overwritten and lost for future calculations. Reverse mode therefore must be a two-stage process: first a complete execution of P is necessary to get X_{p-1}(forward sweep $\overrightarrow{P}$), and only then the Jacobian×vector products can be evaluated (reverse sweep $\overleftarrow{P}$) [17]. But then X_{p-2} is required, whereas instructionI_{p-1} may have overwritten it. This is the main drawback of the reverse mode of AD. There are mainly two ways to cope with that, called the Recompute-All (RA) and the Store-All (SA) approaches [16]: RA increases the execution time, on the other hand SA consumes a great deal of memory.

- Recompute-All (RA): the X_k are recomputed when needed, by restarting the program P on input X_0 until instruction I_k. Figure 2.3 graphically illustrates the RA strategy. The cost is extra execution time, approximately proportional to the square of the number of run-time instructions p. The $\overleftarrow{I_k}$ instructions and backwards arrows represent the execution of the differentiated instructions, which effectively compute $\overline{Y}_{k-1} = f_k'^T(X_{k-1}) \times \overline{Y}_k$. The big black and white dots represent respectively the storage of all variables needed to restart execution from a given point, and restoration of these variables to be able to restart computation. RA strategy has essentially a quadratic time cost with respect to the total number of run-time instructions p.

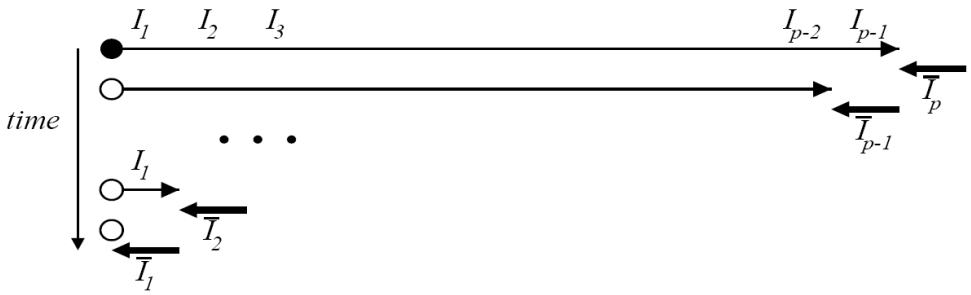

Figure 2.3: The Recompute-All strategy [16]

- Store-All (SA): this strategy consists in storing in a stack all the values of X_k during a preliminary execution of the program, the forward sweep $\overrightarrow{P}$, thus making them accessible when required; the X_k are consequently restored from the stack when needed. The differentiated instructions are computed during the second run, the backward sweep $\overleftarrow{P}$. Figure 2.4 summarizes this tactic graphically. The small black and white dots represent respectively the storage of intermediate values just before they are overwritten by an instruction I_k, and their corresponding

retrieval during the backward sweep. SA strategy as a linear memory cost with respect to p.

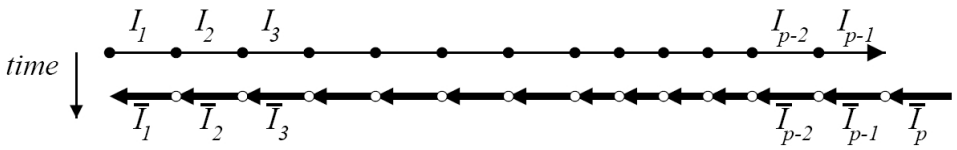

Figure 2.4: The Store-All strategy [16]

Both modes, tangent and reverse, implement elements of the Jacobian matrix, but depending on the dimension of the input (n) and output (m) spaces, it is possible to understand which mode to apply to a given program. In figure 2.5 is shown a comparison between tangent and reverse mode of AD. The program $\dot{\mathrm{P}}$ resulting from the tangent mode, which costs a small multiple of P's execution time, returns only a column of the Jacobian matrix. To obtain the full Jacobian, or equivalently the gradient when the dimension of the output space $m = 1$, one must run P once for each element of the cartesian basis of the input space. Therefore the cost of computing the Jacobian using the tangent mode is proportional to the dimension of the input space. In contrast, the program $\dot{\mathrm{P}}$ resulting from the reverse mode, which also costs a small multiple of P's execution time, returns a row of the Jacobian matrix. To obtain the full Jacobian, one must run P once for each element of the cartesian basis of the output space.

If $n \gg m$, that is the gradients of a small number of function outputs are required with respect to a large number of function inputs, the reverse mode of AD provides the gradient at a much cheaper cost. It is therefore suggested to use reverse mode each time m is smaller than n, which is the typical case of a cost function ($m = 1$) in optimization. Generally, the reverse mode has much grater memory requirements than the forward mode, but can offer better performance when the number of scalar independent variables is significantly grater than the number of scalar dependent variables.

2.4.3 An example of automatic differentiation

To better understand how AD works in practice (source transformation process), we introduce a special notation that will help us for a correct implementation. First of all,

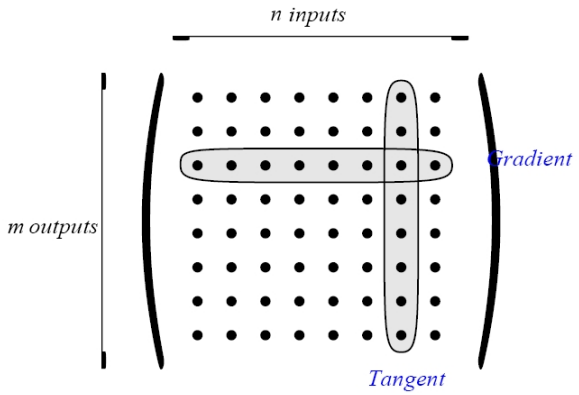

Figure 2.5: Tangent and Reverse AD modes [15]

we assume that the function

$$\begin{array}{rccc} g: & \mathbb{R}^{n_x} \times \mathbb{R}^{n_y} & \rightarrow & \mathbb{R}^m \\ & (X,\, Y) & \rightarrow & g\,(X,\, Y) \end{array} \tag{2.13}$$

is implemented by the routine $\texttt{func}(\texttt{G}, \texttt{X}, \texttt{Y})$, where X and Y are the variables that should contain the $X \in \mathbb{R}^{n_x}$ and $Y \in \mathbb{R}^{n_y}$ respectively, and G is the variables where will be stored the result $g(X,\, Y) \in \mathbb{R}^m$ (i.e. $\texttt{func}(\texttt{G}, \texttt{X}, \texttt{Y})$is a subroutine in Fortran language or a void function in C/C++ terminology) [18].

For differentiation, we need to know which are the independent variables (that are input parameters of the function) and which are the dependent variables (output parameters). For this purpose, we use an arrow over any parameter containing the independent variable and an arrow under any parameter containing the dependent variable, thus, if we want to specify that the routine $\texttt{func}(\texttt{G}, \texttt{X}, \texttt{Y})$, implementing the function $g(X,\, Y)$, has $\texttt{G}$ as output and $\texttt{X}$, $\texttt{Y}$ as input we write

$$\texttt{func}(\underset{\downarrow}{\texttt{G}},\, \overset{\downarrow}{\texttt{X}},\, \overset{\downarrow}{\texttt{Y}}) \tag{2.14}$$

Furthermore, if we would specify that the function is evaluated with some specific values $X = X_0$ and $Y = Y_0$ we'll write

$$\texttt{func}(\underset{g(X_0, Y_0)}{\texttt{G}},\, \overset{X_0}{\texttt{X}},\, \overset{Y_0}{\texttt{Y}}) \tag{2.15}$$

where the value written over a parameter means "value taken by the input variable" and the value under a parameter means "value stored in the output variable".

The last step is to specify which mode we use for differentiation and study the output generated by the AD tool that performs the differentiation required. First of all, we must keep into account that for each independent variable with respect to which we differentiate, we'll have a corresponding dual variable that will be of the same kind (input) if we use forward mode, and of the opposite kind (output) if we use the reverse mode. The same thing happens for the dependent (output) variables: the dual variables will be output variables in the case of forward mode and input variables for reverse mode.

Using the notation previously introduced, forward mode differentiation for the case (2.14) respect to both the independent variables `X` and `Y` gives us

$$\texttt{func\_d}(\texttt{G},\ \texttt{Gd},\ \texttt{X},\ \texttt{Xd},\ \texttt{Y},\ \texttt{Yd}) \tag{2.16}$$

where the new parameters `Gd` (output), `Xd` (input) and `Yd` (input) are the dual variables of `G`, `X` and `Y` (the `d` character after the variables and function name means "direct" differentiation). If we give at the new input parameters `Xd` and `Yd` the values $\dot{X} \in \mathbb{R}^{n_x}$ and $\dot{Y} \in \mathbb{R}^{n_y}$ respectively, we obtain

$$\texttt{func\_d}(\underset{g(X_0,Y_0)}{\texttt{G}},\ \underset{(\frac{\partial g}{\partial X}\big|_{(X_0,Y_0)})\times\dot{X}+(\frac{\partial g}{\partial Y}\big|_{(X_0,Y_0)})\times\dot{Y}}{\texttt{Gd}},\ \overset{X_0}{\texttt{X}},\ \overset{\dot{X}}{\texttt{Xd}},\ \overset{Y_0}{\texttt{Y}},\ \overset{\dot{Y}}{\texttt{Yd}}) \tag{2.17}$$

where the output parameter `Gd` contains the value $\dot{g} = (\frac{\partial g}{\partial X}\big|_{(X_0,Y_0)})\times\dot{X}+(\frac{\partial g}{\partial Y}\big|_{(X_0,Y_0)})\times\dot{Y}$ with $\dot{g} \in \mathbb{R}^m$ (and the derivatives $\frac{\partial g}{\partial X}$ and $\frac{\partial g}{\partial Y}$ are both evaluated at $(X_0,\ Y_0)$).

Reverse mode differentiation of (2.14) gives us

$$\texttt{func\_b}(\texttt{G},\ \texttt{Gb},\ \texttt{X},\ \texttt{Xb},\ \texttt{Y},\ \texttt{Yb}) \tag{2.18}$$

where now we have a new input parameter `Gb` and two new output parameters `Xb` and `Yb` (the `b` character after the variables and function name means "backward" differentiation). Storing the value $\bar{g} \in \mathbb{R}^m$ in the parameter `Gb`, we obtain

$$\texttt{func\_b}(\underset{g(X_0,Y_0)}{\texttt{G}},\ \overset{\bar{g}}{\texttt{Gb}},\ \overset{X_0}{\texttt{X}},\ \underset{(\frac{\partial g}{\partial X}\big|_{(X_0,Y_0)})^T\times\bar{g}}{\texttt{Xb}},\ \overset{Y_0}{\texttt{Y}},\ \underset{(\frac{\partial g}{\partial Y}\big|_{(X_0,Y_0)})^T\times\bar{g}}{\texttt{Yb}}) \tag{2.19}$$

i.e. the output parameters `Xb` and `Yb` will contain the values $\bar{X}_g = (\frac{\partial g}{\partial X}\big|_{(X_0,Y_0)})^T \times \bar{g}$ and $\bar{Y}_g = (\frac{\partial g}{\partial Y}\big|_{(X_0,Y_0)})^T \times \bar{g}$ respectively (with $\bar{X}_g \in \mathbb{R}^{n_x}$, $\bar{Y}_g \in \mathbb{R}^{n_y}$ and the derivatives $\frac{\partial g}{\partial X}$ and $\frac{\partial g}{\partial Y}$ both evaluated at $(X_0,\ Y_0)$). The subscript on the output variables stands to remind

which is the differentiate function: this will be useful when we need to differentiate (in reverse-mode) routines having some common input variables.

For the case where we are differentiating with respect to only some independent variables (X for example) we obtain for forward mode

$$\texttt{func\_dX\_d}(\underset{g(X_0,Y_0)}{\texttt{G}}, \underset{\dot{g}_X=(\frac{\partial g}{\partial X}\big|_{(X_0,Y_0)})\times\dot{X}}{\texttt{Gd\_X}}, \overset{X_0}{\texttt{X}}, \overset{\dot{X}}{\texttt{Xd}}, \overset{Y_0}{\texttt{Y}}) \tag{2.20}$$

where we use the notation $\dot{g}_X = \texttt{Gd\_X}$; and the suffix `dX` in the name of the differentiated routine specifies that the forward mode differentiation is performed only with respect to the independent variable X. In the same manner, we have for the reverse mode

$$\texttt{func\_dX\_b}(\underset{g(X_0,Y_0)}{\texttt{G}}, \overset{\bar{g}}{\texttt{Gb}}, \overset{X_0}{\texttt{X}}, \underset{(\frac{\partial g}{\partial X}\big|_{(X_0,Y_0)})^T\times\bar{g}}{\texttt{Xb}}, \overset{Y_0}{\texttt{Y}}) \tag{2.21}$$

2.4.4 Multi-directional differentiation

As we have previously described, the tangent mode of AD takes as input a single vector dX, which corresponds to the direction in the input space along which the directional derivatives must be computed. Conversely, the reverse mode of AD takes as input a single weight vector $\overline{Y}$ that defines the composite optimization criterion for which the gradient must be computed. Many applications require this computation for several vectors dX or $\overline{Y}$, at the same time and for the same point X in the input space. One example is to get the whole Jacobian $F'(X)$, column by column: for the same X, one must run the differentiated tangent program n times, with dX spanning all the canonical basis of $\mathbb{R}^n$ [19]. This amounts to several runs of the tangent (respectively reverse) program, for the same X.

If X is the same, all instructions from the original program run identically on the same inputs, producing the same results. Actually, it is possible to run the tangent mode simultaneously on several values of dX, and to run the reverse mode simultaneously on several values of $\overline{Y}$. This is called multi-directional tangent or reverse mode. This is functionally equivalent to running the tangent code (respectively the reverse code) many times, with the same value of X but with different values of $\dot{X}$ (respectively $\bar{Y}$). The difference lies in the execution time, because multi-directional code computes the original function only once.

One classical use of multi-directional mode is to compute the complete Jacobian matrix, either column by column through multi-directional tangent mode, or row by

row through multi-directional reverse mode. If the number of rows (i.e. output variables) is conspicuously smaller than the number of columns (i.e. input variables), then the multi-directional reverse mode is recommended. Otherwise the multi-directional tangent mode should be preferred [16].

The multi-directional differentiated model is based on expanding each memory cell that holds a single derivative: instead of holding just a scalar, it holds an array whose dimension is the maximum number of differentiation directions.

2.4.5 Activity analysis

In many situations, when performing automatic differentiation, not all the elements of the Jacobian matrix need to be computed, but what is necessary is only the derivatives of some selected output of the program with respect to some selected inputs. Whatever the differentiation mode, these restrictions allows the AD tool to produce a much more efficient differentiated program. Essentially, fixing some inputs and neglecting some outputs allows AD to just forget about several intermediate differentiated variables. This has two main consequence: several differentiated variables just disappear from the differentiated code, because they will content either null or useless derivatives, therefore memory usage of the differentiated code becomes smaller; several differentiated instructions are simplified or erased because one of their derivative arguments has known trivial value; in this way execution time of the differentiated code becomes shorter [15].

Activity analysis is the specific analysis that detects this situations allowing for a better differentiation code.

We can give the following definitions: an independent variables Y depends on X when the derivative of Y with respect to X is not trivially null; a variable is varied if it depends on at least one independent; conversely we define a variable useful if at least one dependent depends on it; finally we say that a variable is active if it is at the same time varied and useful. In the special case of the tangent mode, when a variable is not varied at some place in the program, then its derivative is certainly null. Conversely when a variable is not useful, then whatever is the value of its derivative, this value does not matter for the final result. Symmetric reasoning applies for the reverse mode of AD: observing that differentiated variables go upstream, we see that a useless variable has a null derivative, in other words the partial derivative of the output with respect to this variable is null. Conversely when a variable is not varied, then whatever is the value of its derivative, this value does not matter for the final result.

Activity analysis is global, running on the complete call graph below the topmost

differentiated procedure. In order to detect active variables, the activity analysis runs three analysis. The first analysis is called differentiable dependency analysis: it computes for basic blocks the differential dependency of every pair of variables. The second analysis is called varied, it computes the set of variables that possibly depends on some independent input. The third analysis is called useful, it computes the set of variables on which some dependent output possibly depends. The intersection of these two sets of variables determine which variables are active [14].

Bibliography

[1] Saltelli A., Ratto M., Andres T., Campolongo F., Cariboni J., Gatelli D., Saisana M., Tarantola S., Global Sensitivity Analysis. The Primer, John Wiley & Sons, 2008.

[2] Aubert P., Dicesare N., Pironneau O., Automatic Differentiation in C++ using Expression Templates and Application to a Flow Control Problem, Accepted in Computer Visualization and Software, 2000.

[3] Bischof C., Carle A., Corliss G., Griewank A., Hovland P., ADIFOR: Generating derivative codes from Fortran programs, Scientific Programming, 1(1): 11-29, 1992.

[4] Elizondo D., Cappelaere B., Faure C., Automatic versus manual model differentiation to compute sensitivities and solve non-linear inverse problems, Computers and Geosciences, 28(3): 309-326, 2002.

[5] Scholz B., Application of a micropolar model to the localization phenomena in granular materials: general model, sensitivity analysis and parameter optimization. Dissertation, Report No. II-15 of the Institute of Applied Mechanics (CE), University of Stuttgart, 2007.

[6] Cusdin P., Müller J.-D., Automatic differentiation and sensitivity analysis methods for computational fluid dynamics, Technical Report QUB-SAE-03-01, QUB School of Aeronautical Engineering, 2003.

[7] Martins J.R.R.A., Kroo I.M., Alonso J.J., An automated method for sensitivity analysis using complex variables, AIAA Paper 2000-0689, 38th Aerospace Sciences Meeting, 2000.

[8] Newman J.C., Anderson W.K., Whitfield D.L., Multidisciplinary Sensitivity Derivatives Using Complex Variables, Technical report - CFD Laboratory - Mississippi State University MSSU-COE-ERC- 98-08, 1998.

[9] Hascoët L., Dauvergne B., Adjoints of large simulation codes through automatic differentiation, European Journal of Computational Mechanics, 17: 63-86, 2008.

[10] Enciu P., Gerbaud L., Wurtz F., Automatic differentiation for sensitivity calculation in electromagnetism, The International Journal for Computation and Maths. in Electrical and Electronic Eng., 28(5): 1313-1326, 2009.

[11] Griewank A., On automatic differentiation, in Iri M. and Tanabe K. (Eds), Mathematical Programming: Recent Developments and Applications, Kluwer Academic Publisher, 83-108, 1989.

[12] Bischof C., Griewank A., Tools for the automatic differentiation of computer programs, in Alefeld G., Mahrenholtz O. and Mennicken R. (Eds.), ICIAM/GAMM 95: Issue 1: Numerical Analysis, Scientific Computing, Computer Science, 267-272, 1996.

[13] Griewank A., Evaluating Derivatives: Principles and Techniques of Algorithmic Differentiation, Frontiers in Applied Mathematics, Siam, 2000.

[14] Araya Polo M., Approaches to assess validity of derivatives and to improve efficiency in automatic differentiation of programs, PhD thesis, University of Nice Sophia Antipolis, 2006.

[15] Hascoët L., Automatic differentiation by program transformation, http://www-sop.inria.fr/tropics/papers/supportCoursDA.pdf, 2007.

[16] Hascoët L., Pascual V., Tapenade 2.1 User's guide, Inria Rapport technique 300, 2004.

[17] Araya-Polo M., Hascoët L., Domain of validity of derivatives computed by automatic differentiation, Inria Rapport de Recherche 5237, 2004.

[18] Martinelli M., Sensitivity Evaluation in Aerodynamic Optimal Design, PhD Thesis, Université de Nice Sophia Antipolis, 2007.

[19] Hascoët L., Static Analyses and Transformations of Programs: from Parallelization to Differentiation, Habilitation, Université de Nice Sophia Antipolis, 2005.

Chapter 3

Mechanics of porous media: mathematical and numerical model

3.1 Introduction

This chapter presents the governing equations for the full dynamic behaviour of a partially saturated porous medium. In particular, we assume that the voids are filled with water and air. The description of multiphase systems made of interpenetrating continuous bodies, such as porous media, is today based either on the mixture theory integrated by the concept of volume fractions, or on averaging theories and from a classical point of view on Biot's theory. Since the averaging theories offer the possibilities of a better understanding of the microscopic situation and its relation to the macroscopic one, which is the natural domain of all continuum mechanical models, we employ in the following the averaging theory based on spatial averaging operators. Within this theory we make use of macroscopic variables which correspond to real measurable quantities directly linked to laboratory practice, e.g. in soil mechanics. It has to be observed that, under appropriate assumptions, the averaging theory yields the same equations as the classical mixture theory, as shown in [1]. Care has to be taken, however, in the linear momentum balance equation as explained in section 3.4.

For the reader mainly interested in the resulting governing equations and their numerical solution, these equations are derived using Biot's theory in [2]. This also permits us to establish a link between the classical, phenomenological approach and the description of the real microscopic composition of the multiphase system. Furthermore, it shows the essential correctness of Biot's findings.

3.2 Averaging principles

Here are briefly summarized the principles necessary for the development of the governing equations. A full description of the averaging theories can be found in references [1, 3, 4, 5, 6, 7, 8, 9]. Sections 3.2, 3.3 and 3.4 follow, in particular, the work by Hassanizadeh and Gray [4, 5, 6, 7, 8] and by de Boer et al. [1].

We introduce the following definitions:

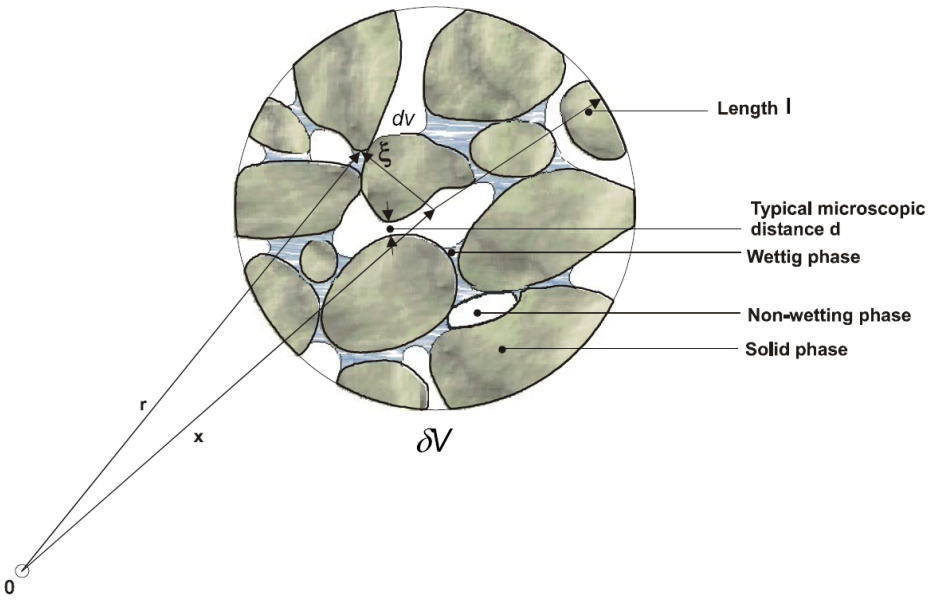

Figure 3.1: Typical averaging volume dv (two phase flow) of porous medium consisting of three constituents [2]

microscopic level: we consider the real non-homogeneous structure of the porous medium domain (figure 3.1). The scale of inhomogeneity is of the same order of magnitude of the dimensions of a pore or a grain, say d. Attention is focused on what happens at a mathematical point within a single phase and the field variables describing the status of a phase are defined only at the points occupied by that phase. For the practical description of the processes taking place in a porous medium, the level of detail given is not needed since microscopic quantities are generally not measurable. Only their average values are measurable.

macroscopic level: the real multiphase system that occupies the porous medium domain is replaced by a model in which each phase is assumed to fill up the entire domain. This means that at every point all phases are supposed present at the same time (overlapping continua). This is the level of interest of continuum mechanics, where we investigate the continuous distribution of the constituents through a macroscopic control

space. At this level, we usually deal with homogeneous media, but non-homogeneities may still be present, e.g. layers. Their scale is of an order of magnitude comparable with the order of magnitude of the entire domain, say L.

megascopic level: at this level the conditions are similar to those of the previously defined level. The difference depends on the fact that some macroscopic inhomogeneities are eliminated by averaging and/or on the fact that the mathematical model is stated in a domain which has less dimensions than the real domain, e.g. a two-dimensional problem with field values averaged over the thickness [10, 11]. Typical applications of this level are found in the simulation of land subsidence problems of regional scale.

3.2.1 Averaging process

We consider a multiphase system occupying a total volume, V, and bounded by surface, A. The multiphase system is a heterogeneous medium composed of $\pi = 1, 2, ..., \kappa$ constituents; each constituent occupies only a portion of V, denoted by V^π. Each point of the total volume V, is considered to be the centroid of a representative elementary volume (REV) or average volume element, dV. Averaging areas, denoted by dA, which are associated with each point on A are also defined. Average quantities are obtained by integrating a microscopic quantity over an averaging volume or area.

The position of the centre of a REV in a global coordinate system is described by the position vector $\mathbf{x}$, while $\mathbf{r}$ indicates the position of a microscopic volume element, dV (i.e. the vector position of a particle with respect to global system), see figure 3.1. The volume of constituent π within a REV, called average volume element dV^π, is obtained by defining a phase distribution function:

$$\gamma^\pi(\mathbf{r},t) = \begin{cases} 1 \text{ for } \mathbf{r} \in \ dV^\pi \\ 0 \text{ for } \mathbf{r} \in \ dV^\alpha \quad \pi \neq \alpha \end{cases} \tag{3.1}$$

$$dV^\pi(\mathbf{x},t) = \int_{dV} \gamma^\pi(\mathbf{r},t) dV \tag{3.2}$$

where $\mathbf{r} = \mathbf{x} + \boldsymbol{\xi}$ and the integration refers to the microscopic local coordinate system with its origin in $\mathbf{x}$ (figure 3.1); $\boldsymbol{\xi}$ is the vector position of a particle with respect to the centre of dV. On the interfaces $\gamma^\pi(\mathbf{r},t)$ is not defined although its right- and left-sided limits exist there.

Similarly we write for the part dA^π of area dA of the REV, occupied by constituent π:

$$dA^{\pi}(\mathbf{x},t) = \int_{dA} \gamma^{\pi}(\mathbf{r},t)dA \tag{3.3}$$

where dA is the microscopic area element.

Knowledge of dV^{π} enables the introduction of the concept of volume fraction, η^{π}, which is of paramount importance in multiphase systems:

$$\eta^{\pi}(\mathbf{x},t) = \frac{dV^{\pi}}{dV} = \frac{1}{dV}\int_{dV} \gamma^{\pi}(\mathbf{r},t)dV \tag{3.4}$$

with

$$\sum_{\pi=1}^{\kappa}\eta^{\pi} = 1 \quad \text{and} \quad 0 \leq \eta^{\pi} \leq 1 \tag{3.5}$$

In fact, substitute continua fill the entire domain simultaneously, instead of the real fluids and the solid, which each fill only part of it. These substitute continua have a reduced density which is obtained through the volume fractions.

The averaging process is used to obtain a field of macroscopic quantities for each phase. In the macroscopic field, an average volume represents and characterizes a physical point. Similarly the averaging area represents and characterizes a physical point on the surface; it is the infinitesimal element of area in the macroscopic field. This element of area is referred to as the representative elementary area (REA). Because these two elementary quantities characterize and represent the infinitesimal element of volume and area respectively, in the macroscopic field it is appropriate to denote them using the symbol dV and dA. Averaged quantities are obtained by integrating (averaging) a microscopic quantity over the volume dV or the area dA of a REV.

We indicate with dV^{π} and dA^{π} respectively the part of volume and the part of area of the constituent π within a REV. Although dV and dA are simply connected regions, dV^{π} and dA^{π} may be a union of isolated multiply connected regions. We can also define $dA^{\pi a}$ as the interface between π phase and α phase that is wholly inside the average volume dV. Similarly to dV^{π} and dA^{π}, $dA^{\pi a}$ are the union of isolated multiply connected regions, and are assumed to be continuous functions of space and time. Note that although the size of dV^{π}, dA^{π}, and $dA^{\pi a}$ depend on the size of averaging volume or area, the ratio of each of these quantities to dV and dA is a macroscopic variable and exhibits the same type of behaviour as depicted in figure 3.2.

The size of a REV is an important choice. Average quantities have to be independent

of the size of the average volume and continuous in space and time. Thus a REV has to fulfil the following requirements: dV has to be small enough to be considered as infinitesimal, i.e. the partial derivatives appearing in the governing equations must make sense; dV must be large enough, with respect to the heterogeneities of the material, to give average quantities without fluctuations depending on the size of the REV (figure 3.2).

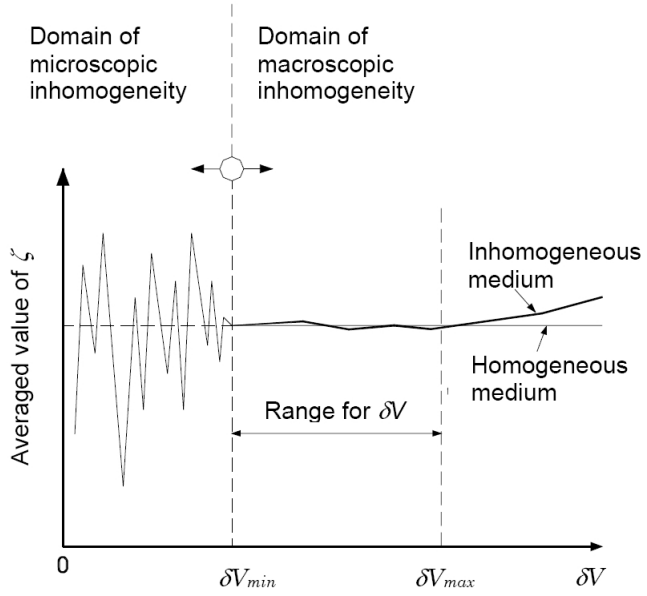

Figure 3.2: Averaged value ζ versus size of the average volume dV [2]

To obtain meaningful average values, the characteristic length l of the average volume must satisfy the inequality $d \ll l \ll L$, where l is dependent on the specific material which constitutes the medium.

Some typical values of the size of the REV can be found in Lemaitre and Chaboche [12]:

Metals	0.5 mm
Plastics	1 mm
Wood	10 mm

Usually there are no boundary conditions associated with a REV, except in the case of the megascopic level or in the case of a medium with periodic structure.

3.3 Microscopic balance equations

The microscopic situation of any π phase is described by the classical balance equations of continuum mechanics. At the interfaces with other constituents, the material properties and thermodynamic quantities may present step discontinuities. The existence of such singular surfaces is conceivable for solid-solid, fluid-solid and immiscible fluid-fluid systems.

For a generic conserved variable, ψ, the conservation equation within the π phase may be written as

$$\frac{\partial(\rho\psi)}{\partial t} + \mathrm{div}(\rho\psi\dot{\mathbf{r}}) - \mathrm{div}\mathbf{i} - \rho b = \rho G \tag{3.6}$$

where $\dot{\mathbf{r}}$ is the local value of the velocity field of the π phase in a fixed point in space, $\mathbf{i}$ is the flux vector associated with ψ, b the external supply of ψ and G is the net production of ψ.

The particular balance laws will be obtained by substituting the proper variables for ψ, $\mathbf{i}$, and b depending on the type of phenomenon being considered. The general balance law (3.6) is not valid at a surface of discontinuity and in particular at the interfaces.

At the interface between two constituents π and α, the jump condition holds

$$[\rho\psi(\mathbf{w} - \dot{\mathbf{r}}) + \mathbf{i}]\big|_{\pi} \cdot \mathbf{n}^{\pi\alpha} + [\rho\psi(\mathbf{w} - \dot{\mathbf{r}}) + \mathbf{i}]\big|_{\alpha} \cdot \mathbf{n}^{\alpha\pi} = 0 \tag{3.7}$$

where $\mathbf{w}$ is the velocity of the interface, $\mathbf{n}^{\alpha\pi}$ the unit normal vector pointing out of the π phase and into the α phase, with

$$\mathbf{n}^{\pi\alpha} = -\mathbf{n}^{\alpha\pi} \tag{3.8}$$

and $|_{\pi}$ indicates that the preceding term [...] must be evaluated with respect to the π phase.

No thermomechanical properties are attributed to these interfaces. This assumption does not exclude the possibility of exchange of mass, momentum or energy between the constituents. Moreover the local thermodynamic equilibrium hypothesis is assumed to hold because the time scale of the modelled phenomena is substantially larger than the relaxation time required to reach equilibrium locally.

The general form of conservation equations for mass, momentum, energy and entropy is given by equation (3.6). The variables introduced in table 3.1 may be substi-

tuted into equations (3.6) and (3.7) to obtain individual microscopic balance equation for each microscopic quantity.

Quantity	ψ	$\mathbf{i}$	b	G
Mass	1	0	0	0
Momentum	$\dot{\mathbf{r}}$	$\mathbf{t}_m$	$\mathbf{g}$	0
Energy	$\mathrm{E} + 0.5\dot{\mathbf{r}} \cdot \dot{\mathbf{r}}$	$\mathbf{t_m}\dot{\mathbf{r}} - \mathbf{q}$	$\mathbf{g} \cdot \dot{\mathbf{r}} + h$	0
Entropy	λ	$\mathbf{\Phi}$	s	φ

Table 3.1: Thermodynamic properties for the microscopic mass balance equations [4, 5]

In table 3.1, E is the specific intrinsic energy, λ the specific entropy, $\mathbf{t}_m$ the microscopic stress tensor, $\mathbf{q}$ a heat flux vector, $\mathbf{\Phi}$ the entropy flux, $\mathbf{g}$ the external momentum supply related to gravitational effects, h the intrinsic heat source, s an intrinsic entropy source and φ denotes an increase of entropy. The constituents are assumed to be microscopically non polar, hence the angular momentum balance equation has been omitted here; this equation shows that the stress tensor is symmetric.

3.4 Macroscopic balance equations

In this section are given the macroscopic balance equations for mass, linear momentum, angular momentum and energy as well as the entropy inequality for a deforming porous material. The starting points are the microscopic balance equations (3.6) where, for each constituent, the generic thermodynamic variable, ψ , is replaced by appropriate microscopic quantities, suitable for a microscopic non polar material. The macroscopic equations have been obtained by systematically applying the averaging procedures to the microscopic balance equations (3.6) as outlined in [4, 5, 6, 13].

For a proper description of the non-isothermal unsaturated porous medium we need to take into account not only heat conduction and vapour diffusion, but also heat convection, liquid water flow due to pressure gradients or capillary effects and latent heat transfer due to water phase change (evaporation and condensation) inside the pores. Furthermore the solid is deformable, resulting in coupling of the fluid, the solid and the thermal fields. All fluid phases are in contact with the solid phase. The constituents are assumed to be immiscible except for dry air and vapour, and chemically reacting; in the following the mixture of dry air and vapour (moist air) will be simply called gas. Below the critical temperature of water, T_{cr}, the liquid phase consists of bound water, which is present in the whole range of moisture content, and capillary water, which

appears when the degree of water saturation exceeds the solid saturation point, S_{ssp}. Above the temperature T_{cr} the liquid phase consists of bound water only. Dissolution of air in water is here neglected. Because of the local thermodynamic equilibrium hypothesis, the temperatures of each constituent at a point in the multiphase medium are taken to be equal. This does not mean that the temperature is uniform throughout the medium but only that at each point one temperature is sufficient to characterize the state. Momentum exchanges due to mechanical interaction are independent of the temperature gradient.

One reminds that stress is defined as tension positive for the solid phase, while pore pressure is defined as compressive positive for the fluids.

3.4.1 Mass balance equations

In the averaging procedure, volume density parameters η^π (volume fractions) appear which are expressed in terms of commonly used variables in multiphase flow.

For solid phase, $\eta^s = 1 - n$ where $n = (dv^w + dv^g)/dv$ is the porosity and dv^π is the volume of constituent π within a REV.

For water $\eta^w = nS_w$ where $S_w = dv^w/(dv^w + dv^g)$ is the degree of water saturation.

For gas $\eta^g = nS_g$ where $S_g = dv^g/(dv^w + dv^g)$ is the degree of gas saturation.

It follows immediately that

$$S_g + S_w = 1 \tag{3.9}$$

In this work we will consider concrete as multiphase porous material: as indicated in [14] concrete is chemically reactive, i.e. it is subjected to chemical reactions such as hydration and dehydration processes, which take place below 105°C and above 120°C respectively.

The temperature role is to accelerate the aging process, with an accelerated hydration reaction, in the first case, while when temperatures overcome 105 °C the hydration stops and the inverse process can starts, involving the hydration products, in particular the cement gel (CSH) and the calcium hydroxide.

If we consider two different states of the material, $s1$ and $s2$, which correspond to two different states in the chemical reaction of dehydration, the dehydration process can be described as in the following:

$$\Delta\rho_{s1} + \Delta Q_{dehydr} \rightarrow \Delta\rho_{s2} + \Delta\rho_w \tag{3.10}$$

where: ΔQ_{dehydr} is the energy absorbed in the unit volume of concrete during dehydration process; ρ_{s1} is the apparent density of the fully hydrated part of solid skeleton; ρ_{s21} is the apparent density of the fully dehydrated part of solid skeleton; $\Delta\rho_w$ is the water released during dehydration of the mass of the solid phase, $m = \rho_{s1}$.

It is clear that, as hydration reaction changes the density of solid skeleton in the time, the dehydration process changes the solid skeleton density too, when temperatures exceed the above mentioned threshold. At the beginning the change is slow, i.e. the dehydration reaction is weak, but in the range 200°C-500°C there is a sharp increasing of water mass content released from the solid matrix.

To take into account such kind of processes it is necessary to introduce the concept of solid skeleton dehydration degree as follow:

$$\Gamma_{dehhydr}(\theta) = \left[\rho_{s1}(\theta_0) - \rho_{s1}(\theta)\right] / \rho_{s1}(\theta_0) \tag{3.11}$$

where θ is the temperature in Kelvin degrees.

Macroscopically we have:

- volumetric mass source of solid phase:

$$\dot{m}_{dehydr} = -\rho_{s1}\gamma_{dehydr}\dot{\Gamma}_{dehydr} \tag{3.12}$$

- volumetric heat source:

$$h_{dehydr} = \dot{m}_{dehydr} \cdot \Delta H_{dehydr} \tag{3.13}$$

where: $\triangle\rho_w/\triangle\rho_{s1} = \gamma_{dehydr}$ and $\triangle Q_{dehydr} = \triangle\rho_w \cdot \triangle H_{dehydr}$; $\triangle H_{dehydr}$ is the enthalpy of dehydration related to unit mass of water released during dehydration, and

$$\dot{\Gamma}_{dehydr} = \dot{\Gamma}_{dehydr}(T) \tag{3.14}$$

is the rate of dehydration and it is a constitutive property of the material (see 3.5.11).

Solid phase

The macroscopic mass balance equation for the solid phase reads:

$$\frac{D^s(1-n)\rho^s}{Dt} + \rho^s(1-n)div\,\bar{\mathbf{v}}^s = (1-n)\rho^s e^s(\rho) \tag{3.15}$$

where ρ^s is the intrinsic phase averaged solid density and $\bar{\mathbf{v}}^s$ is the mass averaged solid velocity. The same simplified notation will be used for the other constituents, once π

is accordingly specified. It is reminded that the intrinsic phase averaged density of a phase is linked to its phase averaged density ρ^π by $\rho_\pi = \eta^\pi \rho^\pi$. For the solid phase of concrete subjected to high temperatures the exchange term $(1-n)\rho^s e^s(\rho)$, i.e. the intrinsic average microscopic exchange of density with the other phases, is not equal to zero because of dehydration process:

$$(1-n)\rho^s e^s(\rho) = \dot{m}_{dehydr} \tag{3.16}$$

where $\dot{m}_{dehydr}$ is the mass source of liquid water (and the corresponding skeleton mass sink) related to the cement dehydration process.

Liquid phase: water

The macroscopic mass balance equation for water has the following form:

$$\frac{D^w n S_w \rho^w}{Dt} + n S_w \rho^w div\, \bar{\mathbf{v}}^w = n S_w \rho^w e^w(\rho) \tag{3.17}$$

where $nS_w\rho^w e^w(\rho)$ is not equal to zero, because water may change into vapour or vice versa and because of the dehydration process. Therefore we have that

$$n S_w \rho^w e^w(\rho) = -\dot{m}_{vap} - \dot{m}_{dehydr} \tag{3.18}$$

is the quantity of water per unit time and volume, lost through evaporation and released through dehydration.

Gaseous phase: dry air and vapour

The gaseous phase here is a multi-component material, composed of two different species: dry air and vapour; these species are miscible. Because the two species are miscible, they have the same volume fraction nS_g.

For vapour ($\pi = gw$) the mass balance equation is

$$\frac{D^g}{Dt}\left(n S_g \rho^{gw}\right) + div\left(n S_g \rho^{gw} \mathbf{u}^{gw}\right) + n S_g \rho^{gw} div\, \bar{\mathbf{v}}^g = \dot{m}_{vap} \tag{3.19}$$

where $\mathbf{u}^\pi$,($\pi = ga,\ gw$), defined as $\mathbf{u}^\pi = \bar{\mathbf{v}}^{\pi g} = \bar{\mathbf{v}}^\pi - \bar{\mathbf{v}}^g$, is the macroscopic diffusive-dispersive velocity.

We introduce now the diffusive-dispersive mass flux of component gw as follows [15]

$$\mathbf{J}_g^{gw} = n S_g \rho^{gw} \mathbf{u}^{gw} \tag{3.20}$$

which allows us to write (3.19) as

$$\frac{D^g}{Dt}\left(nS_g\rho^{gw}\right) + div\,\mathbf{J}_g^{gw} + nS_g\rho^{gw} div\,\bar{\mathbf{v}}^g = \dot{m}_{vap} \tag{3.21}$$

The mass balance equation for dry air ($\pi = ga$) can be written in a similar way as

$$\frac{D^{ga}}{Dt}\left(nS_g\rho^{ga}\right) + nS_g\rho^{ga} div\,\bar{\mathbf{v}}^{ga} = 0 \tag{3.22}$$

The mass balance equation for the whole gaseous phase (mixture of vapour and dry air) is obtained by summing the macroscopic balance equations of the two species and using appropriate definitions for bulk properties of the gaseous phase [7]:

$$\frac{D^g}{Dt}\left(nS_g\rho^{g}\right) + nS_g\rho^{g} div\,\bar{\mathbf{v}}^{g} = \dot{m}_{vap} \tag{3.23}$$

where the density of gas ρ^g is the sum of the densities of dry air ρ^{ga} and vapour ρ^{gw}.

3.4.2 Linear momentum balance equation

The linear momentum balance equation for the π phase has the following, general form

$$div\mathbf{t}^\pi + \rho_\pi\left(\bar{\mathbf{g}}^\pi - \bar{\mathbf{a}}^\pi\right) + \rho_\pi\left[\mathbf{e}^\pi\left(\rho\dot{\mathbf{r}}\right) + \hat{\mathbf{t}}^\pi\right] = 0 \tag{3.24}$$

where $\mathbf{t}^\pi$ is the macroscopic stress tensor in the π .0phase, $\bar{\mathbf{g}}^\pi$ is the external momentum supply, $\rho_\pi\bar{\mathbf{a}}^\pi$ is the volume density of the inertia force, $\rho_\pi\hat{\mathbf{t}}^\pi$ is the volumetric exchange term of linear momentum with other phases due to mechanical interaction and $\rho_\pi\mathbf{e}^\pi\left(\rho\dot{\mathbf{r}}\right)$ is that due to phase changes or chemical reactions.

In the following we make a further assumption that $\rho_\pi\mathbf{e}^\pi\left(\rho\dot{\mathbf{r}}\right) \neq 0$ only for the fluid phases. Then the linear momentum balance equation for the solid becomes

$$div\,\mathbf{t}^s + \rho_s\left(\bar{\mathbf{g}}^s - \bar{\mathbf{a}}^s\right) + \rho_s\hat{\mathbf{t}}^s = 0 \tag{3.25}$$

and for the fluid phase it has the form of (3.24).

The average linear momentum balance equations are subjected to the constraint:

$$\sum_\pi \rho_\pi\left[\mathbf{e}^\pi\left(\rho\dot{\mathbf{r}}\right) + \hat{\mathbf{t}}^\pi\right] = 0 \tag{3.26}$$

3.4.3 Angular momentum balance equation

As indicated in section 3.3, all phases of the semi-saturated porous medium are considered microscopically non-polar. The volume averaged angular momentum balance equation shows [2, 13] that, for non-polar media, partial stress tensor is symmetric also at the macroscopical level

$$\mathbf{t}^{\pi} = (\mathbf{t}^{\pi})^{T} \tag{3.27}$$

3.4.4 Balance of energy equation

The macroscopic energy balance equation for the generic π phase can be written as follows:

$$\rho_{\pi}\frac{D^{\pi}\bar{E}^{\pi}}{Dt} = \mathbf{t}^{\pi} : \mathbf{d}^{\pi} + \rho_{\pi}h^{\pi} - div\,\tilde{\mathbf{q}}^{\pi} + \rho_{\pi}R^{\pi} \tag{3.28}$$

where

$$\rho_{\pi}R^{\pi} = \rho_{\pi}\left[e^{\pi}\left(\rho\hat{E}\right) - e^{\pi}(\rho)\bar{E}^{\pi} + Q^{\pi}\right]$$

represents the exchange of energy between π phase and other phases of the medium due to phase change and mechanical interaction; $\tilde{\mathbf{q}}^{\pi}$ is a macroscopic heat flux vector, h^{π} results from the heat sources and $\mathbf{d}^{\pi}$ is the spatial rate of the deformation tensor. E^{π} accounts for the specific internal energy of the volume element. Equation (3.28) coincides with the energy balance equation in the mixture theory as shown in [1].

The energy balance equations are subject to

$$\sum_{\pi}\rho_{\pi}\left[e^{\pi}\left(\rho\hat{E}\right) + \mathbf{e}^{\pi}\left(\rho\tilde{\dot{\mathbf{r}}}\right)\cdot\bar{\mathbf{v}}^{\pi} + \frac{1}{2}e^{\pi}(\rho)\bar{\mathbf{v}}^{\pi}\cdot\bar{\mathbf{v}}^{\pi} + \hat{\mathbf{t}}^{\pi}\cdot\bar{\mathbf{v}}^{\pi} + Q^{\pi}\right] = 0 \tag{3.29}$$

and physically means that the total balance of energy exchange between all the phases is zero. Phase change and the corresponding supply terms will be considered in the following, only for the fluid phases.

3.4.5 Entropy inequality

Exploitation of entropy inequality is a tool for developing constitutive equations in a systematic manner, leading to a consistent thermodynamic description of the material behaviour at macroscale. The use of entropy inequality further assures that the second

law of thermodynamics is not violated. The procedure was proposed by Coleman and Noll [16]. It has been exploited by Sampaio and Williams [17], and recently by Gray and Hassanizadeh [4] for the development of constitutive equations for unsaturated flow in dry or partially saturated soil, including interfacial phenomena.

The microscopic balance has the following form (see table 3.1):

$$\frac{\partial}{\partial t}(\rho\lambda) + div\,(\rho\lambda\dot{\mathbf{r}}) - div\,\mathbf{\Phi} - \rho s = \rho\varphi \tag{3.30}$$

This equation may be transformed in the usual manner, also making use of the mass balance equation to obtain

$$\rho\frac{D\lambda}{Dt} - div\,\mathbf{\Phi} - \rho s = \varphi \tag{3.31}$$

By identifying the entropy flux, $\mathbf{\Phi}$, and the entropy source, s, respectively with the energy flux vector $\mathbf{q}$ and the energy source h, both divided by the absolute temperature, θ [1], (3.31) may be written as

$$\rho\frac{D\lambda}{Dt} + div\,\frac{1}{\theta}\mathbf{q} - \frac{1}{\theta}\rho h = \rho\varphi \tag{3.32}$$

According to the second law of thermodynamics, the entropy production is zero for reversible processes, while for irreversible processes

$$\rho\varphi \geq 0 \tag{3.33}$$

Equations (3.32) and (3.33) yield the entropy inequality for single component media

$$\rho\frac{D\lambda}{Dt} + div\,\frac{1}{\theta}\mathbf{q} - \frac{1}{\theta}\rho h \geq 0 \tag{3.34}$$

The entropy inequality for the mixture, which is the quantity of interest here, reads

$$\sum_{\pi}\left[\rho^{\pi}\frac{D^{\pi}\bar{\lambda}^{\pi}}{Dt} + \rho_{\pi}e^{\pi}(\rho)\,\bar{\lambda}^{\pi} + div\left(\frac{1}{\theta^{\pi}}\mathbf{q}^{\pi}\right) - \frac{1}{\theta^{\pi}}\rho_{\pi}h^{\pi}\right] \geq 0 \tag{3.35}$$

Again, this corresponds to the form used in the mixture theory as shown in [1]. Before further transformations of the macroscopic balance equations are made, we introduce the constitutive equations for the constituents.

3.5 Constitutive equations

To complete the description of the mechanical behaviour, we now need to specify the constitutive equations. The balance equations developed in the previous sections allow for the introduction of quite elaborate constitutive theories, especially if the balance equations presented in the previous sections for the bulk material are extended to the interfaces, as done by Gray and Hassanizadeh in [18, 19, 20] for the aspects concerning multiphase flow. For the solid phase, second-grade material theories are also possible, where the gradients of relevant thermodynamic properties, such as densities, are considered as independent variables [1]. However, since this thesis is application oriented, i.e. we aim at the quantitative solution of real engineering problems, we make a different choice.

We select constitutive models which are based on quantities currently measurable in laboratory or field experiments, and which have been extensively validated both with reference to known exact solutions and to experiments. Many of these constitutive models correspond to linearizations of more complex arguments. We deal first with the properties of the fluid phases, and only briefly mention the solid phase here, because chapter 5 will be partially devoted to that subject.

3.5.1 Stress tensor in the fluid phase

By applying entropy inequality (3.35) for the bulk material [6, 18], it can been shown that the stress tensor in the fluid phases, appearing in equation (3.24) is

$$\mathbf{t}^{\pi} = -\eta^{\pi} p^{\pi} \mathbf{I} \tag{3.36}$$

where $\mathbf{I}$ is the identity tensor; this operator is equivalent to the Kronecker symbol δ. Quantity p^{π} is the macroscopic pressure of the π phase. The volume fraction η^{π} appears in equation (3.36) because $\mathbf{t}^{\pi}$ is the force exerted on the fluid phase per unit area of multiphase medium. It should be noted that the stress vector in the fluid phase does not have any dissipating part. The macroscopic effects of deviatoric stress components will be accounted for in linear momentum balance equations through momentum exchange terms.

3.5.2 Gaseous mixture of dry air and water vapour

The moist air in the pore system is usually assumed to be a perfect mixture of two ideal gases, i.e. dry air and water vapour. Hence is used the ideal gas law, relating the partial pressure $p_{g\pi}$ of species π, the mass concentration $\rho^{g\pi}$ of species π in the gas phase and the absolute temperature T.

The equations of state of a perfect gas, applied to dry air (ga), vapour (gw) and moist air (g) are

$$\begin{aligned} p^{ga} &= \rho^{ga} T R / M_a \\ p^{gw} &= \rho^{gw} T R / M_w \\ \rho^{g} &= \rho^{ga} + \rho^{gw} \end{aligned} \tag{3.37}$$

$$\begin{aligned} p^{g} &= p^{ga} + p^{gw} \\ M_g &= \left(\frac{\rho^{gw}}{\rho^{g}} \frac{1}{M_w} + \frac{\rho^{ga}}{\rho^{g}} \frac{1}{M_a} \right)^{-1} \end{aligned} \tag{3.38}$$

where M_π is the molar mass of constituent π and R is the universal gas constant. The second equation of (3.38) expresses Dalton's law [21]. For the averaging process it is reminded that dry air, vapour and moist air occupy the same volume fraction nS_g.

3.5.3 Sorption equilibrium

If an oven-dry porous medium is exposed to moist air, the weight of such solid increases because the moisture is adsorbed on the inner surfaces of the pores starting with the finest ones. In the cases of interest here, the water is usually present as a condensed liquid that, because of the surface tension, is separated from its vapour by a concave meniscus (capillary water). There is then a relationship between the relative humidity, the water content (saturation) and the capillary pressure in the pores. The capillary pressure is defined as the pressure difference between the gas phase and the liquid phase, by the capillary pressure equation (see chapter 5):

$$p^c = p^g - p^w \tag{3.39}$$

where p^w is the pressure of the liquid-phase (water). In [19], it is shown that (3.39) is not just a definition, but a derived relationship between two independent quantities p^c

and $p^g - p^w$, at equilibrium.

For the relationship between the relative humidity (RH) and the capillary pressure in the pores, Kelvin-Laplace law is assumed to be valid:

$$RH = \frac{p^{gw}}{p^{gws}} = \exp\left(\frac{p^c M_w}{\rho^w RT}\right) \tag{3.40}$$

The water vapour saturation pressure p^{gws}, which is a function of the temperature only, can be obtained from the Clausius-Clapeyron equation indicated below, or from empirical formulas such as the one proposed by Hyland and Wexler [22].

Assuming zero contact angle between the liquid phase and the solid phase, as is usually accepted for pore water, the capillary pressure can be obtained through the Laplace equation from the pore radius r:

$$p^c = \frac{2\sigma}{r} \tag{3.41}$$

where σ is the surface tension.

These considerations are applicable if the water is present in the pores, as a condensed liquid (capillary region). When, instead, the water is present as one or more molecular layers adsorbed on the surface of a solid because of the Van der Waals and/or other interactions, the capillary pressure no longer has an obvious meaning, even if it can be retained, referring to the broader concept of water potential or moisture stress. In such a case, a direct relationship between the water content and the relative humidity is assumed to hold such as the BET equation [22].

3.5.4 Clausius-Clapeyron equation

The Clausius-Clapeyron equation links the water vapour saturation pressure with temperature as indicated above:

$$p^{gws}(T) = p^{gws0} \exp\left[-\frac{M_w \triangle H_{gw}}{R}\left(\frac{1}{T} - \frac{1}{T_0}\right)\right] \tag{3.42}$$

where T_0 is a reference temperature, p^{gws} is the water vapour saturation pressure at T, p^{gws0} is the water vapour saturation pressure at T_0 and $\triangle H_{gw}$ is the specific enthalpy of evaporation.

3.5.5 Pore size distribution

As it turns out from equations (3.40) and (3.41), the problem is to know the pore size distribution of the considered porous medium, to relate the size of the largest pore filled (on which the capillary pressure depends) with the actual water content. This relationship is obtained through experimental tests, usually centrifuge tests, sorption isotherm measurements or mercury porosimetry. The determination of pore size distribution from sorption isotherms, results of centrifuge tests and mercury porosimetry should then be done following the percolation theory approach [23].

The Rayleigh distribution or the log-normal distributions are often a good estimation of the pore size and often such distribution can be bimodal or multimodal.

For soils and concrete, we need the Kelvin-Laplace equation (3.40), the Clausius-Clapeyron equation (3.42) and the capillary pressure relationship

$$S_\pi = S_\pi \left(p^c, T\right) \tag{3.43}$$

which is directly obtained in laboratory.

3.5.6 Equation of state for water

The equation of state for water has been given by Fernandez [24] as

$$\rho^w = \rho^{w0} \exp\left[-\beta_w T + \alpha_w \left(p^w - p^{w0}\right)\right] \tag{3.44}$$

where the superscript zero indicates an initial steady state at standard conditions; β_w is the thermal expansion coefficient and α_w the compressibility coefficient. By retaining the first order terms of the series expansion of (3.44) we obtain

$$\rho^w = \rho^{w0} \exp\left[1 - \beta_w T + \alpha_w \left(p^w - p^{w0}\right)\right] \tag{3.45}$$

and

$$\frac{1}{\rho^{w0}} \frac{D^w \rho^w}{Dt} = \frac{1}{K_w} \frac{D^w p^w}{Dt} - \beta_w \frac{D^w}{Dt} \tag{3.46}$$

where $K_w = 1/\alpha_w$ is the bulk modulus of water.

Moreover, in [19] an equation of state with dependence on more independent variables is suggested but no practical expression is given.

The equation of state for water can also be obtained from the mass conservation in differential form:

$$\frac{D^w\left(\rho^w V^w\right)}{Dt} = 0 \tag{3.47}$$

In fact, by carrying out the differentiation of a product and keeping in mind that $\rho^w = \rho^w\left(p^w, T\right)$, we ca write

$$\frac{1}{\rho^w}\frac{D^w\rho^w}{Dt} = -\frac{1}{V^w}\frac{D^w V^w}{Dt} = \frac{1}{\rho^w}\left(\frac{\partial\rho^w}{\partial p^w}\frac{D^w p^w}{Dt} + \frac{\partial\rho^w}{\partial T}\frac{D^w T}{Dt}\right) \tag{3.48}$$

Since

$$\begin{aligned} \frac{1}{\rho^w}\frac{\partial\rho^w}{\partial p^w} &= \frac{1}{K_w} = \alpha_w \\ \frac{1}{\rho^w}\frac{\partial\rho^w}{\partial T} &= -\beta_w \end{aligned} \tag{3.49}$$

it fallows that

$$\frac{1}{\rho^w}\frac{D^w\rho^w}{Dt} = \frac{1}{K_w}\frac{D^w p^w}{Dt} - \beta_w\frac{D^w T}{Dt} \tag{3.50}$$

It is reminded that $K_w = 1/C_w$, where C_w is the compressibility coefficient.

3.5.7 Darcy's law

Darcy's law, generalized to allow for relative permeability

$$\eta^\pi\bar{\mathbf{v}}^{\pi s} = \frac{k^{r\pi}\mathbf{k}}{\mu^\pi}\left(-grad\, p^\pi + \rho^\pi\mathbf{g}\right) \tag{3.51}$$

is assumed valid for the transport of both water and gas in slow phenomena; $\mathbf{k}$ is the permeability of the medium (also called intrinsic permeability), μ is the dynamic viscosity and $k^{r\pi}$ is the relative permeability, a dimensionless parameter varying from zero to one.

At macroscopic level we assume the resulting permeability as a product of the intrinsic permeability times the relative permeability $k^{r\pi}$,

$$\mathbf{k}^\pi = k^{r\pi}\mathbf{k} \tag{3.52}$$

as shown in (3.51). The intrinsic permeability varies with the void ratio and with the degree of saturation. For many situations the change of void ratio may be of secondary importance and $k^{r\pi}$ may be satisfactorily defined as a function of the degree of satu-

ration. For each particular porous medium, the relations $k^{r\pi}(S_w)$ are either predicted by models based on some more or less realistic capillary assumption or experimentally determined in laboratory as well as field conditions. For typical curves of relative permeabilities to water and air for soils the reader is referred to Corey [25].

The relative permeability goes to zero before the saturation reaches the value zero. The water saturation at which the relative permeability goes to zero is termed the residual water saturation or displacement residual water saturation.

3.5.8 Fick's law: diffusion of free water vapour

Diffusive-dispersive mass flux is governed by Fick's law

$$\mathbf{J}_\alpha^\pi = -\rho^\alpha \mathbf{D}_\alpha^\pi \, grad\left(\frac{\rho^\pi}{\rho^\alpha}\right) \tag{3.53}$$

where $\mathbf{D}_\alpha^\pi$ is the effective dispersion tensor, π is the diffusing phase and α is the phase in which diffusion takes place (α = w, g). $\mathbf{D}_\alpha^\pi$ is a function of the tortuosity factor, which accounts for the tortuous nature of the pathway in soil; because of mechanical dispersion, $\mathbf{D}_\alpha^\pi$ is also correlated with seepage velocity.

For dry air and water vapour (binary system) we have in particular that

$$\mathbf{J}_g^{ga} = -\rho^g \frac{M_a M_w}{M_g^2} \mathbf{D}_g \, grad\left(\frac{p^{ga}}{p^g}\right) = \rho^g \frac{M_a M_w}{M_g^2} \mathbf{D}_g \, grad\left(\frac{p^{gw}}{p^g}\right) = -\mathbf{J}_g^{gw} \tag{3.54}$$

It is worthwhile to emphasize that gas diffusion can take place even in the absence of a gas pressure gradient, i.e. when its mass weighted velocity $\bar{\mathbf{v}}^g$, is zero.

3.5.9 Fick's law: diffusion of physically adsorbed water

The layers of physically bound water (or adsorbed water) are interested by a phenomenon of mass transport which is similar to a diffusion. For sake of simplicity in the model the movement of this adsorbed water has been modelled by using a relationship similar to Fick's law:

$$\mathbf{J}_d^{bw} = -\rho^w \mathbf{D}_d^{bw} \frac{\partial S_b}{\partial p_c} \, grad\, p^c \tag{3.55}$$

where $\mathbf{D}_d^{bw}$ is the effective tensor of surface diffusion of water on the skeleton and S_b is the degree of saturation of physically adsorbed water.

The diffusion tensor multiplied for the derivative of degree of saturation of bound water on capillary pressure is a kind of equivalent diffusion tensor. Further the material is considered isotropic, hence the adsorbed water diffusion tensor can be seen as

$$\mathbf{D}_d^{bw} = D_d^{bw}\mathbf{I}$$

where D_d^{bw} is the bound water diffusive coefficient. The physically bound water is of importance especially below the so called solid saturation point S_{ssp} where it is the unique liquid phase present in the porous material, and close to the critical point of water where the saturation degree is really small, so the quantity of adsorbed water on the walls of pores is comparable to the remaining capillary free water.

3.5.10 Stress tensor in the solid phase and total stress

From the entropy inequality written in [20] for unsaturated flow, including interfacial phenomena, it can be shown that the total stress tensor of the solid phase is defined as:

$$\mathbf{t}^s = \boldsymbol{\tau}^s - \mathbf{I}p^s \tag{3.56}$$

where $\boldsymbol{\tau}^s$ is the Bishop effective stress tensor of the the skeleton and p^s is called the solid phase pressure and is actually the pressure exerted on the solid phase by the surrounding fluid

$$p^s = p^w S_w + p^g\left(1 - S_w\right) \tag{3.57}$$

The Bishop's stress $\boldsymbol{\sigma}'$ (also called effective stress tensor), is defined as the stress which controls stress–strain, volume change and strength behavior in a porous medium, independent of the magnitude of the pore pressure:

$$\boldsymbol{\sigma}' = (1-n)\,\boldsymbol{\tau}^s \tag{3.58}$$

The total stress tensor, considered as the sum of the single phase stress tensors multiplied by the appropriate volume fraction, is then given by

$$\begin{aligned} \boldsymbol{\sigma} &= \eta^s\mathbf{t}^s + \eta^w\mathbf{t}^w + \eta^g\mathbf{t}^g \\ &= \eta^s\boldsymbol{\tau}^s - p^s\mathbf{I} = (1-n)\,\boldsymbol{\tau}^s - p^s\mathbf{I} \end{aligned} \tag{3.59}$$

Note also, that at the micro-scale the fluids occupy separate parts of the pore space. At the macroscale, they are considered to be overlapping continua that occupy fractions of the same space. Equation (3.57) states that the pressure contributions of the fluids to the solid stress tensor are proportional to the volume fraction each fluid occupies. This implies that even if a fluid is not in contact with the solid, it will contribute to the solid stress.

Equation (3.59) can be put in the usual soil mechanics form, by means of (3.58), as

$$\boldsymbol{\sigma} = \boldsymbol{\sigma}' - \mathbf{I}\left[p^w S_w + p^g \left(1 - S_w\right)\right] \tag{3.60}$$

or

$$\boldsymbol{\sigma}' = \boldsymbol{\sigma} + \mathbf{I}\left[p^w S_w + p^g \left(1 - S_w\right)\right] \tag{3.61}$$

From (3.61) it follows that the relationship between effective stress and total stress, in partially saturated porous media, is no longer independent of the soil type because of the saturations(3.43).

The effective stress, (3.58) or (3.61) is responsible for all major deformations in the skeleton and is linked to the strain rate tensor $\mathbf{D}^s$ by means of a constitutive relationship

$$\frac{D\boldsymbol{\sigma}'}{Dt} = \mathbf{D}_T\left[\left(\mathbf{D}^s - \mathbf{D}_0^s\right)\right] \tag{3.62}$$

where

$$\mathbf{D}_T = \mathbf{D}_T\left(\mathbf{D}^s, \boldsymbol{\sigma}', T\right) \tag{3.63}$$

is a fourth order tensor and $\mathbf{D}_0^s$ represents the increment of all other strains not directly associated with stress changes. For small strain assumptions

$$\mathbf{D}^s = \boldsymbol{\varepsilon} dt \tag{3.64}$$

where $\boldsymbol{\varepsilon}$ is the linear strain tensor.

3.5.11 Solid density

When considering the solid phase as compressible, a relationship for the material time derivative of the solid density can be obtained from the mass conservation equation in

differential form

$$\frac{D^s\left(\rho^s V^s\right)}{Dt} = 0 \tag{3.65}$$

By assuming that the solid density is a function of p^s (3.57), of temperature and of the first invariant of the effective stress, we proceed as in section (3.5.6):

$$\begin{aligned} &\frac{1}{\rho^s}\frac{D^s\rho^s}{Dt} = -\frac{1}{V_s}\frac{D^s V_s}{Dt} = \\ &= \frac{1}{K_s}\frac{D^s p^s}{Dt} - \beta_s\frac{D^s T}{Dt} - \frac{1}{3\left(n-1\right)K_s}\frac{D^s\left(tr\,\boldsymbol{\sigma}'\right)}{Dt} - \frac{1}{\rho^s}\frac{\partial\rho^s}{\partial\Gamma_{dehydr}}\frac{D^s\Gamma_{dehydr}}{Dt} \end{aligned} \tag{3.66}$$

where K_s is the bulk modulus of the grain material, β_s is the thermal expansion coefficient for the solid and $tr\,\boldsymbol{\sigma}' = \mathbf{I}_{1\boldsymbol{\sigma}'}$ the first stress invariant. In (3.66) the last term at the right hand side takes into account the dehydration process. In fact, as mentioned in the previous sections, the solid skeleton density varies also because of this chemical reaction which take place between the liquid phase and the hydrated products.

Usually, the solid skeleton density is experimentally determined in the form:

$$\rho^s = \rho^s\left(T\right) \tag{3.67}$$

which is a constitutive law for the solid skeleton. The degree of dehydration Γ_{dehydr}, function of temperature, as defined with the equation (3.11), is another constitutive law of the solid skeleton, determined from experimental tests:

$$\Gamma_{dehydr} = \Gamma_{dehydr}\left(T\right) \tag{3.68}$$

Concrete can recover only a part of the dehydrated cement paste during a decrease of temperature, i.e. during a freezing process because of condensation, hence the level of dehydration substantially depends on the maximum temperature T_{max} reached during the heating phase, i.e. during the dehydration process. This means that (3.68) should be rewritten in the following manner:

$$\Gamma_{dehydr} = \Gamma_{dehydr}\left(T_{max}\right) \tag{3.69}$$

Corresponding to the degree of dehydration, the dehydration rate can be defined as:

$$\dot{\Gamma}_{dehydr} = \frac{\partial\Gamma_{dehydr}}{\partial T}\frac{\partial T}{\partial t} \tag{3.70}$$

and it depends on temperature history in the material.

Defining further Biot's constant [26] as

$$1-\alpha=\frac{K_T}{K_s} \tag{3.71}$$

where K_T is the bulk modulus of the skeleton, different from that of the grain material, we obtain

$$\begin{aligned}\frac{1}{\rho^s}\frac{D^s\rho^s}{Dt}=\frac{1}{1-n}\left[(\alpha-n)\,\frac{1}{K_s}\frac{D^sp^s}{Dt}-\beta_s\,(\alpha-n)\,\frac{D^sT}{Dt}-(1-\alpha)\,div\,\bar{\mathbf{v}}^s\right]\\ -\frac{1}{\rho_s}\frac{\partial\rho^s}{\partial\Gamma_{dehydr}}\frac{D^s\Gamma_{dehydr}}{Dt}\end{aligned} \tag{3.72}$$

For incompressible grain material $1/K_s=0$, $\alpha=1$. This does not imply that the solid skeleton is rigid, because of rearrangements of the voids. The necessary evolution equation for this is the mass balance equation for the solid phase (3.15).

3.5.12 Fourier's Law

A constitutive assumption for the heat flux is the generalized Fourier's Law

$$\tilde{\mathbf{q}}=-\boldsymbol{\chi}_{eff}\,grad\,T \tag{3.73}$$

where $\boldsymbol{\chi}_{eff}$ is the effective thermal conductivity tensor and $\tilde{\mathbf{q}}$ is the heat flux of the multiphase medium, sum of the partial heat fluxes $\tilde{\mathbf{q}}^\pi$. For isotropic media (3.73) becomes the well known empirical Fourier's Law

$$q=-\chi_{eff}\,grad\,T \tag{3.74}$$

where χ_{eff} is the effective thermal conductivity. The effective thermal conductivity can be predicted theoretically as well as determined experimentally.

For porous building materials, for instance, the following linear relationship may be used, which represents with sufficient accuracy the data by Bomberg and Shirtliffe [23]:

$$\chi_{eff}=\chi_{dry}\left(1+4\frac{nS^w\rho^w}{(1-n)\,\rho^s}\right) \tag{3.75}$$

3.6 General field equations

The macroscopic balance laws are now transformed, and the constitutive equations introduced, to obtain the general field equations, which will be used in the subsequent chapters. The averaging symbol, overbar, will be omitted in the remainder of this thesis, because all quantities belong to the macroscopic situations.

3.6.1 Mass balance equations

The macroscopic mass balance equation for the solid phase (3.15), divided by ρ^s is

$$\frac{(1-n)}{\rho^s}\frac{D^s\rho^s}{Dt} - \frac{D^s n}{Dt} + (1-n)div\,\mathbf{v}^s = \frac{\dot{m}_{dehydr}}{\rho^s} \tag{3.76}$$

The macroscopic mass balance equation for liquid water (capillary and physically adsorbed) is expressed by equation (3.17); by introducing the water relative velocity and the material derivative of water density, with respect to the moving solid, it can be written as follows:

$$\frac{D^s\rho_w}{Dt} + \mathbf{v}^{ws}\cdot grad\,\rho_w + \rho_w\,div\,(\mathbf{v}^s + \mathbf{v}^{ws}) = -\dot{m}_{dehydr} - \dot{m}_{vap} \tag{3.77}$$

where $\mathbf{v}^{\pi s}$ means the π phase relative velocity with respect to the skeleton. After some algebraic transformations we obtain

$$\begin{aligned}\frac{D^s n}{Dt} + \frac{n}{\rho^w}\frac{D^s\rho^w}{Dt} + \frac{n}{S_w}\frac{D^s S_w}{Dt} + \frac{1}{S_w\rho^w}div\,(nS_w\rho^w\mathbf{v}^{ws}) + n\,div\,\mathbf{v}^s \\ = -\frac{\dot{m}_{dehydr} + \dot{m}_{vap}}{S_w\rho^w}\end{aligned} \tag{3.78}$$

Summation with (3.76), to eliminate the time derivative of porosity from the latter equation, enables to obtain the mass conservation equation of liquid water and solid skeleton as follows:

$$\begin{aligned}\frac{(1-n)}{\rho^s}\frac{D^s\rho^s}{Dt} + div\,\mathbf{v}^s + \frac{n}{\rho^w}\frac{D^s\rho^w}{Dt} + \frac{n}{S_w}\frac{D^s S_w}{Dt} + \frac{1}{S_w\rho^w}div\,(nS_w\rho^w\mathbf{v}^{ws}) = \\ = -\frac{\dot{m}_{dehydr} + \dot{m}_{vap}}{S_w\rho^w} + \frac{\dot{m}_{dehydr}}{\rho^s}\end{aligned} \tag{3.79}$$

Introduction of constitutive relationships (3.50) and (3.72) for the material derivatives of the solid and water densities along with (3.57) gives

$$\frac{\alpha - n}{K_s}\frac{D^s}{Dt}\left(S_w p^w + S_g p^g\right) - \beta_s\left(\alpha - n\right)\frac{D^s T}{Dt} + \alpha\, div\,\mathbf{v}^s + n\left(\frac{1}{K_w}\frac{D^s p^w}{Dt} - \beta_w\frac{D^s T}{Dt}\right) + \frac{n}{S_w}\frac{D^s S_w}{Dt} - \frac{(1-n)}{\rho^s}\frac{\partial \rho^s}{\partial \Gamma_{dehydr}}\frac{D^s \Gamma_{dehydr}}{Dt} + \frac{1}{S_w \rho^w} div\left(n S_w \rho^w \mathbf{v}^{ws}\right) = -\frac{\dot{m}_{dehydr} + \dot{m}_{vap}}{S_w \rho^w} + \frac{\dot{m}_{dehydr}}{\rho^s} \tag{3.80}$$

Because of (3.11) we have

$$\frac{D^s S_g}{Dt} = -\frac{D^s S_w}{Dt} \tag{3.81}$$

Carrying out derivatives of p^s, collecting terms and reminding (3.81) yields then

$$\left(\frac{\alpha - n}{K_s} S_w^2 + \frac{n S_w}{K_w}\right)\frac{D^s p^w}{Dt} + \frac{\alpha - n}{K_s} S_w S_g \frac{D^s p^g}{Dt} + \alpha S_w\, div\,\mathbf{v}^s - \beta_{sw}\frac{D^s T}{Dt} + \left(\frac{\alpha - n}{K_s} p^w S_w - \frac{\alpha - n}{K_s} p^g S_w + n\right)\frac{D^s S_w}{Dt} - \frac{(1-n)\, S_w}{\rho^s}\frac{\partial \rho^s}{\partial \Gamma_{dehydr}}\frac{D^s \Gamma_{dehydr}}{Dt} + \frac{1}{\rho^w} div\left(n S_w \rho^w \mathbf{v}^{ws}\right) = -\frac{\dot{m}_{dehydr} + \dot{m}_{vap}}{\rho^w} + \frac{\dot{m}_{dehydr}}{\rho^s} S_w \tag{3.82}$$

where $\beta_{sw} = S_w\left[\left(\alpha - n\right)\beta_s + n\beta_w\right]$

For incompressible grains, i.e. $\alpha = 1$, $1/K_s = 0$, and incompressible water, i.e. $1/K_w = 0$, equation (3.82) may be simplified as follows

$$S_w\, div\,\mathbf{v}^s - \beta^*_{sw}\frac{D^s T}{Dt} + n\frac{D^s S_w}{Dt} - \frac{(1-n)\, S_w}{\rho^s}\frac{\partial \rho^s}{\partial \Gamma_{dehydr}}\frac{D^s \Gamma_{dehydr}}{Dt} + \frac{1}{\rho^w} div\left(n S_w \rho^w \mathbf{v}^{ws}\right) = -\frac{\dot{m}_{dehydr} + \dot{m}_{vap}}{\rho^w} + \frac{\dot{m}_{dehydr}}{\rho^s} S_w \tag{3.83}$$

with $\beta^*_{sw} = S_w\left[\left(1 - n\right)\beta_s + n\beta_w\right]$.

The mass balance equation for gas as a mixture of dry air and vapour is dealt with next. Using the same procedure described for the fluid phase, starting from (3.23), we obtain:

$$\frac{\alpha-n}{K_s}S_wS_g\frac{D^sp^w}{Dt}+\frac{\alpha-n}{K_s}S_g^2\frac{D^sp^g}{Dt}-\left(n+\frac{\alpha-n}{K_s}p^cS_g\right)\frac{D^sS_w}{Dt}-\beta_s\left(\alpha-n\right)S_g\frac{D^sT}{Dt}$$
$$+\alpha S_g\,div\,\mathbf{v}^s+\frac{nS_g}{\rho^g}\frac{D^s\rho^g}{Dt}-S_g\frac{(1-n)}{\rho^s}\frac{\partial\rho^s}{\partial\Gamma_{dehydr}}\frac{D^s\Gamma_{dehydr}}{Dt}$$
$$+\frac{1}{\rho^g}div\left(nS_g\rho^g\mathbf{v}^{gs}\right)=\frac{\dot{m}_{vap}}{\rho^g}+\frac{\dot{m}_{dehydr}}{\rho^s}S_g \tag{3.84}$$

For incompressible solid grains this equation is simplified as

$$-n\frac{D^sS_w}{Dt}-\beta_s\left(1-n\right)S_g\frac{D^sT}{Dt}+S_g\,div\,\mathbf{v}^s+\frac{nS_g}{\rho^g}\frac{D^s\rho^g}{Dt}+\frac{1}{\rho^g}div\left(nS_g\rho^g\mathbf{v}^{gs}\right)$$
$$-S_g\frac{(1-n)}{\rho^s}\frac{\partial\rho^s}{\partial\Gamma_{dehydr}}\frac{D^s\Gamma_{dehydr}}{Dt}=\frac{\dot{m}_{vap}}{\rho^g}+\frac{\dot{m}_{dehydr}}{\rho^s}S_g \tag{3.85}$$

For heat transfer analysis, in partially saturated porous media, it is more convenient to consider the mass balance equation for dry air separately from that of vapour and to sum the mass balance equations for both water species, liquid water and water vapour. In this way, the mass rate of water evaporation $\dot{m}_{vap}$ disappears from the mass balance equations, while $\dot{m}_{dehydr}$ is still present, and this means that an explicit constitutive law for the mass rate of dehydration is required, whereas, in this way, no constitutive model for the mass rate of water evaporation is needed. An evolution equation for $\dot{m}_{vap}$ is however necessary and this will be given by the energy balance equation in an implicit manner.

The mass balance equation for dry air (3.22) is transformed in the following equation

$$\frac{D^g}{Dt}\left(nS_g\rho^{ga}\right)+div\,\mathbf{J}_g^{ga}+nS_g\rho^{ga}\,div\,\mathbf{v}^g=0 \tag{3.86}$$

Equation (3.86) is now transformed as the mass balance equation for the fluid phase in this section. The resulting equation is divided by $\rho^{ga}S^g$ and summed with (3.76). After introduction of equations (3.57) and (3.72) we obtain

$$\frac{\alpha-n}{K_s}S_gS_w\frac{D^sp^w}{Dt}+\frac{\alpha-n}{K_s}S_g^2\frac{D^sp^g}{Dt}-\left(n+\frac{\alpha-n}{K_s}p^cS_g\right)\frac{D^sS_w}{Dt}-\beta_s\left(\alpha-n\right)S_g\frac{D^sT}{Dt}$$
$$+\alpha S_g\,div\,\mathbf{v}^s+\frac{nS_g}{\rho^{ga}}\frac{D^s\rho^{ga}}{Dt}+\frac{1}{\rho^{ga}}div\,\mathbf{J}_g^{ga}+\frac{1}{\rho^{ga}}div\left(nS_g\rho^{ga}\mathbf{v}^{gs}\right)$$
$$-S_g\frac{(1-n)}{\rho^s}\frac{\partial\rho^s}{\partial\Gamma_{dehydr}}\frac{D^s\Gamma_{dehydr}}{Dt}=\frac{\dot{m}_{dehydr}}{\rho^s}S_g \tag{3.87}$$

Again for incompressible solid grains this equation is simplified as

$$-n\frac{D^s S_w}{Dt} - \beta_s (1-n) S_g \frac{D^s T}{Dt} + S_g \, div \, \mathbf{v}^s + \frac{n S_g}{\rho^{ga}} \frac{D^s \rho^{ga}}{Dt} + \frac{1}{\rho^{ga}} div \, \mathbf{J}_g^{ga}$$
$$+\frac{1}{\rho^{ga}} div \, (n S_g \rho^{ga} \mathbf{v}^{gs}) - S_g \frac{(1-n)}{\rho^s} \frac{\partial \rho^s}{\partial \Gamma_{dehydr}} \frac{D^s \Gamma_{dehydr}}{Dt} = \frac{\dot{m}_{dehydr}}{\rho^s} S_g \qquad (3.88)$$

The way to derive the mass balance equation for vapour is identical to that of dry air and results, for the case of incompressible solid grains,

$$-n\frac{D^s S_w}{Dt} - \beta_s (1-n) S_g \frac{D^s T}{Dt} + S_g \, div \, \mathbf{v}^s + \frac{n S_g}{\rho^{gw}} \frac{D^s \rho^{gw}}{Dt} + \frac{1}{\rho^{gw}} div \, \mathbf{J}_g^{gw}$$
$$+\frac{1}{\rho^{gw}} div \, (n S_g \rho^{gw} \mathbf{v}^{gs}) - S_g \frac{(1-n)}{\rho^s} \frac{\partial \rho^s}{\partial \Gamma_{dehydr}} \frac{D^s \Gamma_{dehydr}}{Dt} = \frac{\dot{m}_{dehydr}}{\rho^s} S_g + \frac{\dot{m}_{vap}}{\rho^{gw}} \qquad (3.89)$$

This equation is now multiplied by ρ^{gw} and added to the mass balance equation of liquid water (3.83), in turn multiplied by ρ^w. This sum gives the mass balance equation for the water species, liquid and vapour, without mass rate of water evaporation; in the case of incompressible solid grains and incompressible water we have:

$$n (\rho^w - \rho^{gw}) \frac{D^s S_w}{Dt} + (\rho^w S_w + \rho^{gw} S_g) \, \alpha \, div \, \mathbf{v}^s - \beta^*_{swg} \frac{D^s T}{Dt} + S_g n \frac{D^s \rho^{gw}}{Dt} + div \, \mathbf{J}_g^{gw}$$
$$+div \, (n S_w \rho^w \mathbf{v}^{ws}) + div \, (n S_g \rho^{gw} \mathbf{v}^{gs}) - (\rho^w S_w + \rho^{gw} S_g) \frac{(1-n)}{\rho^s} \frac{\partial \rho^s}{\partial \Gamma_{dehydr}} \frac{D^s \Gamma_{dehydr}}{Dt}$$
$$= \frac{\dot{m}_{dehydr}}{\rho^s} (\rho^w S_w + \rho^{gw} S_g - \rho^s) \qquad (3.90)$$

where $\beta^*_{swg} = \beta_s (1-n) (\rho^{gw} S_g + \rho^w S_w) + n \beta_w \rho^w S_w$.

In these equations Darcy's law for the fluid velocities relative to the solid, Fick's law for diffusive flux and Dalton's law and Clapeyron laws for ideal gases have still to be introduced. In particular, as far as Darcy's law is concerned, it was introduced in section 3.5.7 and will be derived again in its generalized form in the next section from the linear momentum balance equations.

3.6.2 Linear momentum balance equation

Fluids

A more suitable form for the linear momentum balance equation for the fluid phases (3.24) is now obtained by introducing kinematic equations and constitutive relationships. The acceleration of the π phase is given by

$$\mathbf{a}^{\pi} = \mathbf{a}^{s} + \mathbf{a}^{\pi s} + \mathbf{v}^{\pi s} \cdot grad\, \mathbf{v}^{\pi} \tag{3.91}$$

where $\mathbf{a}^{\pi s}$ is the relative acceleration. Introduction in (3.24) of (3.91), (3.36) and of the intrinsic phase averaged density yields

$$\begin{aligned} &-\eta^{\pi}\rho^{\pi}\left[\mathbf{a}^{s} + \mathbf{a}^{\pi s} + \mathbf{v}^{\pi s} \cdot grad\, \mathbf{v}^{\pi}\right] - div\left(\eta^{\pi} p^{\pi} \mathbf{I}\right) \\ &+\eta^{\pi} p^{\pi} \mathbf{g} + \eta^{\pi} p^{\pi} e^{\pi}\left(\rho \dot{\mathbf{r}}\right) - \mathbf{R}^{\pi} \eta^{\pi} \mathbf{v}^{\pi s} = 0 \end{aligned} \tag{3.92}$$

After some transformations [2], we obtain the linear momentum balance equation for fluids:

$$\eta^{\pi} \mathbf{v}^{\pi s} = \frac{\mathbf{k} k^{r\pi}}{\mu^{\pi}}\left[-grad\, p^{\pi} + \rho^{\pi}\left(\mathbf{g} - \mathbf{a}^{s} - \mathbf{a}^{\pi s}\right)\right] \tag{3.93}$$

Finally, neglecting the soil acceleration and the relative acceleration terms, it yields Darcy's law in the form (3.51)

$$\eta^{\pi} \mathbf{v}^{\pi s} = \frac{\mathbf{k} k^{r\pi}}{\mu^{\pi}}\left(-grad\, p^{\pi} + \rho^{\pi} \mathbf{g}\right) \tag{3.94}$$

Due to the simplifications introduced, this law is valid as a first approximation for slow flow of a macroscopically inviscid fluid through a porous medium with incompressible grains.

Solid phase

Taking into account (3.56), (3.57) and (3.58) the linear momentum balance equation (3.25) for the solid phase becomes

$$\begin{aligned} &div\left[\boldsymbol{\tau}^{s} - \mathbf{I}\left[p^{w} S_{w} + p^{g}\left(1 - S_{w}\right)\right]\right] + \left(1 - n\right)\rho^{s} \mathbf{g} \\ &-\left(1 - n\right)\rho^{s} \mathbf{a}^{s} + \mathbf{R}^{w} \eta^{w} \mathbf{v}^{ws} + \mathbf{R}^{g} \eta^{g} \mathbf{v}^{gs} = 0 \end{aligned} \tag{3.95}$$

Multiphase medium

By summing the momentum balance equations (3.92), written for water and gas-phase respectively, with that of the solid phase (3.95), by taking into account the definition of total stress (3.61), assuming continuity of stress at the fluid-solid interfaces and by introducing the averaged density of the multiphase medium

$$\rho = (1-n)\,\rho^s + nS_w\rho^w + nS_g\rho^g \tag{3.96}$$

we obtain the linear momentum balance equation for the whole multiphase medium

$$\begin{aligned} -\rho\mathbf{a}^s - nS_w\rho^w\left[\mathbf{a}^{ws} + \mathbf{v}^{ws}\cdot grad\,\mathbf{v}^w\right] - nS_g\rho^g\left[\mathbf{a}^{gs} + \mathbf{v}^{gs}\cdot grad\,\mathbf{v}^g\right] \\ +div\,\boldsymbol{\sigma} + \rho\mathbf{g} = 0 \end{aligned} \tag{3.97}$$

3.6.3 Enthalpy balance equation

The macroscopic volume averaged enthalpy balance equation for the π phase, after neglecting some terms related to viscous dissipation and mechanical work, caused by density variations due to temperature changes and caused by volume fraction changes, has the following general form [2, 13]:

$$\rho_\pi C_p^\pi \frac{D^\pi T^\pi}{Dt} = \rho_\pi h^\pi - div\,\tilde{\mathbf{q}}^\pi + \rho_\pi R_H^\pi - \rho_\pi e^\pi(\rho)\,H^\pi \tag{3.98}$$

where $H^\pi = H^\pi(\bar{p}^\pi,\, T^\pi)$ is the specific enthalpy of the π phase, $C_p^\pi = (\partial H^\pi/\partial T^\pi)_{\bar{p}}$ is the specific heat at constant pressure and $\rho_\pi C_p^\pi$ is the heat capacity of the π phase. In concrete at high temperature all heat sources, except those related to phase changes and dehydration process, can be neglected.

We assume that the phases of partially saturated porous medium are locally in a state of thermodynamic equilibrium. It means that averaged temperatures of all phases are assumed equal at each point in the multiphase system, $T^\pi = T\,(\pi = s,\, w,\, g)$. These temperatures may however vary throughout the domain.

Summing up, the enthalpy balances for all the phases of the medium, taking into account the mass sources, specific for the particular constituents, and transforming all material time derivatives into those with respect to the solid skeleton, as well as having in mind that [2, 13]:

$$\sum_\pi \rho_\pi R_H^\pi = 0 \tag{3.99}$$

one obtains the following enthalpy balance equation for the whole medium:

$$\begin{aligned}(\rho C_p)_{eff}\frac{\partial T}{\partial t}+\left(\rho_w C_p^w \mathbf{v}^w+\rho_g C_p^g \mathbf{v}^g\right)\cdot grad\,T-div\,(\chi_{eff} grad\,T)\\ =-\dot{m}_{vap}\triangle H_{vap}+\dot{m}_{dehydr}\triangle H_{dehydr}\end{aligned} \tag{3.100}$$

where

$$\begin{aligned}&(\rho C_p)_{eff}=\rho_s C_p^s+\rho_w C_p^w+\rho_g C_p^g\\ &\chi_{eff}=\chi^s+\chi^w+\chi^g\\ &\triangle H_{vap}=H^{gw}-H^w\\ &\triangle H_{dehydr}=H^w-H^{ws}\end{aligned} \tag{3.101}$$

3.7 Initial and boundary conditions

The final mathematical model consists of the following balance equations: mass conservation of solid skeleton, mass conservation of dry air, mass conservation of the water species, enthalpy conservation of the whole medium and linear momentum of the multiphase system. They are completed by an appropriate set of constitutive and state equations, as well as some thermodynamic relationships.

The governing equations of the model, are expressed in terms of the chosen state variables: gas pressure p^g, capillary pressure p^c, temperature T and displacement vector of the solid matrix $\mathbf{u}$.

For the model closure the initial and boundary conditions are needed. The initial conditions specify the full fields of primary state variables at time instant $t=0$, in the whole analysed domain Ω and on its boundary Γ, ($\Gamma=\Gamma_\pi\cup\Gamma_\pi^q$, $\pi=g,\,c,\,T,\,u$)

$$p^g=p_0^g,\quad p^c=p_0^c,\quad T=T_0,\quad \mathbf{u}=\mathbf{u}_0\quad \text{on } (\Omega\cup\Gamma) \tag{3.102}$$

The boundary conditions (BCs) can be of Dirichlet's type on Γ_π

$$\begin{aligned}&p^g(t)=\hat{p}^g(t) &&\text{on}\,\Gamma_g\\ &p^c(t)=\hat{p}^c(t) &&\text{on}\,\Gamma_c\\ &T(t)=\hat{T}(t) &&\text{on}\,\Gamma_T\\ &\mathbf{u}(t)=\hat{\mathbf{u}}(t) &&\text{on}\,\Gamma_u\end{aligned} \tag{3.103}$$

or of Cauchy's type (the mixed BCs) on Γ_π^q:

$$\begin{aligned}
&(nS_g\rho^{ga}\mathbf{v}^{gs} + \mathbf{J}_d^{ga}) \cdot \mathbf{n} = q^{ga} && \text{on } \Gamma_g^q \\
&(nS_w\rho^w\mathbf{v}^{ws} + nS_g\rho^{gw}\mathbf{v}^{gs} + \mathbf{J}_d^{gw}) \cdot \mathbf{n} = q^{gw} + q^w + \beta_c\left(\rho^{gw} - \rho_\infty^{gw}\right) && \text{on } \Gamma_c^q \\
&(nS_w\rho^w\mathbf{v}^{ws}\triangle H_{vap} - \chi_{eff}\mathrm{grad}\, T) \cdot \mathbf{n} = q^T + \alpha_c\left(T - T_\infty\right) + e\sigma_0\left(T^4 - T_\infty^4\right) && \text{on } \Gamma_T^q \\
&\boldsymbol{\sigma}' \cdot \mathbf{n} = \bar{\mathbf{t}} && \text{on } \Gamma_u^q
\end{aligned} \tag{3.104}$$

where $\mathbf{n}$ is the unit normal vector, pointing toward the surrounding gas, q^{ga}, q^{gw}, q^w and q^T are, respectively, the imposed fluxes of dry air, vapour, liquid water and the imposed heat flux, and $\bar{\mathbf{t}}$ is the imposed traction, ρ_∞^{gw} and T_∞ are the mass concentration of water vapour and the temperature in the far field of undisturbed gas phase, e is emissivity of the interface, σ_0 the Stefan-Boltzmann constant, while α_c and β_c are convective heat and mass exchange coefficients. The convective boundary conditions usually occur at the interface between the porous media and the surrounding fluid. When concrete behaviour at high temperature is analysed, the radiative boundary conditions are usually of importance.

The boundary conditions, with only imposed fluxes given, are called Neumann's BCs. The purely convective boundary conditions for heat and moisture exchange are also called Robin's BCs.

3.8 Numerical solution

Discretization in space of the governing equations in their weak form is performed by means of the finite element method (FEM) [28, 29]. The unknown primary variables are expressed by their nodal values and the shape functions:

$$\begin{aligned}
p^g(t) &= \mathbf{N}_p\bar{\mathbf{p}}^g(t), \qquad & p^c(t) &= \mathbf{N}_p\bar{\mathbf{p}}^c(t) \\
T(t) &= \mathbf{N}_t\bar{\mathbf{T}}(t), \qquad & \mathbf{u}(t) &= \mathbf{N}_u\bar{\mathbf{u}}(t)
\end{aligned} \tag{3.105}$$

The variational or weak form of the model equations, applying also the other ones required to complete the model, is obtained in [14] by means of Galerkin's method (weighted residuals), and can be written in matrix form as:

$$\mathbf{C}_{ij}(\mathbf{x})\frac{\partial \mathbf{x}}{\partial t} + \mathbf{K}_{ij}(\mathbf{x})\mathbf{x} - \mathbf{f}_i(\mathbf{x}) = 0 \tag{3.106}$$

with

$$\mathbf{C}_{ij} = \begin{bmatrix} \mathbf{C}_{gg} & \mathbf{C}_{gc} & \mathbf{C}_{gt} & \mathbf{C}_{gu} \\ \mathbf{0} & \mathbf{C}_{cc} & \mathbf{C}_{ct} & \mathbf{C}_{cu} \\ \mathbf{0} & \mathbf{C}_{tc} & \mathbf{C}_{tt} & \mathbf{C}_{tu} \\ \mathbf{0} & \mathbf{0} & \mathbf{0} & \mathbf{0} \end{bmatrix}, \quad \mathbf{K}_{ij} = \begin{bmatrix} \mathbf{K}_{gg} & \mathbf{K}_{gc} & \mathbf{K}_{gt} & \mathbf{0} \\ \mathbf{K}_{cg} & \mathbf{K}_{cc} & \mathbf{K}_{ct} & \mathbf{0} \\ \mathbf{K}_{tg} & \mathbf{K}_{tc} & \mathbf{K}_{tt} & \mathbf{0} \\ \mathbf{K}_{ug} & \mathbf{K}_{uc} & \mathbf{K}_{ut} & \mathbf{K}_{uu} \end{bmatrix}, \quad \mathbf{f}_i = \begin{Bmatrix} \mathbf{f}_g \\ \mathbf{f}_c \\ \mathbf{f}_t \\ \mathbf{f}_u \end{Bmatrix} \tag{3.107}$$

where $\mathbf{x}^T = \left\{\bar{\mathbf{p}}^g, \bar{\mathbf{p}}^c, \bar{\mathbf{T}}, \bar{\mathbf{u}}\right\}$ and the non-linear matrix coefficients $\mathbf{C}_{ij}(\mathbf{x})$, $\mathbf{K}_{ij}(\mathbf{x})$ and $\mathbf{f}_i(\mathbf{x})$are defined in detail in [14].

The time discretization is accomplished through a fully implicit finite difference scheme (Euler backward difference):

$$\left(\frac{\partial \mathbf{x}}{\partial t}\right)_{n+\theta} = \frac{\mathbf{x}_{n+1} - \mathbf{x}_n}{\triangle t}, \quad \mathbf{x}_{n+\theta} = (1-\theta)\,\mathbf{x}_n + \theta \mathbf{x}_{n+1} \quad \text{with}\, \theta = 1 \tag{3.108}$$

where $\triangle t$ is the time step length, n is the time step number, $\mathbf{x}_n$ and $\mathbf{x}_{n+1}$ are the state vectors at times t_n and t_{n+1}. Equation (3.106) at time t_{n+1} becomes:

$$\Psi^i(\mathbf{x}_{n+1}) = \mathbf{C}_{ij}(\mathbf{x}_{n+1}) \frac{\mathbf{x}_{n+1} - \mathbf{x}_n}{\Delta t} + \mathbf{K}_{ij}(\mathbf{x}_{n+1})\mathbf{x}_{n+1} - \mathbf{f}_i(\mathbf{x}_{n+1}) = \mathbf{0} \tag{3.109}$$

where superscript $i\,(i = g,\, c,\, t,\, u)$ denotes the state variable.

The coupled system of equations (3.109) is unsymmetric and non-linear; it requires a linearization by means of a monolithic Newton–Raphson type iterative procedure [2]:

$$\Psi^i(\mathbf{x}^k_{n+1}) = -\left.\frac{\partial \Psi^i}{\partial \mathbf{x}}\right|_{\mathbf{x}^k_{n+1}} \Delta \mathbf{x}^k_{n+1} \tag{3.110}$$

$$\begin{aligned} &\frac{1}{\triangle t}\left[\frac{\partial}{\partial \mathbf{x}}\mathbf{C}\left(\mathbf{x}^k_{n+1}\right)\left(\mathbf{x}^k_{n+1} - \mathbf{x}_n\right) + \mathbf{C}\left(\mathbf{x}^k_{n+1}\right)\right] \triangle \mathbf{x}^k_{n+1} \\ &+ \left[\frac{\partial}{\partial \mathbf{x}}\mathbf{K}\left(\mathbf{x}^k_{n+1}\right)\mathbf{x}^k_{n+1} + \mathbf{K}\left(\mathbf{x}^k_{n+1}\right) - \frac{\partial}{\partial \mathbf{x}}\mathbf{f}\left(x^k_{n+1}\right)\right] \triangle \mathbf{x}^k_{n+1} \\ &= -\left[\mathbf{C}\left(\mathbf{x}^k_{n+1}\right)\frac{\mathbf{x}^k_{n+1} - \mathbf{x}_n}{\triangle t} + \mathbf{K}\left(\mathbf{x}^k_{n+1}\right)\mathbf{x}_{n+1} - \mathbf{f}\left(x^k_{n+1}\right)\right] \end{aligned} \tag{3.111}$$

where k is the iteration index, the Jacobian matrix is defined by

$$\left.\frac{\partial \Psi^i}{\partial \mathbf{x}}\right|_{\mathrm{x}_{n+1}^k} = \left[\begin{array}{cccc} \frac{\partial \Psi^g}{\partial \bar{\mathbf{p}}^g} & \frac{\partial \Psi^g}{\partial \bar{\mathbf{p}}^c} & \frac{\partial \Psi^g}{\partial \bar{\mathbf{T}}} & \frac{\partial \Psi^g}{\partial \bar{\mathbf{u}}} \\ \frac{\partial \Psi^c}{\partial \bar{\mathbf{p}}^g} & \frac{\partial \Psi^c}{\partial \bar{\mathbf{p}}^c} & \frac{\partial \Psi^c}{\partial \bar{\mathbf{T}}} & \frac{\partial \Psi^c}{\partial \bar{\mathbf{u}}} \\ \frac{\partial \Psi^t}{\partial \bar{\mathbf{p}}^g} & \frac{\partial \Psi^t}{\partial \bar{\mathbf{p}}^c} & \frac{\partial \Psi^t}{\partial \bar{\mathbf{T}}} & \frac{\partial \Psi^t}{\partial \bar{\mathbf{u}}} \\ \frac{\partial \Psi^u}{\partial \bar{\mathbf{p}}^g} & \frac{\partial \Psi^u}{\partial \bar{\mathbf{p}}^c} & \frac{\partial \Psi^u}{\partial \bar{\mathbf{T}}} & \frac{\partial \Psi^u}{\partial \bar{\mathbf{u}}} \end{array}\right]\Bigg|_{\mathrm{x}_{n+1}^k} \tag{3.112}$$

and the increment vector of the primary variables is:

$$\triangle \mathbf{x}_{n+1}^k = \left[(\triangle \bar{\mathbf{p}}^g)_{n+1}^k\,,\,(\triangle \bar{\mathbf{p}}^c)_{n+1}^k\,,\,\triangle \bar{\mathbf{T}}_{n+1}^k,\,\triangle \bar{\mathbf{u}}_{n+1}^k\right]^T \tag{3.113}$$

During the computation for each time step, the primary variable vector $\mathbf{x}_{n+1}$ is updated at the end of each iteration, i.e.:

$$\mathbf{x}_{n+1}^{k+1} = \mathbf{x}_{n+1}^k + \triangle \mathbf{x}_{n+1}^k \tag{3.114}$$

The convergence and error analysis of the method applied here can be found in reference [30].

Bibliography

[1] de Boer R., Ehlers W., Kowalski S., Plishka J., Porous media, a survey of different approaches, Forschungsbericht aus dem Fachbereich Bauwesen, 54, Universität-Gesamthochschule Essen, 1991.

[2] Lewis R.W., Schrefler B.A., The finite element method in the static and dynamic deformation and consolidation of porous media, 2nd ed., John Wiley & Sons, Chichester, 1998.

[3] Bedford A., Drumheller D.S., Theories of immiscible and structured mixtures, Int. J. Engng. Sci., 21(8): 863-960, 1983.

[4] Hassanizadeh S.M., Gray W.G., General conservation equations for multiphase systems: 1. Averaging procedure, Adv. Water Resources, 2: 131-144, 1979.

[5] Hassanizadeh S.M., Gray W.G., General conservation equations for multiphase systems: 2. Mass, momenta, energy and entropy equations, Adv. Water Resources, 2: 191-203, 1979.

[6] Hassanizadeh S.M., Gray W.G., General conservation equations for multiphase systems: 3. Constitutive theory for porous media flow, Adv. Water Resources, 3: 25-40, 1980.

[7] Hassanizadeh S.M., Derivation of basic equations of mass transport in porous media, Part. 1. Macroscopic balance laws, Adv. Water Resources, 9: 196-206, 1986.

[8] Hassanizadeh S.M., Derivation of basic equations of mass transport in porous media, Part. 2. Generalized Darcy's law and Fick's law, Adv. Water Resources, 9: 207-222, 1986.

[9] Bear J., Bachmat Y., Transport phenomena in porous media - basic equations, in Bear J. and Corapcioglu M.Y. (Eds.), Fundamentals of Transport Phenomena in Porous Media, Nato ASI Series, Nijhoff, Dordrecht, 5-61, 1984.

[10] Bear J., Corapcioglu Y., Mathematical model for regional land subsidence due to pumping. 2. Integrated aquifer subsidence equation for vertical and horizontal displacements, Water Resour Research, 17(4): 947-958, 1981.

[11] Simoni L., Schrefler B.A., F.E. solution of a vertically averaged model for regional land subsidence, Int. J. Num. Meth. Eng., 27(1): 215-230, 1989.

[12] Lemaitre J., Chaboche J.L., Mécanique des matériaux solides, Dunod, Paris, 1988.

[13] Schrefler B.A., Mechanics and thermodynamics of saturated-unsaturated porous materials and quantitative solutions, Applied Mechanics Reviews, 55(4): 351-388, 2002.

[14] Pesavento F., Non linear modelling of concrete as multiphase porous material in high temperature conditions, PhD Thesis, University of Padova, 2000.

[15] Eringen A.C., Suhubi E.S., Nonlinear Theory of simple microelastic solids, Int. J. Engng. Sci., 2: 189-203, 1964.

[16] Coleman B.D., Noll W., The thermodynamics of elastic materials with heat conduction and viscosity, Arch. Ration. Mech. Anal., 13: 168-178, 1963.

[17] Sampaio R., Williams W.O., Thermodynamics of diffusing mixtures, Journal de Méchanique, 18(1): 19-45, 1979.

[18] Gray W.G., Hassanizadeh S.M., Unsaturated flow theory including interfacial phenomena, Water Resources Res., 27(8): 1855-1863, 1991.

[19] Gray W.G., Hassanizadeh S.M., Paradoxes and realities in unsaturated flow theory, Water Resources Res., 27(8), 1847-1854, 1991.

[20] Hassanizadeh S.M., Gray W.G., Mechanics and thermodynamics of multiphase flow in porous media including interphase boundaries, Adv. Water Resources, 13(4): 169-186, 1990.

[21] Moran M.J., Shapiro H.N., Fundamentals of Engineering Thermodynamics, 2nd ed., John Wiley & Sons, New York, 1993.

[22] ASHRAE Handbook, Fundamentals Volume, ASHRAE, Atalanta, 1993.

[23] Bomberg M., Shirtliffe C.J., Influence of moisture gradients on heat transfer through porous building materials. Thermal transmission measurements of insulation, ASTM STP 660, R.P. Tye ed., ASTM, Philadelphia, 211-233, 1978.

[24] Fernandez R.T., Natural convection from cylinders buried in porous media, Ph. D. Thesis, University of Calif., Berkley, 1972.

[25] Corey A.T., Measurement of water and air permeability in unsaturated soil, Soil Sci. Soc. Am. Proc., 21(1): 7-10, 1957.

[26] Biot M.A., Willis P.G., The elastic coefficients of the theory of consolidation, J. Appl. Mech., 24: 594-601, 1957.

[27] Gawin D., Pesavento F., Schrefler B.A., Modelling of hygro-thermal behaviour of concrete at high temperature with thermo-chemical and mechanical material degradation, Comput. Methods Appl. Mech. Engrg., 192: 1731-1771, 2003.

[28] Zienkiewicz O.C., Taylor R.L., in: The Finite Element Method, vol. 1: The Basis, Butterworth-Heinemann, Oxford, 2000.

[29] Zienkiewicz O.C., Taylor R.L., in: The Finite Element Method, vol. 2: The Solid Mechanics, Butterworth-Heinemann, Oxford, 2000.

[30] Gawin D., Schrefler B.A., Thermo-hydro-mechanical analysis of partially saturated porous materials, Engng. Comput., 13(7): 113-143, 1996.

Chapter 4

Mechanical behaviour of concrete

4.1 Continuous damage for concrete

Continuous damage models are constitutive relations in which the mechanical effect of cracking and void growth is introduced with internal state variables which act on the elastic stiffness of the material [1]. The simplest model was proposed by Kachanov and Rabotnov in order to describe void nucleation and void growth in alloys subjected to creep [2].

In most cases, continuous damage is a phenomenological approach to the description of an elastic material containing voids or cracks. There are, however, several possibilities for introducing, in the framework of damage mechanics, the effect of micro-cracking on the elastic stiffness of a quasi-brittle material. The different constitutive relations are distinguished by the mathematical nature of the damage state variable. The difference lies in the description of the effect of micro-structural changes, i.e. micro cracking and void growth, on the mechanical behaviour as the material undergoes damage. The choice of a scalar variable implies that damage is due to the growth of spherical voids, or randomly distributed defects such as cracks. Hence, the elastic response of the material remains isotropic if the material is initially isotropic. A second order damage tensor implies that there exist principal directions along which cracking or void growth is oriented. If the material is initially elastic, damage induces anisotropy and the elastic response of the damaged material is no longer isotropic. To sum-up, there is a connection between the micro-structure of the material, its evolution as damage progresses, and the internal state variable, which describes at the phenomenological level the effect of damage.

It is not surprising that one of the result of such analysis is strain-softening, indepen-

dently from the mathematical nature of the damage internal variable. As the micro-crack density increases, the strength of the damaged material decreases and reaches zero eventually. This is also typical of fracture mechanics in linear elastic analysis. Accordingly, phenomenological damage models exhibit strain-softening which results into major difficulties:

- Well-posedness of boundary-initial value problems is lost at the onset of strain and damage localisation in statics-dynamics. Consequently, finite element calculations are severely mesh dependent and failure is predicted to occur without energy dissipation, which is physically incorrect [3].

- The length scale of the damage distribution decreases when localisation occurs; damage localises over a very narrow region of the continuum. The characteristic length governing the variations of damage falls down far below the scale at which the state variables, strain and damage, can be regarded as quantities which describe the response of a continuum. In other words, the wave length of the damage distribution is predicted to be much smaller than the size of the material heterogeneities.

Motivated by the fundamental mathematical difficulties related to strain-softening, a regularized form of these strain-softening constitutive relations was proposed. This model also called "non local damage model" tries to remedy the difficulties associated to strain localisation. It has been generalized in the form of a non local continuum with local strain. The variable which controls softening is defined as an averaged quantity over a domain, the size of which is related to the material heterogeneities. Thus, this type of constitutive relation appears to be one of the possibility for modelling the response of concrete in tension with a continuum model in spite of the inherent discontinuous nature of cracking at the microscopic and macroscopic level.

4.2 The effective stress concept

The influence of damage on physical quantities can be measured and used to define properly the damage variable: density change, which can be interpreted as a damage variable in ductile failure; resistivity change, which leads to very similar damage measures to that for mechanical parameters (see below); change in the fatigue limit, which can be interpreted in terms of the remaining life; change in the mechanical behaviour of the material, interpreted through the effective stress concept: "a damaged volume of

material under the applied stress σ shows the same strain response as the undamaged one submitted to the effective stress $\tilde{\sigma}$ " [4, 5].

If the damage D represents the loss of effective area taking into account decohesions and local stress concentrations, one can write:

$$\tilde{\sigma} = \sigma \frac{S}{\tilde{S}} = \frac{\sigma}{1-D} \tag{4.1}$$

where S denotes the section surface of one volume element whit outer normal $\mathbf{n}$, and $\tilde{S}$ denotes the effective resistant surface ($\tilde{S} < S$).

The measure of damage, with respect to the normal $\mathbf{n}$, is given by the following relationship:

$$D_n = \frac{S - \tilde{S}}{S} \tag{4.2}$$

If we consider that the defaults are uniformly distributed in each direction (isotropic damage), damage does not depend on $\mathbf{n}$ and $D_n = D$. D is a scalar such as $0 < D < 1$, with $D = 0$ (undamaged material) and $D = 1$ (completely damaged material).

Damage measures through the effective stress concept have been performed in several situations. Let us mention the case of ductile rupture and of brittle creep damage [4].

Ductile rupture measures the change of the elastic modulus. From elasticity equations for both damaged and undamaged material

$$\sigma = \tilde{E}\varepsilon_e \qquad \tilde{\sigma} = E\varepsilon_e \tag{4.3}$$

one obtains:

$$\tilde{\sigma} = \frac{E}{\tilde{E}}\sigma = \frac{\sigma}{1-D} \;\rightarrow\; D = 1 - \frac{\tilde{E}}{E} \tag{4.4}$$

Brittle creep damage uses the power law to describe secondary creep, which can be considered as an undamaged state (for the superalloy, for example):

$$\dot{\varepsilon}_s = \left(\frac{\sigma}{\lambda}\right)^N \tag{4.5}$$

Several tests give the exponent N. Damage follows easily from the measurement of strain rate during tertiary creep and the effective stress concept (4.1):

$$D = 1 - \left(\frac{\dot{\varepsilon}}{\dot{\varepsilon}_s}\right)^{1/N} \tag{4.6}$$

4.3 Isotropic damage model for concrete

In the literature, the damage variable was first defined by Kachanov as the ratio of the resisting (net) area of material to the initial area of a specimen in which voids are growing under sustained loads [1]. More generally, the influence of damage on the response of the material is a degradation of its elastic stiffness. The stress-strain relation reads:

$$\sigma_{ij} = E_{ijkl}^{damaged} \varepsilon_{kl} \tag{4.7}$$

where σ_{ij} is the stress component, ε_{kl} is the strain component, and damaged E_{ijkl} is the stiffness coefficient of the damaged material. It is clear from this "simple" definition that, in a phenomenological approach, the damage variable can be chosen as a scalar, several scalars, a second order tensor, a fourth order tensor or even a eight order tensor. More importantly, the differences of description resulting from different choices are not obvious *a priori*. Ladevèze proposed a rational method for the derivation of the internal damage variable. In this chapter, however, we will focus attention on the simple, isotropic, scalar damage model because it is the most widely damage model employed and also because it has been proved to be an efficient model for the description of the tensile failure of concrete and reinforced concrete structural components.

The stress strain relation of an isotropic damaged elastic material, as obtained by Ladevèze, contains two damage variables D and δ:

$$\varepsilon_{ij} = \frac{3}{2E_0\left(1-D\right)}\left(\sigma_{ij} - \frac{\sigma_{kk}}{3}\delta_{ij}\right) + \frac{\left(1-2\nu_0\right)}{2E_0\left(1-\delta\right)}\left[\sigma_{kk}\delta_{ij} - \sigma_{ij}\right] \tag{4.8}$$

where E_0, ν_0 are the Young's modulus and Poisson's ratio of the undamaged isotropic material respectively, and δ_{ij} is the Kronecker symbol. The damage variables D and δ are equal to 0 initially (for the undamaged material). At complete failure, the elastic stiffness of the material vanishes and the two variables are equal to 1. The subsequent assumption $D = \delta$ yields the stress-strain relationship proposed by Mazars [2, 6, 7] which we will use:

$$\varepsilon_{ij} = \frac{1+\nu_0}{E_0\left(1-D\right)}\sigma_{ij} - \frac{\nu_0}{E_0\left(1-D\right)}\left[\sigma_{kk}\delta_{ij}\right] \tag{4.9}$$

According to this equation, the Poisson's ratio is not affected by damage. During a uniaxial test, the ratio of the longitudinal strain to the transverse strain remains constant. Out of the two elastic constants which describe the undamaged material,

only one is modified by the evolution of damage, the Young's modulus. The elastic (i.e. free) energy per unit mass of material is:

$$\rho\Psi = \frac{1}{2}\left(1 - D\right)\varepsilon_{ij}E^0_{ijkl}\varepsilon_{kl} \tag{4.10}$$

where E^0_{ijkl} is the stiffness tensor of the undamaged material. This energy is assumed to be the state potential, which means that the thermodynamic forces associated to the two variables describing the material, the strain tensor and the damage variable, derive from this potential:

$$\begin{aligned} \sigma_{ij} &= \rho\frac{\partial\Psi}{\partial\varepsilon_{ij}} \\ Y &= -\rho\frac{\partial\Psi}{\partial D} = \frac{1}{2}\varepsilon_{ij}E^0_{ijkl}\varepsilon_{kl} \end{aligned} \tag{4.11}$$

Note that the first of equations (4.11) is exactly the same as equation (4.9). Y is called the damage energy release rate. The meaning of Y is clear from the calculation of the energy dissipation rate. The dissipation rate is the difference between the total (internal) variation of mechanical energy for any arbitrary rate of strain and the elastic (recoverable) energy rate:

$$\dot{\phi} = \sigma_{ij}\dot{\varepsilon}_{ij} - \rho\dot{\Psi} \tag{4.12}$$

Substitution of equations (4.9)-(4.11) yields the dissipation rate $\dot{\phi}$ as a function of the damage variable:

$$\dot{\phi} = Y\dot{D} \tag{4.13}$$

Therefore, Y is the energy released per unit rate of damage. In this constitutive relation (with a single damage variable), the second principle of thermodynamics constrains the time derivative of damage to be zero or positive. Damage cannot decrease because the rate of dissipation cannot decrease according to the Clausius-Duhem inequality.

The evolution of damage requires the definition of a loading function and an evolution law which can be similar to the evolution equation in associated plasticity. The constitutive relation is sometimes given in an integrated format. For example, damage is computed explicitly as a function of the maximum equivalent strain ever encountered in the material during the previous loading history in the model proposed by Mazars [6, 7]. The equivalent strain is a scalar measure of the tensile strains for a general, tridimensional, state of deformation.

4.4 Non local damage models

Fracture mechanics and crack interaction considerations have shown that defining damage as a weighted average seems more appropriate, especially with regard to the description of localization of cracking in an elastic material containing a distribution of micro cracks. A non local variable enables the description of micro structural changes that a local variable cannot accommodate. Such a phenomenological model has been investigated by Bazant and by Pijaudier-Cabot [6], along with a constitutive relation where the variable which controls damage is averaged, instead of averaging damage itself. As far as computations are concerned, the two models yield similar results.

Scalar non local damage models are presented. These models bear the essential characteristics pertaining to a non local integral model. Similar developments could be performed starting from a plasticity model, with a Gurson model or with an anisotropic damage model.

In the literature, there are two non local scalar damage models which have been proposed. The differences between these two constitutive relations are in the definition of the loading function and in the definition of the variable which controls damage [1]:

- In the first model, damage is controlled by the energy release rate and there is no distinction between the effect of damage in tension and in compression. The absolute value of the material strength is the same in uniaxial tension as in uniaxial compression. The format of the constitutive relation follows exactly that of associated plasticity. For this reason, this model has been mostly used for analytical studies, especially the analysis of strain localization.

- In the second model, damage is described by coupling the compression and tension effects to define a single damage variable [6]. The evolution of damage depends also on the state of stress. Hence, it is possible to describe the differences of behaviour in uniaxial tension and in uniaxial compression, including the variations of strength. This model represents very well the behaviour of concrete.

4.4.1 Energy-based model

In the energy-based model the constitutive relation is exactly the same as for the local damage model (4.9). The difference relies in the evolution of damage; the growth of damage is defined by a loading function f:

$$f(\bar{y}, D) = \int_0^{\bar{y}} F(z)\, dz - D \tag{4.14}$$

where F is a function of the strain tensor which is deduced from experimental data. Instead of depending on the local energy release rate $y(x)$, the loading function depends on $\bar{y}(x)$, the average energy release rate due to damage at point x of the solid:

$$\bar{y}(x) = \frac{1}{V_r(x)} \int_V \Psi(x-s)\, y(s)\, dv \quad \text{and} \quad V_r(x) = \int_V \Psi(x-s)\, dv \tag{4.15}$$

V is the volume of the solid, and $y(s)$ is the energy release rate due to damage at point s defined by:

$$y(s) = \frac{1}{2} \varepsilon(s) \,:\, E \,:\, \varepsilon(s) \tag{4.16}$$

$\Psi(x-s)$ is the weight function:

$$\Psi(x-s) = \Psi_0 \exp\left(-\frac{\|x-s\|^2}{2l_c^2}\right) \tag{4.17}$$

l_c is the internal length of the non local continuum and Ψ_0 is a normalizing factor. This factor is such that for an infinite body $V_r(x) = 1$. The internal length of the non local continuum depends on the size of the heterogeneities in the material. This length was taken in the calculations as $l_c \approx 3d_a$ in which d_a is the maximum size of the aggregate in concrete.

The evolution law is prescribed as in plasticity models:

$$\dot{D} = \delta \frac{\partial g}{\partial \bar{y}} \tag{4.18}$$

with the Kuhn-Tucker conditions $\delta \geq 0$, $f \leq 0$ and $\delta f = 0$. The function g is the evolution potential controlling the growth of damage and is here the damage multiplier. In this chapter, we have set $g = \bar{y}$. For concrete in tension, the evolution of damage is [1]:

$$F(\bar{y}) = \frac{b_1 + 2b_2(\bar{y} - Y_0)}{\left[1 - b_1(\bar{y} - Y_0) + b_2(\bar{y} - Y_0)^2\right]^2} \tag{4.19}$$

with the constants $b_1 = 605\, MPa^{-1}$, $b_2 = 5.24 \cdot 10^4\, MPa^{-1}$, $Y_0 = 60 \cdot 10^{-6}\, MPa$.

4.4.2 Strain based model

This model is the non local extension of the constitutive relation due to Mazars [6, 7]. The positive strains control the growth of damage which is mainly due to micro crack opening in mode I (tensile mode). The following norm called equivalent strain is defined:

$$\tilde{\varepsilon} = \sqrt{\sum_{i=1}^{3} \left(\langle \varepsilon_i \rangle_+ \right)^2}, \qquad \left(\langle x \rangle_+ = \frac{|x| + x}{2} \right) \tag{4.20}$$

where $\langle \varepsilon_i \rangle_+ = 0$ if $\varepsilon_i < 0$ and $\langle \varepsilon_i \rangle_+ = \varepsilon_i$ if $\varepsilon_i \geq 0$; and $\varepsilon_i \, (i \in [1,3])$ are the principal strains. The non local variable $\bar{\varepsilon}$, which represents the average of the equivalent strain over the representative volume surrounding each point in the material, is the variable that controls the growth of damage:

$$\bar{\varepsilon}(x) = \frac{1}{V_r(x)} \int_V \Psi(x - s)\, \tilde{\varepsilon}(s)\, dv \tag{4.21}$$

V is the volume of the structure, $V_r(x)$ is the representative volume at point x, and $\Psi(x - s)$ is the weight function, the same as for the previous model (4.17). The evolution of damage is specified according to following conditions:

$$\begin{aligned} & f(\bar{\varepsilon}) = \bar{\varepsilon} - \kappa \\ & and \\ & if \;\; f(\bar{\varepsilon}) = 0 \; and \; \dot{f}(\bar{\varepsilon}) = 0 \; then \; D = F(\bar{\varepsilon}) \\ & if \;\; f(\bar{\varepsilon}) < 0 \; or \; if \;\; f(\bar{\varepsilon}) = 0 \; and \; \dot{f}(\bar{\varepsilon}) < 0 \; then \; D = 0 \end{aligned} \tag{4.22}$$

Equation (4.22) defines the damage surface and the growth of damage. In (4.22) κ is the softening parameter and takes the largest value of $\bar{\varepsilon}$ ever reached during the previous loading history at a given time and at the considered point in the medium. Initially $\kappa = \kappa_0$, where κ_0 is the threshold of damage; κ_0 is the tensile strain at which damage is initiated, that is when the maximum tensile stress f_t is reached in a uniaxial test:

$$\kappa_0 = \frac{f_t}{E_0} \tag{4.23}$$

The evolution law, denoted as $F(\bar{\varepsilon})$ in equation (4.22), is a function of the strain, instead of the strain rate. It is integrated with respect to time so that damage can be directly computed at any state of deformation. Damage is decomposed into two parts: D_t for tension and D_c for compression. D is from the relation (4.24), which combines

these two types of damage:

$$D = \alpha_t D_t + \alpha_c D_c \tag{4.24}$$

The factors α_t and α_c are such that in uniaxial tension $\alpha_t = 1$, $\alpha_c = 0$ and $D = D_t$, and in uniaxial compression $\alpha_t = 0$, $\alpha_c = 1$ and $D = D_c$. The damage variables are functions of the average equivalent strain:

$$\begin{aligned} D_t &= 1 - \frac{\kappa_0 (1 - A_t)}{\bar{\varepsilon}} \frac{A_t}{\exp\left(-B_t \left(\bar{\varepsilon} - \kappa_0\right)\right)} \\ D_c &= 1 - \frac{\kappa_0 (1 - A_c)}{\bar{\varepsilon}} \frac{A_c}{\exp\left(-B_c \left(\bar{\varepsilon} - \kappa_0\right)\right)} \end{aligned} \tag{4.25}$$

and constants A_c, B_c, A_t, B_t are model parameters; these coefficients characterize the hardening/softening response of concrete. The factors α_t and α_c are expressed as non dimensional functions of the principal strains.

$$\begin{aligned} \langle \varepsilon_i \rangle &= \varepsilon_{ti} + \varepsilon_{ci} \\ \alpha_t = \sum_{i=1}^{3} \left(\frac{\varepsilon_{ti} \langle \varepsilon_i \rangle_+}{\tilde{\varepsilon}^2} \right)^{\beta} & \qquad \alpha_c = \sum_{i=1}^{3} \left(\frac{\varepsilon_{ci} \langle \varepsilon_i \rangle_+}{\tilde{\varepsilon}^2} \right)^{\beta} \end{aligned} \tag{4.26}$$

in which ε_{ti} is the positive strain due to positive stresses and ε_{ci} is the positive strain due to negative stresses (Poisson's effect). The purpose of exponent β is to reduce the effect of damage on the response of the material under shear compared to tension. Usually $\beta \approx 1.05$. Typical values for model parameters are:

$E_0 = 23400\, MPa$; $\nu_0 = 0.2$; $\beta = 1.05$; $A_t = 1.0$; $B_t = 15000$; $A_c = 1.2$; $B_c = 649$.

4.5 Thermo-chemical and mechanical damage in concrete

During heating, concrete at high temperature is exposed to complicated physical and chemical transformations, causing changes of its inner structure, what has also a sensible influence on the material properties. From a practical point of view, among the most important macroscopic consequences of these processes are concrete dehydration and crack development, resulting in a significant decrease of mechanical properties of

concrete. The material stress–strain behaviour in such conditions is highly non-linear and depends not only on the temperature and dehydration degree, but also on the history of mechanical loading during heating [8].

Degradation of concrete at high temperature, arising from a coupled hygro-thermal, chemical (dehydration) and mechanical interaction, can be modelled by means of the isotropic non-local damage theory of Mazars [2] and Mazars and Pijaudier-Cabot [6]. Thermo-chemical effect are also taken into account [9, 10].

As far as the mechanical constitutive relationships are concerned, in the case of concrete exposed to high temperature, we introduce damage into the elastic constitutive law in a classical manner. We consider that only the elastic properties of the material are affected by the total damage parameter D, defined by (4.34), accounting for both mechanical and thermo-chemical damage components, d and V, see equations (4.32)-(4.33), and that the dependence on damage is introduced through the stiffness matrix, $\mathbf{\Lambda} = \mathbf{\Lambda}(D)$:

$$\boldsymbol{\tau}^s = \mathbf{\Lambda}(D) : \boldsymbol{\varepsilon}^s \tag{4.27}$$

In equation (4.27) $\boldsymbol{\varepsilon}^s$ is the strain tensor for infinitesimal deformations and $\boldsymbol{\tau}^s$ is the effective stress tensor (see section 3.5.10). Application of the true stress concept

$$\boldsymbol{\tau}^s = \mathbf{\Lambda}(1-D)\,\tilde{\boldsymbol{\tau}}^s \tag{4.28}$$

where $\tilde{\boldsymbol{\tau}}^s$ is the "net effective stress" (in the sense of damage mechanics), leads to the following form of the constitutive relationship for the solid phase:

$$\tilde{\boldsymbol{\tau}}^s = \mathbf{\Lambda}_0 : \boldsymbol{\varepsilon}^s \tag{4.29}$$

where $\mathbf{\Lambda}_0$ is the initial stiffness.

Taking into account (4.28) and (4.29), the "net effective stress tensor" may be expressed as follows:

$$\tilde{\boldsymbol{\tau}}^s = \frac{\mathbf{t}^s + p^s\mathbf{I}}{(1-D)} \tag{4.30}$$

The damage theory defines a "modified effective stress" $\tilde{\sigma}$ and takes into account both the mechanical damage $d\,(0 \leq d \leq 1)$ and the thermo-chemical damage $V\,(0 \leq V \leq 1)$ resulting in a reduction of the material strength properties,

$$\tilde{\sigma} = \frac{\sigma'}{(1-d)\,(1-V)} \tag{4.31}$$

σ' is the effective stress tensor (called also Bishop's stress), responsible for deformations of the material skeleton.

The changes of concrete strength properties can be expressed not only as functions of the mechanical damage and temperature, but also of the thermally induced material deterioration [9]. The latter one may be of importance for proper assessment of the state of concrete structure exposed to high temperature, e.g. after fire or nuclear accident, because thermo-chemical deterioration is irreversible.

The parameter which describes the degree of the thermally induced material deterioration advancement is called thermo-chemical damage, V: it accounts for changes of material stiffness, both due to thermally induced microcracks, caused mainly by stresses at micro- and meso-level, (e.g. resulting from different thermal expansion coefficients of cement paste and aggregate, and from local increase of dehydration products volume), and due to decrease of concrete strength properties caused by the dehydration process, thus related to the Γ_{dehydr} value.

The thermo-chemical damage parameter V is defined in terms of the experimentally determined evolution of Young's modulus of mechanically undamaged material (i.e. heated to a given temperature, without any additional mechanical load), E_0, expressed as a function of temperature

$$V = 1 - \frac{E_0(T)}{E_0(T_a)} \tag{4.32}$$

where $T_a = 20°\mathrm{C}$ is room temperature.

Mechanical damage of concrete is considered following the scalar isotropic model described in section 4.4. In this model, the damaged material at given temperature, T, is supposed to behave elastically and to remain isotropic. The mechanical damage parameter d, being a measure of cracks volume density in the material, can be determined using the experimental data of the Young's modulus for a mechanically undamaged material at a given temperature T (i.e. only heated, without any mechanical load), $E_0\,(T)$, and for the mechanically damaged material at the same temperature $E\,(T)$

$$d = 1 - \frac{E(T)}{E_0(T)} \tag{4.33}$$

A total effect of the mechanical and thermo-chemical damages, to which the material is exposed at the same time, is multiplicative and not just the sum of the two components of damage. The total damage parameter, D, is defined by the following formula [9]:

$$D = 1 - \frac{E(T)}{E_0(T_a)} = 1 - \frac{E(T)}{E_0(T)} \frac{E_0(T)}{E_0(T_a)} = 1 - (1 - d) \cdot (1 - V) \tag{4.34}$$

Bibliography

[1] Pijaudier-Cabot G., Non local damage, in Mühlhaus H.B. (Ed), Continuum models for materials with microstructure, John Wiley, Chichester, 105-143, 1995.

[2] Mazars J., Application de la mécanique de l'endommagement au comportament non linéaire et à la rupture du béton de structure, Thèse de Doctorat d'état, L.M.T., Université de Paris VI, France, 1984.

[3] Bazant Z.P., Mechanics of distributed cracking, Applied Mech. Review, 39(5): 675-705, 1986.

[4] Chaboche J.L., Continuum damage mechanics: Part I - General Concepts, Journal of Appl. Mech., 55(3): 59-64, 1988.

[5] Lemaitre J., Chaboche J.L., Mécanique des matériaux solides, Dunod, Paris, 1988.

[6] Mazars J., Pijaudier-Cabot G., Continuum damage theory - application to concrete, Journal of Eng. Mechanics, ASCE, 115(2): 345-365, 1989.

[7] Mazars J., Description of the behaviour of composite concretes under complex loadings through continuum damage mechanics, reprinted from Proceedings of the 10th U.S. National Congress of Applied Mechanics, in Lamb J.P. (Eds), ASME, 1986.

[8] Khoury G.A., Majorana C.E., Pesavento F., Schrefler B.A., Modelling of heated concrete, Mag. Concr. Res., 54(2): 1-25, 2002.

[9] Gawin D., Pesavento F., Schrefler B.A., Modelling of hygro-thermal behaviour and damage of concrete at temperature with thermo-chemical and mechanical material degradation, Comput. Methods Appl. Mech. Engr., 192: 1731-1771, 2003.

[10] Gawin D., Alonso C., Andrade A., Majorana C.E., Pesavento F., Effect of damage on permeability and hygro-thermal behaviour of HPCs at elevated temperatures. Part 1. Experimental results, Computers and Concrete, 2(3): 189-202, 2005.

Chapter 5

Hygro-thermal state of concrete and material data

5.1 Introduction

Concrete is a chemically and micro-structurally complex composite material which consists mainly of aggregates bonded together by a softer matrix of hardened cement past surrounding the aggregates in a weak interfacial transition zone. Its structure is highly porous containing up to 40% of capillary pores, and up to 28% gel pores [1]. Those pores are filled partially with liquid, and partially with a gas phase. The liquid phase consists of bound water (or adsorbed water), which is present in the whole range of water contents of the medium, and capillary water (or free water), which appears when water content exceeds the so called solid saturation point S_{ssp} [2]; the gas phase consists of water vapour and dry air.

When moisture is present, a very complex analysis may be required to deal with the coupled heat and mass transfer in concrete pores, involving both liquid mass transfer and vapour mass transfer. In general, moisture transport may include air vapour mixture flow due to forced convection and infiltration through cracks and pores; vapour transport by diffusion; flow of liquid due to capillary action, surface diffusion or gravity; further complications are associated with phase changes due to condensation/evaporation, adsorption/desorption, hydration/dehydration [3].

For concrete, particularly at high temperature, one cannot predict heat transfer from just the traditional thermal properties: thermal conductivity and volumetric specific heat. Movement of air, water, and possibly carbon dioxide through the concrete is accompanied by significant energy transfer, particularly associated with the latent heat

of water and the heats of hydration and dehydration. Because of the high pore pressures that result when high-strength concrete is exposed to a fire, it is necessary to consider forced advection as well as diffusion.

Consider a concrete slab that initially may have small temperature gradients, e.g., due to indoor-to-outdoor temperature differences. At the beginning of a fire, the temperature of the exposed side of the concrete slab will rise rapidly. Free moisture, both liquid and vapour, will migrate toward the cold side of the concrete. Initially, this moisture movement occurs by diffusion and advection processes, where the driving force may be considered to be the gradient in vapour content (commonly expressed as partial vapour pressure, relative humidity, molar or mass fraction) and the pressures of the liquid and gas phase, respectively. As the temperature of the fire-exposed side increases, any free liquid water will evaporate and migrate toward the colder side where some of it will condense. The latent heat required to evaporate the liquid water will retard the rate of temperature rise at that location. When water vapour is transported into a colder region, some of it is absorbed into the concrete, with a heat of sorption that is approximately equal to the latent heat associated with condensation of free water vapour into liquid, so that significant heat is released. As moisture moves into the slab and the interior temperature rises towards 100°C, portions of the slab may experience additional hydration (conversion of free water into chemically bound water), with a connected release of heat. Hydration takes place at room temperature and the process increases with temperature in the presence of moisture up to 80°C or more, resulting in an increase in the mass of the solid skeleton. When the temperature of any portion of the concrete slab exceeds (roughly) the boiling point of water (at the local pressure) some dehydration (release of chemically bound water) will begin to take place, with a simultaneous absorption of heat. Dehydration from the CSH becomes significant above about 110°C, while the dehydration of the calcium hydroxide takes place at about 500°C producing CaO and H_2O. Both produce a reduction in the solid skeleton mass of the cement paste; the dehydration reactions continue up to temperatures in excess of 800°C.

The free water present in the pores of concrete flows toward the cold side. However, high-strength concrete is not very permeable for water vapour and is even less permeable (by, say, roughly two orders of magnitude) to liquid water. Thus the moisture cannot escape as rapidly as it is being released and the pore pressure in the concrete will rise substantially. Eventually, liquid water may fill the concrete pores at a location ahead of the temperature front, creating a condition known as moisture clog, where the liquid water blocks the transfer of water vapour toward the cold side of the slab. Under such

conditions, the existing pore pressure will result in forced advectional mass transfer of superheated steam and air to the heated side of the slab. This situation is particularly emphasized in high performance concrete with low porosity and low permeability and could contribute to explosive spalling.

During temperature exposure of the concrete, its transport properties for both heat and mass can change quite significantly due to differential thermal expansion opening up microcracks and changes in the solid structure associated with chemical decomposition of the cement paste (dehydration) and of any carbonate aggregates (conversion to oxides), both processes leading to less dense material and thus lower thermal conductivity and thermal diffusivity, and higher mass transport properties.

Also phenomena of absorption and desorption by concrete cannot be neglected. For moisture transfer at temperatures below the boiling point of water (at the local pressure), absorption effects are quite important and the mass storage of water, and the associated enthalpy storage, need to be considered. Absorption/desorption of water vapour is usually described in terms of sorption isotherms, curves which relate the equilibrium of the absorbed moisture content of a medium, at a specific temperature, to the moisture content (usually expressed as vapour pressure or humidity) to which it is exposed.

Therefore in this chapter we will analyse the processes which occur during concrete heating first of all from thermodynamic physical point of view, then studying the inner microstructure of the material and its changes with temperature.

5.2 Thermodynamic relationships

Due to the curvature of the interface between the capillary or bound water and the gas phase inside the pores of the medium (considered as a capillary porous body) the equilibrium water vapour pressure p^{gw} differs from the saturation pressure p^{gws} and can be obtained from the Kelvin equation [4, 5],

$$p^{gw} = p^{gws}(T) \cdot RH = p^{gws}(T) \exp\left(-\frac{p^c M_w}{\rho^w RT}\right) \tag{5.1}$$

where RH is relative humidity, and the water vapour saturation pressure p^{gws}, depending only upon temperature T, can be calculated from the Clausius-Clapeyron equation (chapter 3) or from empirical correlations, e.g. the formula proposed by Hyland and Wexler, (see equation (5.25)).

The radius of the curvature of the interface, R_c, being in the mechanical equilibrium state with water vapour, and corresponding to its pore radius r, is given by the Young-Laplace equation,

$$p^c = \frac{\sigma_{wa}}{R_c} \tag{5.2}$$

where for spherical meniscus (capillary water) its curvature is equal to

$$\frac{1}{R_c} = \frac{2 \cdot \cos\vartheta}{r - t_a} \tag{5.3}$$

while for cylindrical interface (bound water) it is

$$\frac{1}{R_c} = \frac{1}{r - t_a} \tag{5.4}$$

σ_{wa} is the surface tension of water-air interface, ϑ is the wetting angle, usually assumed to be zero, hence $\cos\vartheta = 1$, and t_a is the thickness of the adsorbed water layer in the pore.

It should be emphasized that equations (5.1) and (5.2) are valid both for the capillary and bound water. In the latter case pressure p^c should be understood as the matric potential ϕ, being a thermodynamic potential referring to the bound water, which cannot be identified to the pressure. Nevertheless, for the sake of brevity we have used the same notation for capillary water and bound water.

For a mixture of N components, the equilibrium between a liquid (l) and its vapour (v) can be expressed using the chemical potential μ as [4]

$$\mu_{l_i} = \mu_{v_i} \quad i = 1,\, 2,\, ...,\, N \tag{5.5}$$

or, since for a pure substance the chemical potential μ is equal to the molar Gibbs function g of each phase, the equilibrium can also be expressed as

$$g_l = g_v \tag{5.6}$$

The differential of the chemical potential for a single phase of a pure substance can be expressed as

$$dg = -\lambda dT + v dp + \mu dx - dL_\sigma \tag{5.7}$$

where λ is the molar entropy, v the specific molar volume, x the molar fraction and dL_σ the amount of work made by the surface tension to extend the phase separation

surface. The phase interface is assumed to have a constant area (i.e., $dL_\sigma = 0$) and for a pure substance the molar fraction x is always a constant, then the variation of the molar Gibbs function is

$$dg = -\lambda dT + vdp \tag{5.8}$$

Since $d\mu_l = d\mu_v$ (and thermodynamic equilibrium requires thermal equilibrium, i.e., equal temperature in the two phases $dT_l = dT_v = dT$), we can write

$$-\lambda_l dT + v_l dp_l = -\lambda_v dT + v_v dp_v \tag{5.9}$$

5.2.1 Derivation of the Clausius-Clapeyron equation

The Clapeyron–Clausius equation can be obtained from (5.5) and (5.9) remembering that at equilibrium on a flat interface the pressures are equal $p_v = p_l = p$ and the system has only one degree of freedom (Gibbs rule applied to a phase change), hence

$$\frac{dp}{dT} = \frac{\lambda_v - \lambda_l}{v_v - v_l} \tag{5.10}$$

Since the enthalpy of vaporization $\triangle h_{vap}$ is equal to $T(\lambda_v - \lambda_l)$, (5.10) can be rewritten as

$$\frac{dp}{dT} = \frac{\triangle h_{vap}}{T\left(v_v - v_l\right)} \tag{5.11}$$

This is the well-known Clapeyron–Clausius equation that can be applied to a phase change of a pure vapour at constant temperature and pressure. Some judgment should be exercised when integrating the Clapeyron's equation (5.11) over extended temperature intervals, because in such case the fact that the enthalpy of vaporization $\triangle h_{vap}$ is a function of the temperature, i.e., $\triangle h_{vap} = \triangle h_{vap}(T)$, and that the specific volumes v_v and v_l also change with temperature, should be taken in account. More accurate results can often be obtained using empirical correlations such as Hyland and Wexler [6].

When the specific volume v_l of the liquid water is negligible with respect to that of the vapour v_v , i.e., the system is far away from the critical point (at ambient temperatures, for example, they differ more than three orders of magnitude) and the specific volume of vapour v_v can be expressed through the ideal gas law, the Clapeyron's

equation (5.11) can be expressed as

$$\frac{dp}{dT} \approx \frac{\triangle h_{vap}}{T v_v} = \frac{p \triangle h_{vap}}{RT^2} \tag{5.12}$$

or

$$\frac{\mathrm{d} \ln p}{\mathrm{d}T} = \frac{\triangle h_{vap}}{RT^2} \tag{5.13}$$

5.2.2 Derivation of the Kelvin equation

The Kelvin's formula can be obtained remembering that the capillary pressure p_c is defined as

$$p_c = p_v - p_l \tag{5.14}$$

and hence in differential form

$$dp_c = dp_v - dp_l \tag{5.15}$$

Both the liquid and the vapour phase are governed by a Gibbs–Duhem equation

$$\begin{aligned} \lambda_l dT - v_l dp_l + d\mu_l = 0 \\ \lambda_v dT - v_v dp_v + d\mu_v = 0 \end{aligned} \tag{5.16}$$

At constant temperature $dT = 0$ and equation (5.16), together with (5.5), becomes

$$v_l dp_l = v_v dp_v \quad T = \text{constant} \tag{5.17}$$

and substituting (5.15) in (5.16) to eliminate p_l:

$$dp_c = \frac{v_l - v_v}{v_l} dp_v = dp_v - \frac{v_v}{v_l} dp_v \tag{5.18}$$

Assuming that the vapour behaves as an ideal gas, i.e. $p_v v_v = RT$, equation (5.18) becomes

$$dp_c = dp_v - \frac{RT}{v_l} \frac{dp_v}{p_v} \tag{5.19}$$

Integrating between the initial limits $p_c = 0$ and $p_v = p_{v0}$ (i.e., flat surface $H_0 = 0$) and the final values p_c, p_v and assuming constant and molar volume for the liquid v_l (i.e.,

incompressible liquid $\alpha_l = 0$), equation (5.23) becomes

$$p_c = (p_v - p_{v0}) - \frac{RT}{v_l} \ln\left(\frac{p_v}{p_{v0}}\right) \tag{5.20}$$

When the molar volume of the liquid v_l is negligible with respect to that of the vapour v_v (i.e., the vapour pressure p_v is not too high) the first term on the right-hand side of (5.20) can be omitted obtaining

$$p_c = -\frac{RT}{\bar{v}_l} \ln\left(\frac{p_v}{p_{v0}}\right) \tag{5.21}$$

that is usually known as the Kelvin's equation. From Kelvin equation it follows that the equilibrium vapour pressure p_v over a concave meniscus must be less than the saturation pressure p_{v0} over a flat surface ($p_c = 0$) and then capillary condensation of a vapour to a liquid can happen.

5.3 Liquid water and moisture properties

5.3.1 State equation of water

The state equation of liquid water is rather complex and usually creates numerical problems [5]: it should take into account a considerable, non-linear decrease of water density in temperature range close to the critical point of water. As a sufficient approximation of the dependence of the bulk density of liquid water upon its temperature and pressure, the following formula may be used:

$$\rho^w = \rho^{w0} \left[1 - \beta_w \left(T - T_0\right) + \alpha_w \left(p_w - p_0\right)\right] \tag{5.22}$$

where $\rho^{w0} = 999.84\, kg/m^3$ is the water density at the reference temperature T_0 and pressure p_0, $\beta_w = (1/\nu_w) \,/\, (\partial \nu_w / \partial T)_p$ is volume thermal expansion coefficient of the water, $\alpha_w = (1/\nu_w) \,/\, (\partial \nu_w / \partial p)_T$ is the isothermal compression modulus of water ($\alpha_w = 4.3 \cdot 10^{-9}$ Pa^{-1}), and $\nu_w = \rho_w^{-1}$ is the water specific volume. The coefficient β_w change in non-linear manner with temperature (e.g. $\beta_w = 0 \cdot 68 \cdot 10^{-4}\, K^{-1}$ at $T = 273.15\, K$ and $\beta_w = 10.1 \cdot 10^{-4}\, K^{-1}$ at $T = 420\, K$), thus the average value for the temperature range under interest should be used in calculations. The state equation (5.22), basically valid for the bulk (free) liquid water, is often used also for the description of the capillary and bound water, e.g. [5, 7, 8]. However, because of a very complex nature of interaction

between the water and skeleton, its applicability is questionable, especially as far as pressure dependence is concerned (although capillary water is in traction, but its density is not expected to be lower than that for bulk water). Nevertheless, equation (5.22) may be used, taking into account that close to critical point of water a sharp increase of volume thermal expansion coefficient takes place and assuming water incompressibility, i.e. $\alpha_w = 0$. At lower relative humidities, usually encountered at higher temperatures, most of the liquid water consists of the physically adsorbed water, which is exposed to strong interaction with the solid skeleton, resulting in an increase of the water density. At the same time one can expect a decrease of the density with an increase of the capillary pressure (decrease of the water pressure), what is the case in heated concrete. Having in mind these two opposite trends, as well as lack of sufficient experimental data, we have assumed here incompressibility of the liquid water inside the pores of concrete [9].

Another relationship that can be used as state equation of water is a nonlinear expression of empirical nature due to Furbish [10]. Also in this case the incompressibility of water can be supposed. The density of liquid water is very well approximated by a fifth-order polynomial:

$$\begin{aligned}\rho^w = &\left[b_0 + b_1 T + b_2 T^2 + b_3 T^3 + b_4 T^4 + b_5 T^5\right] \\ &+ \left(p_{w1} - p_{wrif}\right)\left[a_0 + a_1 T + a_2 T^2 + a_3 T^3 + a_4 T^4 + a_5 T^5\right]\end{aligned} \tag{5.23}$$

where: $p_{w1} = 1 \cdot 10^7\, Pa$ and $p_{wrif} = 2 \cdot 10^7\, Pa$; the coefficients a_i and b_i in equation (5.23) are shown in table 5.1:

a_0	a_1	a_2	a_3	a_4	a_5
$4.89 \cdot 10^{7}$	$-1.65 \cdot 10^{-9}$	$1.86 \cdot 10^{-12}$	$2.43 \cdot 10^{-13}$	$-1.60 \cdot 10^{-15}$	$3.37 \cdot 10^{-18}$
b_0	b_1	b_2	b_3	b_4	b_5
$1.02 \cdot 10^{-3}$	$-7.74 \cdot 10^{-1}$	$8.77 \cdot 10^{-3}$	$-9.21 \cdot 10^{-5}$	$3.35 \cdot 10^{-7}$	$-4.40 \cdot 10^{-10}$

Table 5.1: Coefficients of equation (5.23)

The relationship of equation (5.23) is reported in figure 5.1 where is evident the dependence of water density on temperature and the thermal expansion of water close to critical point.

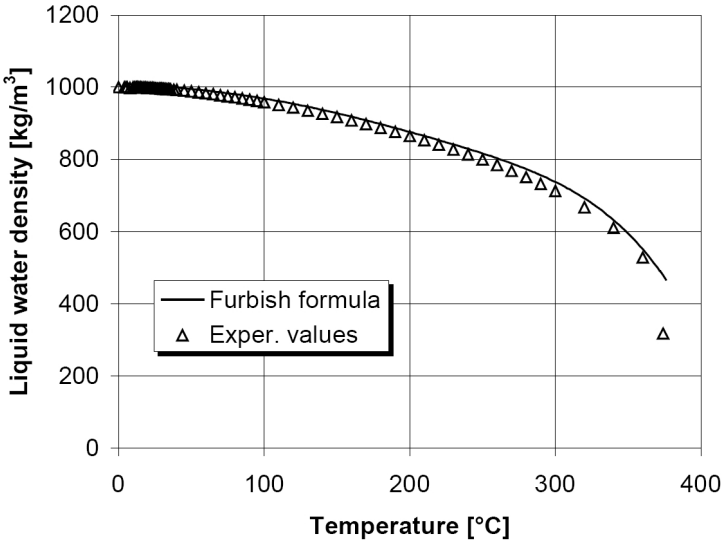

Figure 5.1: Water density: comparison between Furbish formula (5.23) and experimental values [11]

5.3.2 Saturated vapour pressure

The saturated water vapour pressure, i.e. the vapour pressure with flat surface (H=0), can be calculated through the well known Clasius-Clapeyron equation as a function of temperature (see chapter 3):

$$p^{gws}(T) = p^{gws0} \cdot RH = p^{gws0} \exp\left[-\frac{M_w \triangle h_{vap}}{RT}\right] \tag{5.24}$$

Anyway, this relationship should be used carefully over extended temperature intervals, because enthalpy of vaporization is not constant but it is a function of temperature, i.e. $\Delta h_{vap} = \Delta h_{vap}(T)$, specific volumes of liquid water v_w and of water vapour v_w, respectively.

More accurate results can be obtained using empirical correlations such as Hyland-Wexler relationship:

$$p^{gws}(T) = \exp\left[C_1/T + C_2 + C_3 T + C_4 T^2 + C_5 T^3 + C_6 \ln(T)\right] \tag{5.25}$$

where $C_1 = 5800.2206$, $C_2 = 1.3914993$, $C_3 = -4.8640293 \cdot 10^{-2}$, $C_4 = 4.1764768 \cdot 10^{-5}$, $C_5 = -1.4452093 \cdot 10^{-8}$, $C_6 = 6.5459673$.

5.3.3 Enthalpy of evaporation

The enthalpy of evaporation is considered temperature dependent and is approximated by means of the Watson formula, [12]:

$$\triangle h_{vap} = 2.672 \cdot 10^5 (T - T_{cr})^{0.38} \tag{5.26}$$

where $T_{cr} = 647.3\,K$ is the critical temperature of water.

5.3.4 Viscosity of liquid water

The dynamic viscosity of liquid water depends strongly upon temperature [13] and can be evaluated, with sufficient accuracy in a wide temperature range, using the following approximate formula, [14]

$$\mu^w = 0.6612 \cdot (T - 229)^{-1.562} \tag{5.27}$$

5.3.5 Viscosity of moist air

The dynamic viscosity of moist air, which depends upon the temperature and the ratio of the vapour and gas pressures, can be approximated using the following formula [15]:

$$\mu^g = \mu^{gw} + (\mu^{ga} - \mu^{gw}) \left(\frac{p^{ga}}{p^g} \right)^{0.608} \tag{5.28}$$

where:

(p^{ga}/p^g) is the mole fraction of dry air in the gas phase;
$\mu^{gw} = \mu^{gw0} + \alpha_v (T - T_0)$ is the water vapour dynamic viscosity,
with $\mu^{gw0} = 8.85 \cdot 10^{-6}\,Pa \cdot s$, $\alpha_v = 3.53 \cdot 10^{-8}\,Pa \cdot s \cdot K^{-1}$;
$\mu^{ga} = \mu^{ga0} + \alpha_a (T - T_0) + \beta_a (T - T_0)^2$ is the dry air dynamic viscosity,
with $\mu^{ga0} = 17.17 \cdot 10^{-6}\,Pa \cdot s$, $\alpha_a = 4.73 \cdot 10^{-8}\,Pa \cdot s \cdot K^{-1}$, $\beta_a = 2.22 \cdot 10^{-11}\,Pa \cdot s \cdot K^{-2}$.

5.4 Mechanism of moisture transport in concrete

5.4.1 Darcean flows

Permeability is defined as the property that governs the rate of flow of a fluid through a porous material and is defined from the Darcy's law.

For fluid phases the multiphase Darcy's law has been applied as constitutive equation, thus for capillary water and gas phase flow we have [11]:

$$\mathbf{v}^w = -\frac{\mathbf{k}^w}{\mu^w}\left(\nabla p^g - \nabla p^c - \rho^w \mathbf{b}\right) + \mathbf{k}^{wg}\mathbf{v}^g + \mathbf{k}^{w\triangle\sigma}\nabla\sigma \tag{5.29}$$

$$\mathbf{v}^g = -\frac{\mathbf{k}^g}{\mu^g}\left(\nabla p^g - \nabla p^c - \rho^g \mathbf{b}\right) + \mathbf{k}^{gw}\mathbf{v}^w + \mathbf{k}^{g\triangle\sigma}\nabla\sigma \tag{5.30}$$

where $\mathbf{k}_w$ and $\mathbf{k}_g$ are permeability tensors of the liquid and gaseous phases, $\mathbf{v}^w$ and $\mathbf{v}^g$ are the volume averaged velocities of capillary water and gaseous phase relative to the solid phase, and the vector $\mathbf{b}$ indicates the specific body force term (normally corresponding to the acceleration of gravity).

The second terms in the right hand side of (5.29) and (5.30) represent the viscous drag of one fluid upon the other and $\mathbf{k}^{wg}$ and $\mathbf{k}^{gw}$ are the related permeability tensors.

The third terms in the right hand side of equations (5.29) and (5.30) represent the effect of surface tension gradient. In fact, the tangential force balance shows that the gradient of the surface tension can influence the interfacial motion; the result is an extra driving force in the volume averaged momentum equations (Marangoni effect).

However, the evaluation of these additional terms, especially in high temperature conditions, appears to be really difficult, so also these terms will be neglected in the formulation of Darcy's formula. As far as the remaining coefficients in equations (5.29) and (5.30) is concerned, $\mathbf{k}^w$ and $\mathbf{k}^g$ are the most studied coefficients and almost all studies are empirical.

Muskat and Meres (1936) recommended that the permeabilities of the liquid and the gaseous phases, $\mathbf{k}^w$ and $\mathbf{k}^g$, are treated as isotropic and given by:

$$\begin{aligned} \mathbf{k}^w &= \mathbf{k}k^{rw} \\ \mathbf{k}^g &= \mathbf{k}k^{rg} \end{aligned} \tag{5.31}$$

where $\mathbf{k}$ is the absolute or intrinsic permeability used in the single phase flows; k^{rw} and k^{rg} are the relative permeability of the w and g phases, respectively.

Then the relative permeability accounts for the phase distributions, i.e.:

$$k^{r\pi} = k^{r\pi}\left(\text{matrix structure}, S, \sigma, \vartheta, \frac{\rho_\pi}{\rho^\alpha}, \text{history}\right)$$

where S is the liquid phase saturation, σ the surface tension and ϑ is the contact

angle. Therefore, the approach taken by Muskat and Meres was the simplification of this relation to a saturation dependence only, i.e.,:

$$k^{rw} = k^{rw}(S)$$
$$k^{rw} = k^{rg}(S) \tag{5.32}$$

which is still in popular usage.

Since the simultaneous flow of the two phases has been made analogous to that of the Darcean single-phase flow, the flow of each phase at a given local saturation depends on how the two phases are distributed over the representative elementary volume (REV). The factors that can be influencing the phase distributions are the local saturation, matrix (or pore) structure, history, contact angle, surface tension and density ratio. These effects are generally determined experimentally.

The local saturation, i.e., the extent to which the liquid fills the pores in the REV, influences the phase distributions in this volume and in turn influences the resistance to the flow of each phase. Considering the complexity of the phase distribution function, the local flow through the channels in which each phase flows is a complex function of S.

The excess resistance, i.e $1/k^{rw}$, also becomes a complex function of local saturation. One of the important features of the excess resistances $1/k^{rw}$ and $1/k^{rg}$ is that the simultaneous flow of the phases causes excess resistances for both phases. This means that in general for a given saturation we have:

$$k^{rw} + k^{rg} < 1 \tag{5.33}$$

The intermediate saturations correspond to a mutual and significant resistance offered by each phase to the flow of the other phase.

The solid phase distribution influences the distribution of the w and g phases and, in turn the relatives permeabilities. Since the w and g phases flow through the passages that are nonuniform in cross section, the distributions of the phases (and their point velocities) are significantly influenced by the topology of the passages. The absolute permeability K is a measure of the average throat size, but it does not give all the information about the microstructure.

The simplest way to evaluate relative permeabilities coefficients, is to consider a simple dependence on the only saturation, similar to equation (5.32). In this sense, two different approach exists, depending on the fact that the liquid phase is continuous

(funicolar zone) or discontinuous (pendular zone) in the porous medium. By taking into account an irreducible saturation level S_{irr}, the liquid phase continuity is disrupted when the saturation falls below S_{irr}, so that liquid flow is not longer possible. This behaviour is described by introducing a k^{rw} model which can be represented as follows:

$$k^{rw} = \left(\frac{S - S_{irr}}{1 - S_{irr}}\right)^{A_w} \quad \text{for } S > S_{irr} \tag{5.34}$$

where S_{irr} is the irreducible saturation, which is discussed in detail in [2, 16] and A_w is a constant, with the value from the range <1,3>, [2, 8, 16].

On the other hand, if S_{irr} is zero, i.e. the liquid phase remains continuous, that is in funicolar state, during the overall nonhygroscopic region, one has the following form of relative permeability for the liquid phase, see figure 5.2:

$$k^{rw} = S^{A_w} \tag{5.35}$$

where, typically the exponent A_w varies in the range <1,6>.

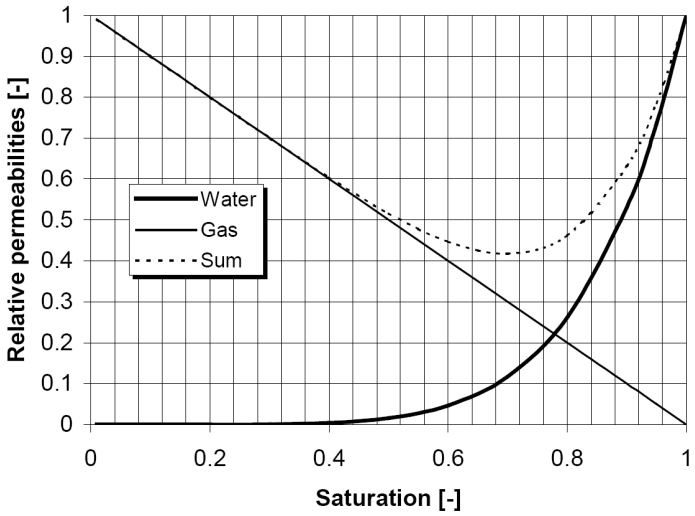

Figure 5.2: Relative permeability for liquid water, gas and their sum, according to formula (5.35) with $A^w = 6$ and (5.37) with $A^g = 1$, $S_{cr} = 1$ [11]

In the first formulation, i.e. with irreducible saturation, there is not liquid phase transport in the pendular zone. This means that in this region there is only vapour diffusion flux driven by vapour concentration. Withaker has shown that in such condition the convective flux, driven by pressures, is not enough to overcome the diffusive flux, which is from the region of high temperature to the region of low temperature.

But experimentally it is known that drying processes globally is a loss of mass from the inner part of material toward the exposed surface. Because of this in the mathematical model a singularity is produced.

In the second formulation, i.e. without the irreducible saturation concept, a continuous moisture flux toward the surface exists, also between S_{irr} and 0 (solid saturation point) and in such case the problem of singularity is avoided. In reality, a sharp increase of the capillary water flux is observed for concrete, when the relative humidity RH reaches the value higher than about 75% [17].

Such a kind of behaviour can be described by the following relationship:

$$k^{rw} = \left[1 + \left(\frac{1 - RH}{0.25}\right)^{B_w}\right]^{-1} S^{A_w} \tag{5.36}$$

where B_w is a constant, see figure 5.3.

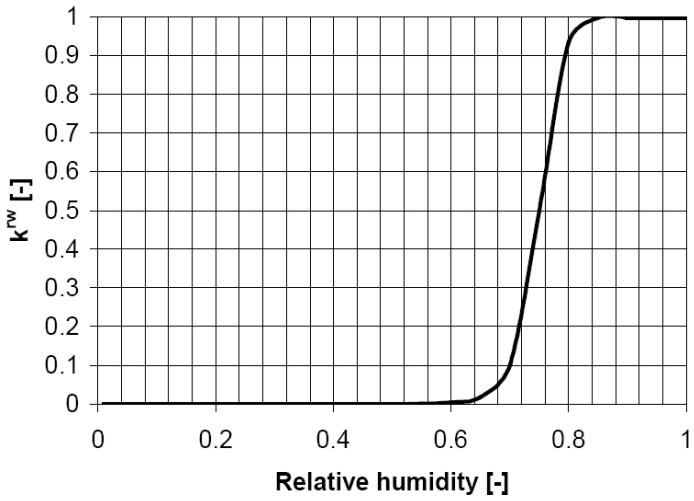

Figure 5.3: Relative permeability of liquid water as function of R.H. according to equation (5.36) [11]

The term in square brackets has a form originally proposed in [17] for the water diffusivity (with $B_w = 6$ or 16). It has good numerical properties and allows to avoid the use of irreducible saturation concept which creates serious theoretical and numerical problems [2]. The gas relative permeability for concrete, similarly as for most capillary porous materials, may be described by the formula of the form, [2, 8, 14]:

$$k^{rg} = 1 - \left(\frac{S}{S_{cr}}\right)^{A_g}, \quad \text{for } S < S_{cr} \tag{5.37}$$

where S_{cr}, variable with temperature, is the critical saturation value, above which there

is no gas flow in the medium, and A_g is a constant, which usually has value from the range <1,3>, see figure 5.2.

5.4.2 Bound water flow

For the bound water flow, the following generalized constitutive law is applied [11]:

$$\mathbf{v}_d^{bw} = -\mathbf{D}_d^{bw} \nabla S_b \tag{5.38}$$

where $\mathbf{D}_d^{bw} = \mathbf{D}_d^{bw}(S_b)$ is the bound water diffusion tensor, and the degree of saturation with adsorbed water, S_b, is given by

$$S_b = \begin{cases} S & \text{for } S \leq S_{ssp} \\ \\ S_{ssp} & \text{for } S > S_{ssp} \end{cases} \tag{5.39}$$

According to the adsorption theory, the latter depends upon the partial vapour pressure (or the relative humidity of the moist air), and because of the Kelvin-Laplace equation, also upon the matric potential p^c (see the remarks after equation (5.2) about the notation used):

$$S_b = S_b(p^{gw}) = S_b(p^c) \tag{5.40}$$

Equations (5.38)-(5.40) show clearly, that the driving force for the bound water flow is, in fact, the matric potential. The relationship (5.40), results from the adsorption theory where the adsorbed water content or volume fraction were introduced as additional state variables, not related to the vapour pressure value, hence also with the matric potential. In order to obtain a formulation containing directly a variable state (p^c), equation (5.38) can be written as:

$$\mathbf{v}_d^{bw} = -\mathbf{D}_d^{bw} \frac{\partial S_b}{\partial p^c} \mathrm{grad} p^c \tag{5.41}$$

so the diffusion tensor multiplied for the derivative of degree of saturation of bound water on capillary pressure is a kind of equivalent diffusion tensor. The bound water diffusion coefficient for concrete was found in [18] to be given as

$$D_d^{bw} = D_{d_0}^{bw} \exp\left(-2.08 \frac{S}{S_{ssp}} \frac{T}{T_0}\right) \tag{5.42}$$

where $D_{d_0}^{bw} = 1.57 \cdot 10^{-11}\, m^2/s$ and reference temperature $T_0 = 295\, K$.

5.4.3 Diffusion of water vapour

For the description of the diffusion process of the binary gas species mixture, dry air and water vapour, Fick's law is applied:

$$\begin{aligned}\mathbf{v}_g^{ga} &= -\frac{M_a M_w}{M_g^2}\mathbf{D}_g^{ga}\mathrm{grad}\left(\frac{p^{ga}}{p^g}\right)\\ &= \frac{M_a M_w}{M_g^2}\mathbf{D}_g^{gw}\mathrm{grad}\left(\frac{p^{gw}}{p^g}\right) = -\mathbf{v}_g^{gw}\end{aligned} \tag{5.43}$$

where

$$\frac{1}{M_g} = \frac{\rho^{gw}}{\rho^g}\frac{1}{M_w} + \frac{\rho^{ga}}{\rho^g}\frac{1}{M_a}$$

and $\mathbf{D}_g^{ga} = \mathbf{D}_g^{gw} = \mathrm{D}_{eff}$ is the effective diffusion coefficient of vapour species in the porous medium (isotropic material).

The effective diffusion coefficient of vapour inside the pores of partially saturated concrete varies with saturation, temperature and gas pressure changes and may be described as [18]:

$$D_{eff} = n\,(1-S)^{A_v}\,f_S D_{v0}\left(\frac{T}{T_0}\right)^{B_v}\frac{p_0}{p^g} \tag{5.44}$$

where $D_{v0} = 2.58{\cdot}10^{-5}\,m^2/s$ is the diffusion coefficient of vapour species in the air at the reference temperature $T_0 = 273.15\,K$ and pressure $p_0 = 101325\,Pa$, A_v is a constant, usually from the range <1,3>, B_v is a constant, which for the value $B_v = 1.667$ gives good correlation with the experimental data concerning vapour diffusion at different temperatures, and f_S is the structure coefficient, which takes into account that concrete inner structure influences a vapour diffusion process.

Another formulation of effective vapour diffusivity (which reads $j = a\,\mathrm{or}\,v$):

$$\mathbf{v}_d^{gw} = -\frac{1}{\phi_g}F\frac{D_{va}}{p^j}grad\left(\frac{p^j}{p^g}\right) \tag{5.45}$$

where $\phi_g = \phi(1-S)$ represents the ratio of material volume occupied by the gas phase (moist air), D_{va}/p^g is the coefficient of free diffusion of vapour in air [19]:

$$D_{va} = D_{va}\,(T) = 0.217 p_{atm}\left(\frac{T}{T_0}\right)^{1.88} \tag{5.46}$$

and where the factor F, function of S, accounts simultaneously for the tortuosity effects

and the reduction of space offered to gas diffusion; F is the one by Millington:

$$F = F(S) = n^{4/3}(1 - S)^{10/3} \tag{5.47}$$

However, this formulation does not take into account the high temperatures effects, so it can be considered valid only in a range of temperatures close to the ambient ones.

5.5 Physico-chemical phase changes

Phase changes take place which can be physical or chemical in nature [20, 21].

Phase changes in concrete are incorporated directly in the transport mechanism of the concrete model (table 5.2). For Portland cement based concretes, they are: CSH (i.e. cement gel) and CH dehydration/hydration, evaporation/condensation, sorption/desorption, aggregate physical phase changes (e.g. $\alpha - \beta$ transformation of quartz at 573°C), and decarbonation of calcium carbonate above 650°C.

Phases	Process	Energy	Phase change process
Dehydration	Chemical	Loss	Solid matrix (CSH or CH) ⇒water - energy + matter (C or C_yS)
Hydration		Gain	Water + matter (C or C_yS)⇒solid matrix (CSH or CH) + energy
Evaporation	Physical	Loss	Capillary water⇒water vapour - energy
Condensation		Gain	Water vapour⇒water + energy
Desorption	Physical	Loss	Physically adsorbed water⇒water vapour - energy
Sorption		Gain	Water vapour⇒physically adsorbed water + energy
Decarbonation	Chemical	Loss	Calcium carbonate⇒CO_2 - energy
Carbonation		Gain	CO_2⇒calcium carbonate + energy
$\alpha - \beta$ inversion	Physical	Loss	Endothermic during heating up at 573°C with expansion
$\beta - \alpha$ inversion		Gain	Exothermic during heating down at 573°C with contraction

Table 5.2: Brief description of some phase changes in concrete

Hydration, being of chemical nature, takes place at room temperature and the process increases with temperature in the presence of moisture up to 80°C or more, resulting in an increase in the mass of the solid skeleton. It should be noted that if cement paste is heated above 100°C in the presence of moisture under hydro-thermic conditions, de-

pending upon the C/S ratio, a chemical transformation of tobermorite will take place to produce C_2SH(A) hydrate which is a weak, porous and crystalline material. Further chemical changes take place at higher temperatures under hydrothermal conditions. In addition, reactive silica in the concrete (aggregate or cement replacement) would also react beneficially with water and CH to produce CSH phases. The use of cement replacements such as silica fume, pfa or slag reduces the amount of CH produced upon hydration and increases the amount of CSH produced, thus creating a stronger and less permeable material.

Dehydration (i.e. release of chemically bound water) from the CSH becomes significant above about 110°C, while the dehydration of the calcium hydroxide takes place at about 500°C producing CaO and H_2O. Both produce a reduction in the solid skeleton mass of the cement past; however the strength of concrete is more related to CSH than the CH. The release of chemically bound water contributes moisture to the gas phase and contributes to vapour pressure which becomes significant in high performance concrete with low porosity and low permeability, and could contribute to explosive spalling. The temperature at which dehydrations occur depend upon the activation energy of the chemical. The CSH is a complex chemical with a range of activation energies for its constituents.

Evaporation of capillary water (physical phenomenon) from concrete increases with temperature particularly close to 100°C, depending upon the pressure. The loss of capillary water does not significantly influence the mechanical properties of the cement paste but the loss of physically adsorbed water has a major influence on the mechanical properties. For a small element of concrete at atmospheric pressure the capillary water would evaporate completely by about 100°C. However, for relatively large elements, the evaporation from the surface, especially for dense concretes, may not be rapid enough to release all the capillary water from the body by 100°C and some water may in fact be driven down the temperature gradient into the material (so called thermo-diffusion of liquid water). Therefore, capillary water may remain within the body for a period during heating up to temperatures in excess of 100°C, particularly for dense concrete, thus contributing to the chemical hydrothermal changes mentioned above and to explosive spalling. No capillary or free-water is possible above the critical point of water, $T_{cr} = 374.15$°C, at which point capillary water and capillary pressure disappear while only some chemically bound water and water vapour (usually under considerable pressure) exist above this temperature.

The $\alpha-\beta$ transformation of quartz (of physical nature) occurs at 573°C in aggregates

and sands containing quartz. This is an endothermic reaction during heating, and exothermic during cooling when the transformation is reversed.

Decarbonation (chemical process) occurs at temperatures above 650°C, whenever, $CaCO_3$ is present in the aggregate (e.g. limestone and carbonate aggregates). This produces lime (CaO) and Carbon dioxide (CO_2).

On cooling, the CaO produced from the dehydration of CH and decarbonation of the $CaCO_3$ absorbs water and rehydrates (chemical process called rehydration of lime) into $Ca(OH)_2$ with a corresponding 40 per cent increase in volume.

Concluding, it should be underlined, that all the phase changes are strongly influenced by temperature, and are strictly thermodynamically not fully reversible, although reversibility is often assumed in mathematical modelling.

5.5.1 Adsorption-desorption phenomena

Capillary condensation of water vapour plays an important role during hygro-thermo-mechanical processes in mesoporous materials [22]. Physical phenomena associated with capillary condensation are taken into account by means of sorption isotherms, which represent the dependence of saturation on relative humidity. For each relative humidity value, a sorption isotherm indicates the corresponding free water content value at a given, constant temperature.

When the relative humidity of the air contained inside the pore space changes at constant temperature, the amount of condensed water vapour adsorbed by solid skeleton, being in thermodynamic equilibrium state with it, will change too. The relationship describing quantitatively this phenomenon is called sorption isotherm. It is an important characteristic of the inner pore structure, since a pore size distribution curve can be calculated by using this relationship together with the Kelvin equation (5.21).

Because of the complexity of sorption process, the isotherms cannot be determined by calculation, but must be measured experimentally with respect to capillary pressure and the level of saturation. During experimental sorption tests at constant temperature, a family of adsorption and desorption curves is usually observed, dependent on initial and final moisture content of the medium. When the adsorption process starts from oven dry moisture conditions, we shall obtain the primary adsorption curve. Similarly, starting from fully water saturated state we obtain the primary desorption isotherm. These two primary isotherms are, respectively, lower and upper limits for all possible "inner" adsorption (AB) and desorption (BC) curves, which are shown schematically in figure 5.4.

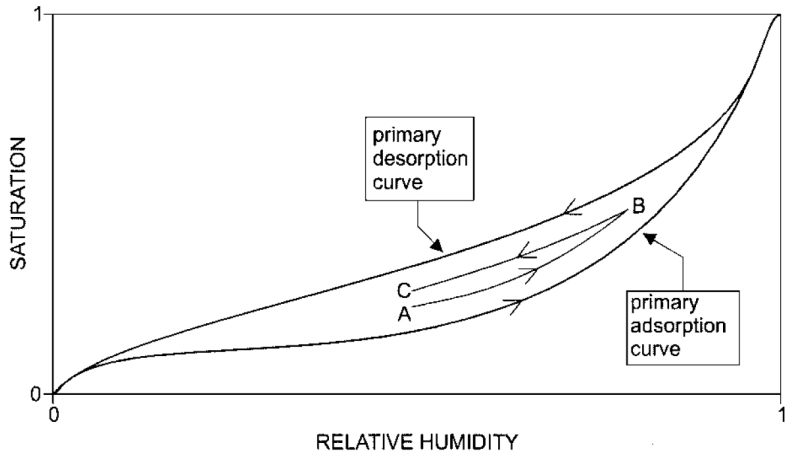

Figure 5.4: Schematic adsorption and desorption isotherms: primary and inner ones [22]

The difference between adsorptional and desorptional degree of saturation at the same relative humidity and temperature (e.g. CA in figure 5.4) can be considerable for mesoporous materials resulting in capillary condensation hysteresis.

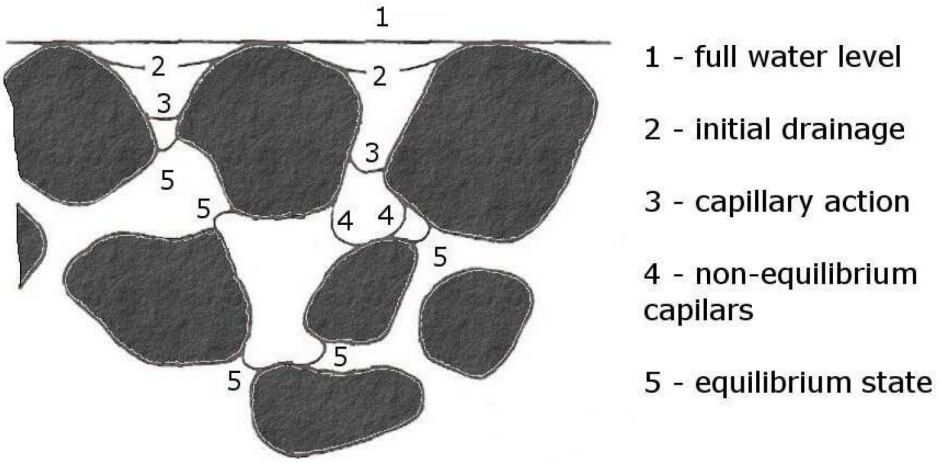

Figure 5.5: Gradual drainage [23]

The process of gradual drainage from the top of the specimen is illustrated in figure 5.5, where successive stage of this process are numerated from 1 till 5 [23]. At first, at 1 stage the pore structure is fully saturated with water. Next, when the fluid is drained from the surface of the sample and air is introduced on the top of that, there is a water-air interaction and menisci can form at interface 2. The radius of curvature at every point on a meniscus depends on the pressure difference between water pressure and air pressure. This difference can be written using Laplace formula (5.2) that indicates that

the greatest capillary pressure can be maintained by the local interface, corresponds to the smallest radius curvature (stage 3). On the other hand the channels which support a larger radius (stage 4), because of the reduced boundary area, are in a non equilibrium stage and the water needs to continue to retreat until the local equilibrium position is obtained (stage 5). The complete withdrawal of the liquid corresponds to the fully unsaturated specimen when the pore structure is completely filled with gas. The relationship which describes the quantity of fluid present in the void space is a function of the saturation S and is called adsorption/desorption curve.

The degree of saturation with liquid water S (considering together hygroscopic and capillary water, if the latter is contained in the pores), is an experimentally determined function of capillary pressure (matric potential) p^c and temperature T [11]. Because of the difficulties to obtain from experimental tests such a kind of curve in temperature, particularly above 100°C, and the processes which are of interest for our aims are heating of concrete, i.e. globally are drainage processes even if a local condensation is possible, hysteresis phenomena are not considered here, so isotherms curves are assumed to be a unique function of capillary pressure:

$$S = S\left(p^c,\, T\right) \tag{5.48}$$

The relationship (5.48) is clearly fundamental for realistic modelling of hygro-thermic behaviour of the specific concrete, thus it must be determined during sorption tests at several temperatures. An example of such dependence, obtained using the concrete data from Bazant [24] is the following:

$$S = S\left(p^c,\, T\right) = \left\{h\left(p^c,\, T\right)\right\}^{1/m_{(T)}} \tag{5.49}$$

where h is the relative humidity and m is a coefficient function of T determined correcting experimentally the values obtained from the thermodynamic tables of water and water vapour.

$$m\left(T\right) = 1.04 - \frac{T'}{22.34 + T'}, \qquad T' = \left(\frac{T + 10}{T_0 + 10}\right)^2 \tag{5.50}$$

Using such a kind of isotherms in a multiphase model like the present one, a problem can arise when the temperature builds up to critical point of water. In fact, Bazant's model follows a typical phenomenological approach where the single phases in the pores of material are undistinguished and only a general "fluid phase" is present in the voids of concrete. In this manner it is possible to not consider the critical point of water, simply

keeping a certain quantity of water also above T_{crit}. It is evident, as Bazant pointed out in his numerous papers on this subject, that when the temperature is under the critical one, the water content in these isotherms is to consider as liquid water, i.e. free water plus a small percentage for bound water, while when T overcomes the critical point, the residual water has to be considered as gas water or a monolayer of physically bound water. While, with this formulation a consistent lot of water is present also above critical temperature, representing the gas phase and the chemically bound water in this zone, which are separately computed in the model presented in this work.

In fact, in a micro-mechanical approach where the three phases are clearly distinct it is necessary that, thinking to isotherms as curves of "liquid water", the value of saturation tends to zero approaching the critical point of water and it is practically zero above this point.

For this reason, another formulation for desorption isotherms due to Baroghel-Bouny [19] has been considered. In this formulation the following relationship between capillary pressure and saturation, for "ordinary" concrete and high performance concrete at ambient temperature, is defined:

$$p^c = p^c(S) = a\left(S^{-b} - 1\right)^{\left(1-\frac{1}{b}\right)} \tag{5.51}$$

where the coefficients a and b in equation (5.51) are material dependent; their values are $a = 18.6237\,MPa$, $b = 2.2748$ for ordinary performance concrete, and $a = 49.9364\,MPa$, $b = 2.0601$ for high performance concrete.

The formulation given with equation (5.51) has been changed to take into account high temperatures effects, keeping constant the parameter b, and modifying the parameter a which is now a function of temperature, in the following manner [11]:

$$\begin{aligned} a &= \text{constant} \quad \text{if}\, T < 100^\circ \\ a &= Q_0 + Q_2 \quad \text{if}\, T > 100^\circ \end{aligned}$$

where Q_2 is a constant, while Q_0 is a polynomial or an exponential function of temperature,

$$S = (G+1)^{(-1/b)} \tag{5.52}$$

where G is a function of temperature and capillary pressure:

$$G = G(T,\, p^c) = \left[\frac{E}{a}p^c\right]^{\frac{b}{b-1}} \tag{5.53}$$

and where the parameter E is a function of temperature which has different form depending on the value of temperature.

5.5.2 Dehydration

The changes of the hydrated water content with temperature and the source term related to it, is given by [11]:

$$\triangle \dot{m}_{dehydr} = \frac{\partial}{\partial t} \left[\triangle m_{dehydr} \left(T \right) \right] = \frac{\partial}{\partial T} \left(\triangle m_{dehydr} \right) \frac{\partial T}{\partial t} \tag{5.54}$$

and should be measured during laboratory tests. For the temperature range below the critical point of water, the dehydrated water content $\triangle m_{dehydr}\left(T\right)$ increases, when temperature increases, approximately following a step function where there is a sharp change between 200°C and 500°C. For an ordinary concrete, in fact, the rise at the beginning of the phenomenon, i.e. when the hydration process stops around 105°C, is rather small and only around 200°C the dehydrated amount of water assumes significant values.

$$\triangle m_{dehydr} = f_s \, m \, c \, f \left(T \right) \tag{5.55}$$

where f_s is stechiometric factor, m is ageing degree of concrete (between 0 and 1), c is the cement content and $f(T)$ is an function of temperature, i.e.:

$$\begin{aligned} &if\, T < 105^{\circ}\mathrm{C} \quad f(T) = 0 \\ &if\, T > 105^{\circ}\mathrm{C} \quad f(T) = \frac{\left[1 + \sin\left(3.1416/2\left(1\text{-}2\exp\left(-0.004\left(T - 105\right)\right)\right)\right)\right]}{2} \end{aligned} \tag{5.56}$$

The function $f(T)$ is reported in the following figure:

5.6 Hygro-thermal-mechanical properties of concrete

5.6.1 Porosity

Concrete porosity is not constant, but it changes with increase of the temperature; its dependence on temperature can be approximated by a linear relationship [5, 11]:

$$n = n_0 + A_n \left(T - T_0 \right) \tag{5.57}$$

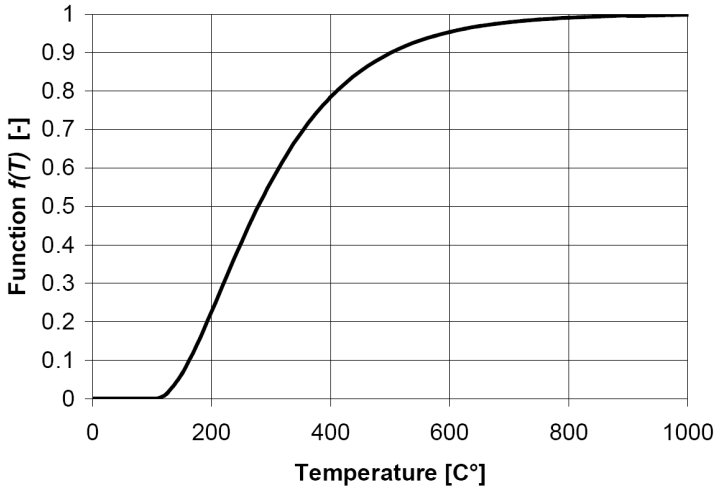

Figure 5.6: Dimensionless function of T of equation (5.56) [11]

where A_n is a constant dependent on the type of concrete.

It should be reminded, that the porosity, n, and the hydrated water source term, $\partial\left(\triangle m_{hydr}\right)/\partial T$, as well as the density of the solid phase, ρ_s, must fulfil the solid mass balance equation

$$\frac{(1-n)}{\rho^s}\frac{D^s\rho^s}{Dt} - \frac{D^s n}{Dt} + (1-n)\,\mathrm{div}\mathbf{v}^s = \frac{\dot{m}_{dehydr}}{\rho^s} \tag{5.58}$$

Thus, assuming that the first two parameters depend upon temperature according to equations (5.57) and (5.55), the change of solid density, caused by dehydration process, may be easily calculated through equation (5.58) in the temperature range (T_{ho}, T), where T_{ho} is temperature, at which dehydration process starts. Otherwise, knowing n and ρ_s as function of temperature from experimental tests, it is possible, always using equation (5.58), to evaluate the change of porosity related to dehydration process.

5.6.2 Intrinsic permeability

The intrinsic permeability, also called absolute permeability, is a material characteristic describing the penetration of gases or liquids through a porous material due to pressure head and it is generally determined by means of experimental tests performed using gas or water. Theoretically, the intrinsic permeability coefficient of a given concrete should be the same regardless of whether a gas or a liquid is used in the tests. For gases, the compressibility as well as the viscosity of the gas must be considered in order to derive

the coefficient of permeability:

$$k_g = \mu \frac{Ql}{tA} \frac{2p}{(p_1 - p_2)(p_1 + p_2)} \tag{5.59}$$

where capillary flow has been considered as laminar and where:

k_g = coefficient of permeability $[m^2]$

μ = viscosity of the gas $[Ns/m^2]$

Q = volume of gas flowing $[m^3]$

l = thickness of penetrated section $[m]$

A = penetrated area $[m^2]$

p = pressure at which Q is measured $[Pa]$

p_1 = gas entry pressure $[Pa]$

p_2 = gas exit pressure $[Pa]$

t = time $[s]$

Among liquids penetrating through concrete, water represents the most important fluid. In contrast to gases, liquids may be considered as incompressible, and equation (5.59) may be then rewritten. If the viscosity is taken into consideration and a laminar flow is assumed, the coefficient of (water) permeability is given by:

$$k_w = \frac{Ql}{tA} \frac{\mu}{\triangle p} \tag{5.60}$$

where:

k_w = coefficient of permeability $[m^2]$

μ = viscosity $[Ns/m^2]$

Q = volume of liquid flowing $[m^3]$

l = thickness of penetrated section $[m]$

A = penetrated area $[m^2]$

p = pressure difference $[Pa]$

t = time $[s]$

As above mentioned, the coefficient of permeability measured using (5.59) and (5.60) represents a material characteristic, i.e. it depends only on the microstructure of the concrete, and is independent of the properties of the fluid. Instead, there are large differences between values obtained using water or gases. The gas values are consistently higher, the difference being greater at lower permeability coefficients, even if the material is practically dried.

The problem concerning the measure of absolute permeability is decisively more complex if the temperature is not constant, in particular at high temperature, i.e. above 100°C. Heating concrete from ambient temperature to 120°C increases k by up to 2 orders of magnitude. Moreover, drying (e.g. in the range 120-600°C) causes internal structural damage and dehydration of the cement, resulting (a) in an increase in k value, and (b) in k values which are time dependent initially on re-wetting. The damage increases with increase of temperature, thus resulting in progressively increasing of k with temperature increase. The curing treatments are of importance, too. In fact, with particular curing during heating of concrete it is possible to minimize damage degree, resulting in a lower k increase. Hence, damage plays a role really important and should be taken into account. For the evaluation of intrinsic permeability temperature dependence, different approaches can be followed. A phenomenological approach is usually applied for the description of changes of concrete physical properties during complex hygro-thermal and mechanical phenomena at high temperature. It means that all these changes are expressed as a function of temperature, moisture content and gas pressure, i.e. physical quantities measured directly during experimental tests. However results of such tests are strongly dependent upon the form and dimensions of a test sample, as well as physical conditions during experiment. Hence application of the results of these tests for prediction of concrete behaviour in conditions that differ significantly from the experimental ones is rather questionable.

Because of this there is a need for mechanistic mathematical models which assume certain physical models of the phenomena analysed. As above mentioned, significant increase of concrete intrinsic permeability at high temperature is mainly generated by arising of micro-cracks and by changes of material inner structure, as well as by crack-opening due to high gas pressure values. As a result, it depends not only upon temperature, moisture content and gas pressure, as assumed for a phenomenological approach, but also upon a degree of cracks development, which may be described by use of damage parameter D [5, 11]:

$$k = k_0 10^{f(T)} \left(\frac{p^g}{p_0^g} \right)^{A_P} \cdot 10^{A_D D} \tag{5.61}$$

where A_P and A_D are material constants. The term related to damage describes the effect of concrete cracking, and the gas pressure term the effect of cracks' opening, on increase of the permeability. Function $f(T) = A_T^2 (T - T_0)^2 + A_T^1 (T - T_0)$ takes into account the influence of the dehydration process on the permeability of concrete

at high temperature. Parameter A_P in (5.61) has a clear physical interpretation, because it describes the effect of crack opening, caused by pressure rise, on the material permeability increase. The value of parameter A_D in (5.61) takes into account the permeability increase caused by cracking (both mechanical and thermally induced), which may be described in terms of damage parameter.

5.6.3 Thermal conductivity

Thermal conductivity is a key thermal property in predicting heat and mass transport in concrete exposed to fire conditions. Thermal conductivity is defined in terms of the ratio of the heat flux to the temperature gradient, in the absence of any mass flow. In general, there is no practical way to stop mass flow to occurring. For materials with low permeability and low mass diffusivity, the diffusive mass flow may be small enough that it should be possible to carry out transient thermal test to determine thermal conductivity and/or thermal diffusivity before significant mass transfer can occur. However, evaporation and subsequent condensation of moisture can transfer large quantities of heat even for small mass flows, so separation of conducted heat from the heat associated with mass transfer can be very difficult.

For the description of heat conduction in heterogeneous material as concrete, Fourier's law is used

$$\tilde{\mathbf{q}} = -\chi_{eff}\mathrm{grad}T \tag{5.62}$$

where

$$\chi_{eff} = \chi^s + \chi^w + \chi^g \tag{5.63}$$

is effective thermal conductivity, dependent on the temperature and moisture content.

Usually this effective value is measured experimentally and takes into account not only pure heat conduction, but also several micro-scale phenomena inside pores, like radiation and micro-convection. Often tests are performed only for the dry material at various temperatures. In such a case effective thermal conductivity of moist concrete may be evaluated from the formula [4]:

$$\chi_{eff} = \chi_d\left(T\right)\left(1 + \frac{4n\rho^w S}{\left(1-n\right)\rho^s}\right) \tag{5.64}$$

where $\chi_d(T)$ is thermal conductivity of a dry material, which temperature dependence

may be usually approximated by a linear relationship

$$\chi_d = \chi_{d0} \left[1 + A_\chi \left(T - T_0\right)\right] \tag{5.65}$$

5.6.4 Specific heat and thermal capacity

The thermal capacity of partially saturated concrete can be expressed as a combination of the thermal capacities of its constituents, [5, 8, 26]

$$\rho C_p = \left(1 - n\right) \rho^s C_{ps} + n \left[S \rho^w C_{pw} + \left(1 - S\right) \left(\rho^g C_{pga} + \rho^{gw} \left(C_{pgw} - C_{pga}\right)\right)\right] \tag{5.66}$$

where thermal capacities $C_{p\pi}$ depend upon the temperature of the material. A temperature dependence of the thermal capacity $(\rho C)_{ps}$ for the solid skeleton may be approximated by a linear relationship

$$\rho C_{ps} = \rho C_{ps0} \left[1 + A_0 \left(T - T_0\right)\right] \tag{5.67}$$

where C_{ps0} is the thermal capacity of the solid skeleton at the reference temperature T_0 and A_c is a coefficient.

It is possible to give a direct dependence of thermal capacity, or specific heat, of partially saturated porous media, from the state variables T and p^c, without considering a combination of the thermal capacities of single constituents, i.e.:

$$\rho C_p = \rho C_p \left(T, \, p^c\right) \tag{5.68}$$

5.6.5 Density of the solid skeleton

The density of concrete and its constituents is needed to compute the thermal capacity, which is needed for the theoretical model used to predict heat transport in fire-exposed concrete.

For what concerns the density of the solid skeleton, its variation over the temperature range of interest is due to the dehydration process. Accordingly, information as to mass variation is important in determining the enthalpy of a specimen.

In this case, a phenomenological formula, valid for the concrete type used in the analysis, has been used [25]:

$$\rho_s = \rho_{s0} + A_s \left(T - T_0\right) \tag{5.69}$$

where ρ_{s0} is the density at the reference state and A_s is a constant.

5.6.6 Young's modulus, tensile and compressive strength

Young's modulus, tensile and compressive strength are dependent upon temperature. The specific form of these dependencies are determined experimentally for the concrete under consideration within the Brite Euram "Hiteco Project" [27].

Due to damage and chemical transformations of concrete (generally called dehydration), Young's modulus and the strength properties of concrete degrade gradually with increase in temperature:

$$E = E_0 - \alpha \left(T - T_0\right) \tag{5.70}$$

$$\begin{aligned} f_c &= f_{c0} - \beta_1 \left(T - T_0\right) \\ f_t &= f_{t0} - \beta_2 \left(T - T_0\right) \end{aligned} \tag{5.71}$$

where E_0, f_{c0} and f_{t0} are respectively the Young's modulus, the compressive and the tensile strength at the reference temperature T_0, whereas α, β_1 and β_2 are constant depending upon the type of concrete in question.

Bibliography

[1] Neville A.M., Properties of Concrete, 4h ed., Pearson Education Ltd., Harlow, Essex, 2004.

[2] Couture F., Jomaa W., Puiggali J.R., Relative permeability relations: a key factor for a drying model, Transport in Porous Media, 23(3): 303-335, 1996.

[3] Schrefler B.A, Gawin D., Pesavento F., Modelling of concrete as multiphase porous material, with application to fires, IACM Newsletter (Bulletin for The International Association for Computational Mechanics), 12: 16-21, 2002.

[4] Baggio P., Bonacina C., Schrefler B.A., Some considerations on modelling heat and mass transfer in porous media, Transport in porous media, 28: 233-281, 1997.

[5] Gawin D., Majorana C.E., Schrefer B.A., Numerical analysis of hygro-thermal behaviour and damage of concrete at high temperature, Int. J. Mech. Cohes.-Frict. Mater., 4: 37-74, 1999.

[6] ASHRAE Handbook, Fundamentals Volume, ASHRAE, Atalanta, 1993.

[7] Daian J.F., Condensation and isothermal water transfer in cement mortar. Part I - Pore size distribution, equilibrium, water condensation and imbibition, Transport in Porous Media, 3: 563-589, 1988.

[8] Nasrallah S.B., Perre P., Detailed study of a model of heat and mass transfer during convective drying of porous media, Int. J. Heat Mass Transfer, 31(5): 957-967, 1988.

[9] Gawin D., Pesavento F., Schrefer B.A., Modelling of hygro-thermal behaviour of concrete at high temperature with thermo-chemical and mechanical material degradation, Comput. Methods Appl. Mech. Engrg., 192: 1731-1771, 2002.

[10] Furbish D.J., Fluid Physics in Geology. An introduction to fluid motion on earth surface and within its crust, Oxford University Press 4, 1997.

[11] Pesavento F., Non linear modelling of concrete as multiphase porous material in high temperature conditions, PhD Thesis, University of Padova, 2000.

[12] Forsyth P.A., Simpson R.B., A two-phase, two-component model for natural convection in a porous medium, Int. J. for Num. Meth. in Fluids, 12: 655-682, 1991.

[13] Reid R.C., Praunsnitz J.M., Bruce E.P, The Properties of Gases and Liquids, 4th ed., McGraw-Hill, New York, 1987.

[14] Thomas H.R. , Sansom M.R. , Fully coupled analysis of heat, moisture and air transfer in unsaturated soil, J. Engng. Mech., 121(3): 392-405, 1995.

[15] Gawin D., A model of hygro-thermic behaviour of unsaturated concrete at high temperatures, Proc. of 2nd Int. Scientific Conference "Analytical Models and New Concepts in Mechanics of Concrete Structures", 65-71, June 12-14-1996, Lodz, Poland, 1996.

[16] Scheidegger A.E. , The Physics of Flow through Porous Media, 2nd ed., Univ. of Toronto Press, 1960.

[17] Bazant Z.P., Najjar L.J., Nonlinear water diffusion in nonsaturated concrete, Matériaux et Constructions (Paris), 5(25): 3-20, 1972.

[18] Perre P., Degiovanni A., Simulation par volumes finis des transfers couplés en milieux poreux anisotropes: séchage du bois à basse et à haute température, Int. J. Heat Mass Transfer, 33(11): 2463-2478, 1990.

[19] Baroghel-Bouny V., Mainguy M., Lassabatere T., Coussy O., Characterization and identification of equilibrium and transfer moisture properties for ordinary and high-performance cementitious materials, Cement and Concreat. Res., 29: 1225-1238, 1999.

[20] Schrefer B.A., Khoury G.A., Gawin D., Majorana C.E., Thermo-hydro-mechanical modelling of high performance concrete at high temperatures, Engineering Computations, 19(7): 787-819, 2002.

[21] Khoury G.A., Majorana C.E., Pesavento F., Schrefer B.A., Modelling of heated concrete, Mag. of Concrete Research, 54(2): 77-101, 2002.

[22] Gawin D., Lefik M., Schrefler B.A., ANN approach to sorption hysteresis within a coupled hygro-thermo-mechanical FE analysis, Int. J. Numer. Meth. Engng., 50(2): 299-323, 2001.

[23] Bear J., Dynamics of fluids in porous media, American Elsevier, New York, 1972.

[24] Bazant Z.P., Thonguthai W., Pore pressure in heated concrete walls: theoretical prediction, Mag. of Concrete Research, 31(107): 67-76, 1979.

[25] Dal Pont S., Durand S., Schrefler B.A., A multiphase thermo-hydro-mechanical model for concrete at high temperatures-Finite element implementation and validation under LOCA load, Nuclear Engineering and Design, 237: 2137–2150, 2007.

[26] Lewis R.W, Schrefler B.A., The finite element method in the static and dynamic deformation and consolidation of porous media, 2nd ed., John Wiley & Sons, Chichester, 1998.

[27] Brite Euram III BRPR-CT95–0065 Hiteco, Understanding and industrial application of high performance concrete in high temperature environment-Final Report, 1999.

Chapter 6

Parameter sensitivity analysis of concrete mathematical model

6.1 Introduction

In the previous chapters the mathematical model used to describe the full dynamic behaviour of concrete, considered as a partially saturated porous medium, has been presented; moreover different aspects concerning the behaviour of this material subjected to high temperatures and pressures has been analysed.

It has been shown that during heating, one observes several interacting physical and chemical phenomena resulting in significant changes of the material inner structure and properties. The resulting model for the analysis of concrete is therefore very complex and sophisticated because it must considers the whole complexity and mutual interactions of the possible physical processes; moreover it deals with several fields strongly coupled end it requires several number of material parameters.

From this background derives the necessity to systematically determine the influence that the parameters of this model have on the solution of the model itself. Thus enables a reduction in the parameter number, suggesting which parameters should be determined in an accurate way for obtaining acceptable results and which can simply be found from literature; in addition the identification of parameters influence should allows to proceed to a simplification of the mathematical models (model reduction).

The influence that the material parameters have on the solution of the equations set which characterize the model is called parameter sensitivity and can be computed through a sensitivity analysis. As shown in chapter 2 there are many methods for generating the desired sensitivities. First, the parameter sensitivities can be analytically

derived by hand, which is typically most accurate and efficient; however, for complicated problems, like the one taken into consideration, this can be a tedious, error-prone and time-consuming process. Numerical methods are therefore preferred in general; one classical numerical method is finite differencing, which finds approximation formulas of derivatives by truncating a Taylor series of a function about a given point. This technique is very simple to implement, but it requires repeated solutions of the model upon perturbation of each parameter. Moreover it suffers from large truncation and rounding errors, especially for high-order derivatives. Another method to achieve sensitivity analysis consists in automatic differentiation (AD): it is a chain rule based evaluation technique for obtaining the parameter sensitivities of mathematical models, using tools that generate automatically differentiated model equations.

In this work the automatic differentiation technique has been adopted to carry out sensitivity analysis, whereas the finite difference method has been used to validate the obtained results.

In the following the procedure used to perform the sensitivity analysis of the mathematical model for the description of concrete behaviour at high temperature will be described.

6.2 Comes-HTC

Comes-HTC is a software written in Fortran90, developed by Padova University, which implements the mathematical model previously described, for the analysis of the hygro-thermal-mechanical behaviour of concrete structures exposed to high temperature.

Through the mathematical model used to develop the core of Comes-HTC it is possible:

- the evaluation of the different discrete fluid phases effects;
- the analysis of the high temperature concrete behaviour;
- the use of specific high performance concrete constitutive modelling;
- the prediction of the possible occurrence of concrete spalling phenomena.

Comes-HTC can be useful in nuclear and civil engineering, for the analysis of concrete structures of nuclear reactors in hypotetical core-distruptive accidents or in operative conditions, and for the evaluation of fire resistance in industrial and civil concrete structures.

This code is a two dimensional time transient finite element program finalised at the evaluation of the distribution of temperature, gas (moisture), liquid and water vapour, stress and strains fields in concrete structures, under any applied force, thermal and hygrometric conditions, in any temperature range between 20°C and 800°C.

The problem unknowns are the following: temperature, capillary pressure, gas pressure and displacements. These data allow the calculation of derived outputs (saturation, stress-strain fields, water content, damage, etc.). The model is based on four governing equations (see chapter 3): mass conservation of dry air, mass conservation of the water species (both liquid water and vapour, phase change and hydration and dehydration processes are considered), enthalpy conservation of the whole medium and linear momentum of the multiphase system. They are completed by an appropriate set of constitutive and state equations, as well as some thermodynamic relationships.

The system of differential equation governing the problems has been introduced into Comes-HTC, and has been solved following the flowchart given in figure 6.1, where the procedures involved in the sensitivity analysis are depicted.

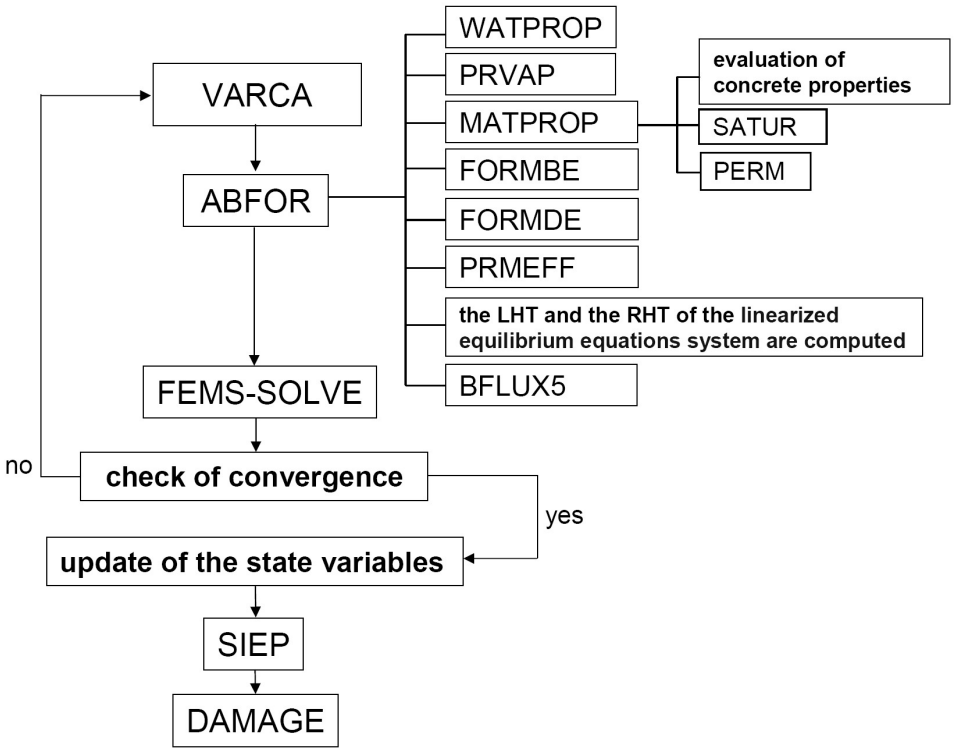

Figure 6.1: Comes-HTC flowchart (only the most important subroutines are shown)

The subroutine VARCA is the main subroutine, with regard to the automatic differ-

entiation process, and contains the Newton-Raphson loop. In VARCA there is the loop over the elements within which ABFOR is called: this subroutine computes, for each element, the left and the right hand side vector of the linearized system of equations (see section 3.8). In ABFOR there are the calls to the procedures necessary to compute the constitutive and thermodynamic relationships for the description of hygro-thermal-chemical and mechanical state of the porous material, and in particular to:

WATPROP: defines the physical properties of liquid water;

PRVAP: evaluates the vapour pressure, the vapour density and the relative humidity;

MATPROP: computes material properties for the chosen type of concrete; MATPROP calls also the subroutine which evaluates gas and water relative permeability (PERM) and the one which evaluates the saturation for the porous material (SATUR);

FORMBE: computes the strain-displacement matrix;

FORMDE: computes the elastic stress-strain matrix;

PRMEFF: evaluates the effective diffusivity of vapour inside the pores of partially saturated concrete and its effective thermal conductivity.

Finally ABFOR calls BFLUX5 which contains the flux boundary conditions formulation for gas pressure, capillary pressure, temperature and displacements.

FEM-SOLVE is the frontal solver: the function of this subroutine is to assemble the contribution of each element to form the global stiffness matrix and the global load vector and to solve the resulting set of linearized equations by gaussian direct elimination (see section 3.8):

$$\begin{aligned} &\frac{1}{\triangle t}\left[\frac{\partial}{\partial \mathbf{x}}\mathbf{C}\left(\mathbf{x}_{n+1}^{k}\right)\left(\mathbf{x}_{n+1}^{k}-\mathbf{x}_{n}\right)+\mathbf{C}\left(\mathbf{x}_{n+1}^{k}\right)\right]\triangle\mathbf{x}_{n+1}^{k} \\ &+\left[\frac{\partial}{\partial \mathbf{x}}\mathbf{K}\left(\mathbf{x}_{n+1}^{k}\right)\mathbf{x}_{n+1}^{k}+\mathbf{K}\left(\mathbf{x}_{n+1}^{k}\right)-\frac{\partial}{\partial \mathbf{x}}\mathbf{f}\left(x_{n+1}^{k}\right)\right]\triangle\mathbf{x}_{n+1}^{k} \\ &=-\left[\mathbf{C}\left(\mathbf{x}_{n+1}^{k}\right)\frac{\mathbf{x}_{n+1}^{k}-\mathbf{x}_{n}}{\triangle t}+\mathbf{K}\left(\mathbf{x}_{n+1}^{k}\right)\mathbf{x}_{n+1}-\mathbf{f}\left(x_{n+1}^{k}\right)\right] \end{aligned} \tag{6.1}$$

Once the convergence is achieved, the primary variables are updated, the mechanical stresses and strains are computed (SIEP) and it is possible to evaluate the thermo-chemical and mechanical damage in concrete. It should be underlined that, to take

into account damage of concrete, caused by a combined action of hygro-thermal and mechanical factors, a two stage solution strategy is applied, allowing to obtain a converging solution at every time step. First an intermediate problem with "fixed" damage value, obtained at the previous time step, is solved using Newton-Raphson method. Then, starting from this intermediate state, the "final" solution with variable damage is obtained by modified Newton-Raphson method, using the tangential or Jacobian matrix from the last iteration of the first stage (initial stress method) [1].

6.3 Tapenade

To perform sensitivity analysis of the fem code Comes-HTC with automatic differentiation we used Tapenade, which is an AD tool developed at INRIA Sophia Antipolis by the TROPICS team [2]. The software is written in Java, and it applies source transformation to codes written in Fortran77, Fortran95, Fortran90 and C. The extension for C has been released in 2008, and is still more experimental than the one for Fortran.

Tapenade is based on the source transformation approach which changes the semantics of the source code: in fact the original code's statements that calculate real valued variables are augmented with additional statements to calculate their derivatives, generating a new program.

Tapenade differentiates computer programs according to the model described in section 2.4; through programs differentiation the relationships between the independent variables, X, and the dependent ones, $Y = F(X)$, can be assessed determining quantitatively how the solution of a model depends on certain parameters in the model formulation.

Tapenade supports three modes of differentiation:

- the tangent mode that computes the directional derivatives or sensitivities: $F'(X) \times \dot{X}$ (where $F'(X)$ is the entire Jacobian matrix);
- the vector or multi-directional tangent mode that computes $F'(X) \times \dot{X}_n$ for several directions X_n simultaneously;
- the reverse mode that computes the gradient $F'^T(X) \times \bar{X}$.

The multi-directional reverse mode is not implemented, although this could be done if needed. In Tapenade a specific mode for the computation of higher degree derivatives

doesn't exist, however they can be obtained through repeated application of tangent AD on tangent and/or reverse AD.

In this work the multi-directional tangent mode analysis has been performed. The multi-directional differentiation is based on spreading each memory cell that holds a single derivative: instead of holding just a scalar, it holds an array whose dimension is represented by the maximum number of differentiation "directions". When performing this type of analysis with Tapenade, several aspects must be noted:

- differentiated variables have an extra dimension with respect to their original variable;

- since Fortran does not allow a function to return an array, differentiated function must become subroutines;

- a simple instruction, as for instance an assignment, produces a differentiated instruction which is a loop that iterates for each differentiation direction. To minimize the number of loops Tapenade performs a data dependencies analysis to reorder the differentiated instructions. The goal is to create sequences of differentiated loops, as long as possible, and then to merge these loops because they have the same iteration space.

Tapenade usually does not produce a perfect differentiated program at first try. After AD, a validation step is necessary to check the computed derivatives [3, 4, 5]. Validation does not represent a disadvantage itself, but rather denies the option of accepting *a priori* AD code as correct.

A common technique to check validation of the derivatives computed by means of the tangent mode, is to compare them with finite differences approximations. Recalling the notations adopted in section 2.4, we differentiate a program P that computes a function F, with input $X \in \mathbb{R}^n$ and output $Y = F(X) \in \mathbb{R}^m$. By applying the formula for a differentiable function f of a scalar variable $x \in \mathbb{R}$:

$$f'(X) = \lim_{\varepsilon \to 0} \frac{f(x+\varepsilon) - f(\varepsilon)}{\varepsilon} \tag{6.2}$$

We recall that for a given direction $\dot{X}$ in the input space, the output of the tangent mode should be $\dot{Y} = F'(X) \times \dot{X}$. Introducing function g of scalar variable h: $g(h) = F(X + h \times \dot{X})$, expanding g' at input $h = 0$ with equation (6.2) (on the left hand side) and with the chain rule (on the right hand side) we can write

$$\lim_{\varepsilon \to 0} \frac{F\left(X + \varepsilon \times \dot{X}\right) - F(X)}{\varepsilon} = g'(0) = F'(X) \times \dot{X} = \dot{Y} \tag{6.3}$$

so that we can approximate $\dot{Y}$ with the forward difference method by running F twice, on X and on $X + \varepsilon \times \dot{X}$. Using the same procedure described for the forward difference it is possible to approximate $\dot{Y}$ with the backward and the central difference method.

6.4 Applying sensitivity analysis to Comes-HTC

The aim of sensitivity analysis, applied to the fem code Comes-HTC, is the computation of the material parameters influence on the hygro-thermal-mechanical behaviour of concrete exposed to thermal loads. The solutions that the fem code Comes-HTC computes are the state variables of the mathematical model: gas pressure, capillary pressure, temperature and displacements; by means of these data the calculation of important derived quantities (e.g. saturation, vapour pressure, relative humidity, stress-strain fields, thermo-chemical damage, etc.) it is possible. The state variables and their derived quantities are the object of sensitivity analysis.

Sensitivity analysis requires the differentiation of the matrices involved in the solution of the equations set governing the problem. Tapenade allows to obtain the differentiated system of the model equations through the analysis of the dependencies between the independent variables of the original code, i.e. the material parameters, and the dependent variables involved in the sensitivity analysis.

The first step in using Tapenade, in particular to derive Comes-HTC, is to identify which subroutines implement the mathematical functions that we want to differentiate. Then the code should be shared in two parts corresponding respectively to the reading of data and initialization of the model, and to the calculation along time. Therefore only the part of the code that achieves the computations must be differentiated.

The next step is to identify the top-level routine, i.e. the routine from which all functions and subroutines, that affect the dependent variables, are called. In this stage one must have selected the appropriate dependent variables, whose derivatives are required, and the independent variables, with respect to which it must differentiate. In our case, the independent variables are the material parameters and the dependent variables are the state variables and their derived quantities.

When defining the top-routine, it is also necessary to supply Tapenade with all the subroutines that are called from the top routine, and whose differentiation is needed for the computation of the sensitivity coefficients.

The main drawback of Automatic Differentiation, applied to complex mathematical model as the one implemented in Comes-HTC, is that the differentiation of the total

program at one time is automatic only theoretically, because Tapenade doesn't detect all the dependencies between the independent variables (material parameters) and the dependent ones (state variables and derived quantities). To properly apply the automatic differentiation, one should have sufficient knowledge of how each model variable is propagated within the code. In practice, to obtain correct results, it is necessary to perform AD on the single subroutines: therefore the variables must be defined as independent or dependent according to the role that they play in each subroutine.

Moreover in Tapenade some little bugs are still present, and sometimes the chain rule, which is used to compute derivatives, is not applied correctly. For these reason, all the derivatives computed by Tapenade have been manually checked.

Tapenade gives as output the differentiated code; after AD a validation step is required and consists in comparing the derivatives (sensitivity coefficients) computed by Tapenade with the ones calculated with the finite differences approximations. With finite differences it is important to pay attention to the choice of the parameter perturbations that can influences the reliability of the method itself.

Initially we used both the central and the forward difference method, and we observed that the second one gives a satisfactory estimation of the derivatives, with a lower numerical effort. Hence, since the finite difference method is one of most computationally expensive strategy, especially in case of long running programs as Comes-HTC, we used the forward method for checking the entire derived code, to not increase the computation cost of the validation step.

6.4.1 Differentiation process on Comes-HTC

As previously explained, sensitivity analysis is a formal procedure to determine quantitatively how the solution of a model depends on certain parameters present in the model formulation. The parameters chosen in this work are the concrete properties at ambient temperature $T_0 = 293.15\,K$. In particular to perform sensitivity analysis we have selected two hygrometric variables, porosity n_0 and intrinsic permeability k_0, two thermal variables, solid thermal conductivity χ_0 and solid specific heat C_{ps0}, and two mechanical variables, Young's modulus E_0 and cubic thermal expansion coefficient β_{s0}. This material parameters are summarized in the vector $\mathbf{p}$:

$$\mathbf{p} = [n_0,\, k_0,\, \chi_0,\, C_{ps0},\, E_0,\, \beta_{s0}] \tag{6.4}$$

The adopted numerical model accounts for strong coupling mechanisms between the different processes that concern concrete elements exposed to high temperature; in fact here we deal with three fields that interact each other: the hygrometric field, the thermal field and the mechanical field. Because of this coupling, all the variables needed to describe concrete behaviour are strongly interconnected.

The differentiation process has required a preliminary identification of all the dependencies between the variables, that in each subroutine are linked following different pathways. After that, we started with AD, giving to Tapenade the single subroutines implemented in Comes-HTC.

The goal of sensitivity analysis is to compute the sensitivity coefficients, i.e. the derivatives, of the state variables and of the quantities from them derived. In order to do this, within the Newton-Raphson loop, for each time step n and at the end of each iteration k, the system of linearized equations governing the problem (6.1), that can be written in the general form

$$\mathbf{A}\left(\mathbf{x}_{n+1}^{k}\right) \triangle \mathbf{x}_{n+1}^{k} = \mathbf{b}\left(\mathbf{x}_{n+1}^{k}\right) \tag{6.5}$$

must be differentiated. In (6.5) $\mathbf{A}\left(\mathbf{x}_{n+1}^{k}\right)$ is the left-hand side, i.e. the Jacobian matrix, $\mathbf{b}\left(\mathbf{x}_{n+1}^{k}\right)$ is the right-hand side, i.e. the residuum vector, and $\triangle \mathbf{x}_{n+1}^{k}$ is the solution vector, which holds the increment of the state variables. It should be underlined, that both $\mathbf{A}\left(\mathbf{x}_{n+1}^{k}\right)$ and $\mathbf{b}\left(\mathbf{x}_{n+1}^{k}\right)$ are function of the material parameters vector $\mathbf{p}$. Differentiating equation (6.5) with respect to the material parameters, we obtain:

$$\mathbf{A}\left(\mathbf{x}_{n+1}^{k}\left(\mathbf{p}\right)\right) \frac{d \triangle \mathbf{x}_{n+1}^{k}\left(\mathbf{p}\right)}{d\mathbf{p}} + \frac{d\mathbf{A}\left(\mathbf{x}_{n+1}^{k}\left(\mathbf{p}\right)\right)}{d\mathbf{p}} \mathbf{x}_{n+1}^{k}(\mathbf{p}) = \frac{d\mathbf{b}\left(\mathbf{x}_{n+1}^{k}\left(\mathbf{p}\right)\right)}{d\mathbf{p}} \tag{6.6}$$

So, the sensitivity coefficient of the increment vector of the state variables is given by the solution of

$$\mathbf{A}\left(\mathbf{x}_{n+1}^{k}\left(\mathbf{p}\right)\right) \frac{d \triangle \mathbf{x}_{n+1}^{k}\left(\mathbf{p}\right)}{d\mathbf{p}} = \frac{d\mathbf{b}\left(\mathbf{x}_{n+1}^{k}\left(\mathbf{p}\right)\right)}{d\mathbf{p}} - \frac{d\mathbf{A}\left(\mathbf{x}_{n+1}^{k}\left(\mathbf{p}\right)\right)}{d\mathbf{p}} \left(\mathbf{x}_{n+1}^{k}\left(\mathbf{p}\right)\right) \tag{6.7}$$

where

$$\begin{aligned} \frac{d\mathbf{b}\left(\mathbf{x}_{n+1}^{k}\left(\mathbf{p}\right)\right)}{d\mathbf{p}} &= \frac{\partial \mathbf{b}\left(\mathbf{x}_{n+1}^{k}\left(\mathbf{p}\right)\right)}{\partial \mathbf{x}} \frac{d\mathbf{x}_{n+1}^{k}\left(\mathbf{p}\right)}{d\mathbf{p}} \\ \frac{d\mathbf{A}\left(\mathbf{x}_{n+1}^{k}\left(\mathbf{p}\right)\right)}{d\mathbf{p}} &= \frac{\partial \mathbf{A}\left(\mathbf{x}_{n+1}^{k}\left(\mathbf{p}\right)\right)}{\partial \mathbf{x}} \frac{d\mathbf{x}_{n+1}^{k}\left(\mathbf{p}\right)}{d\mathbf{p}} \end{aligned} \tag{6.8}$$

Therefore, once the convergence of the system (6.5) is achieved and the increment of state variables $\triangle \mathbf{x}_{n+1}^{k}$ is obtained, it is possible to calculate the sensitivity coefficient of $\triangle \mathbf{x}_{n+1}^{k}$ solving a system in which the left-hand side is exactly the one that is required by (6.5), and the right-hand side can be computed by means of the derivatives of $\mathbf{A}\left(\mathbf{x}_{n+1}^{k}(\mathbf{p})\right)$ and $\mathbf{b}\left(\mathbf{x}_{n+1}^{k}(\mathbf{p})\right)$.

Sensitivity must be computed incrementally, i.e. to obtain either the incremental or, equivalently, end-of-step sensitivity vector one needs to know the sensitivities at the beginning of the step. Consequently, the sensitivity coefficients have to be first computed at the end of the step; next properly updated and then stored for the next step use. Therefore, at the end of each iteration, the sensitivity coefficients of the primary variables are updated, by using the same procedure adopted for the primary variables themselves (see section 3.8):

$$\begin{aligned} \mathbf{x}_{n+1}^{k+1} &= \mathbf{x}_{n+1}^{k} + \triangle \mathbf{x}_{n+1}^{k} \\ \frac{d\mathbf{x}_{n+1}^{k+1}(\mathbf{p})}{d\mathbf{p}} &= \frac{d\mathbf{x}_{n+1}^{k}(\mathbf{p})}{d\mathbf{p}} + \frac{d\triangle \mathbf{x}_{n+1}^{k}}{d\mathbf{p}} \end{aligned} \tag{6.9}$$

For sake of brevity, in the following we will write:

$\mathbf{A}(\mathbf{x}(\mathbf{p}))$	for	$\mathbf{A}\left(\mathbf{x}_{n+1}^{k}(\mathbf{p})\right)$
$\mathbf{b}(\mathbf{x}(\mathbf{p}))$	for	$\mathbf{b}\left(\mathbf{x}_{n+1}^{k}(\mathbf{p})\right)$
$\mathbf{x}(\mathbf{p})$	for	$\mathbf{x}_{n+1}^{k}(\mathbf{p})$
$\triangle \mathbf{x}$	for	$\triangle \mathbf{x}_{n+1}^{k}$

Note that, for each time step Comes-HTC solves a set of linearized equation using the iterative Newton-Raphson iteration that generates a sequences of approximations of the exact solution. The mechanical application of AD on this kind of method gives a sequences of derivatives of the approximate solutions with the same number of iterations as the original solver. The reason is that AD keeps the flow of control of the original program in the differentiated program. In particular the convergence tests are still based only on the non-differentiable variables. One may wonder whether and how AD produced derivatives are reasonable approximations to the desired derivatives of the exact solution. The issues of derivative convergence for iterative solvers in relation to automatic differentiation are discussed in [6, 7].

We want to emphasize here that we did not optimize our differentiated code for speed, e.g. we calculate the derivatives in each Newton-Raphson iteration, whereas it would only be necessary to do this in the last iteration of the time step.

Before continuing, we shall briefly discuss what we mean when we speak about implicit and explicit function dependence, because it concerns the essence of the notion of sensitivity. By saying that a function $F(X)$ is explicitly dependent on the argument X, we mean that the numerical value of X it is directly present in the formulation of the function itself. By saying that a function $F(X)$ is implicitly dependent on the argument X we mean that, given a numerical value of X, in order to compute the value of $F(X)$ some further calculation, usually non trivial and typically requiring the solution of a set of differential equations, are necessary. In other words, having X does not suffice to directly evaluate the value of $F(X)$.

In the following, the main stages of the differentiation process are described, showing how handle the fem code to produce correct derivatives. In particular we will focus on the analysis of the more significant derivatives computed by the subroutines called by Abfor, which is the subroutine which computes the right-hand side and the left hand side of the system of equations (6.5).

6.4.2 Sensitivity coefficients of liquid water properties

WATPROP is the first subroutine called by ABFOR and computes the physical properties of liquid water.

Water properties are: density ρ^w, enthalpy of evaporation $\triangle h_{vap}$, viscosity μ^w, specific heat C_{pw} and thermal conductivity χ^w; the last two water properties are constant therefore they are not involved in the differentiation process. Instead, the first three water properties are all directly dependent on temperature which is in turn implicitly linked to the material parameters.

Thus the following dependencies are given:

$$\begin{aligned} \rho^w &= \rho^w(T(\mathbf{p})) \\ \triangle h_{vap} &= \triangle h_{vap}(T(\mathbf{p})) \\ \mu^w &= \mu^w(T(\mathbf{p})) \end{aligned} \tag{6.10}$$

The sensitivity coefficients of water density, enthalpy of evaporation and water viscosity are obtained deriving equations (5.23), (5.26) and (5.27). It results:

$$\begin{aligned}
\frac{d\rho^w}{d\mathbf{p}} &= \frac{dT}{d\mathbf{p}}\left[b_1 + 2b_2T + 3b_3T^2 + 4b_4T^3 + 5b_5T^4\right] \\
&\quad + \left(p_{w1} - p_{wrif}\right)\frac{dT}{d\mathbf{p}}\left[a_1 + 2a_2T + 3a_3T^2 + 4a_4T^3 + 5a_5T^4\right] \qquad (6.11)\\
\frac{d\triangle h_{vap}}{d\mathbf{p}} &= 0.38 \cdot 12.672 \cdot 10^5 \cdot \left(T - T_{cr}\right)^{0.38-1}\frac{dT}{d\mathbf{p}} \\
\frac{d\mu^w}{d\mathbf{p}} &= -1.562 \cdot 0.6612 \cdot \left(T - 229\right)^{-1.562-1}\frac{dT}{d\mathbf{p}}
\end{aligned}$$

It should be underlined that the state variable T is obviously dependent on the material parameter vector $\mathbf{p}$ only implicitly; the value of the derivative $dT/d\mathbf{p}$ results from equation $(6.9)_2$.

6.4.3 Sensitivity coefficients of terms linked to water vapour

In PRVAP are evaluated the water vapour pressure p^{gw}, and the dynamic viscosity of moist air μ^g.

The first term is assumed function of the water vapour saturation pressure and of the relative humidity; whereas the second term is assumed function of the water vapour and dry air dynamic viscosity, and of the ratio of water vapour and gas pressures. Analyzing how the different variables are interconnected, the following dependencies can be recognized:

$$\begin{aligned}
p^{gw} &= p^{gw}\left(p^{gws},\, RH\right) \\
\mu^g &= \mu^g\left(\mu^{ga},\, \mu^{gw},\, p^{gw},\, p^g\right)
\end{aligned} \qquad (6.12)$$

In order to evaluate p^{gw} and μ^g, PRVAP must also compute the quantities in brackets in the left side of equation (6.12); we have:

$$\begin{aligned}
p^{gws} &= p^{gws}\left(T\left(\mathbf{p}\right)\right) \\
RH &= RH\left(p^c\left(\mathbf{p}\right),\, \rho^w\left(T\left(\mathbf{p}\right)\right),\, T\left(\mathbf{p}\right)\right)
\end{aligned} \qquad (6.13)$$

and

$$\begin{aligned}
\mu^{ga} &= \mu^{ga}\left(T\left(\mathbf{p}\right)\right) \\
\mu^{gw} &= \mu^{gw}\left(T\left(\mathbf{p}\right)\right) \\
p^g &= p^g\left(\mathbf{p}\right)
\end{aligned} \qquad (6.14)$$

By means of this dependencies, the total derivatives of the water vapour pressure can

be obtained deriving equations (5.1) and (5.25):

$$\begin{aligned}
\frac{dp^{gw}}{d\mathbf{p}} &= \frac{dp^{gws}}{d\mathbf{p}} RH + p^{gws}\frac{dRH}{d\mathbf{p}} \\
\frac{dp^{gws}}{d\mathbf{p}} &= p^{gws}\frac{dT}{d\mathbf{p}}\left[\frac{C_1}{T^2} + C_3 + 2C_4T + 3C_5T^2 + \frac{C_6}{T}\right] \\
\frac{dRH}{d\mathbf{p}} &= -RH\frac{M_w}{R\left(\rho^w T\right)^2}\left[\frac{dp^c}{d\mathbf{p}}\rho^w T - p^c\left(\frac{d\rho^w}{d\mathbf{p}}T + \frac{dT}{d\mathbf{p}}\rho^w\right)\right]
\end{aligned} \tag{6.15}$$

while the total derivatives of dynamic viscosity of moist air can be obtained deriving equation (5.28). We remind that, by the state equation for perfect gas, $p^{ga} = p^g - p^{gw}$.

$$\begin{aligned}
\frac{d\mu^g}{d\mathbf{p}} &= \frac{d\mu^{gw}}{d\mathbf{p}} + \left(\frac{d\mu^{ga}}{d\mathbf{p}} - \frac{d\mu^{gw}}{d\mathbf{p}}\right)\left(1 - \frac{p^{gw}}{p^g}\right)^{0.608} \\
&\quad - \left(\mu^{ga} - \mu^{gw}\right)\frac{0.608}{\left(p^g\right)^2}\left(1 - \frac{p^{gw}}{p^g}\right)^{0.608-1}\left(\frac{dp^{gw}}{d\mathbf{p}}p^g - p^{gw}\frac{dp^g}{d\mathbf{p}}\right) \\
\frac{d\mu^{gw}}{d\mathbf{p}} &= \alpha_v\frac{dT}{d\mathbf{p}} \\
\frac{d\mu^{ga}}{d\mathbf{p}} &= \frac{dT}{d\mathbf{p}}\left[\alpha_a + 2\beta_a\left(T - T_0\right)\right]
\end{aligned} \tag{6.16}$$

The total derivatives of capillary and gas pressure, which are present in equations $(6.15)_3$ and $(6.16)_1$, can be obtained by $(6.9)_2$ recalling that these state variables depend implicitly on the material parameter.

6.4.4 Sensitivities coefficients of the material properties

Sensitivity analysis has been performed using as independent variables concrete properties at ambient temperature $T_0 = 293.15\,K$. Nevertheless, as shown in section 5.6, material parameters are not constant, but they change according to the hygro-thermo-mechanical state of the material. The derivatives of material parameters, which depend on the parameter vector $\mathbf{p}$, must be computed because they appear in the definition of the Jacobian matrix $\mathbf{A}$ and of the residuum vector $\mathbf{b}$.

Porosity

Increasing temperature produces an evolution in microstructure characteristics and in particular an increase of porosity. Porosity is taken into account as a function of the parameter vector and of temperature:

$$n = n\left(\mathbf{p},\, \mathbf{T}\left(\mathbf{p}\right)\right) \tag{6.17}$$

More precisely, equation (5.57) shows that porosity n is linked to $\mathbf{p}$ only through its first component, i.e n_0.

The total derivative of n with respect to $\mathbf{p}$ is obtained via:

$$\frac{dn}{d\mathbf{p}} = \frac{\partial n}{\partial \mathbf{p}} + A_n \frac{d\mathbf{T}}{d\mathbf{p}} \tag{6.18}$$

where

$$\frac{\partial n}{\partial \mathbf{p}} = \begin{cases} 1 & \text{if } p_i = n_0 \\ 0 & \text{otherwise} \end{cases} \tag{6.19}$$

Permeability

The computation of permeability highlights the full coupling between the hygral, thermal and mechanical field. Intrinsic permeability, in fact, depends on the hygrometric field through gas pressure and intrinsic permeability itself at temperature T_0, on the thermal field through temperature, and on the mechanical field through the total damage parameter:

$$k = k\left(\mathbf{p},\, p^g\left(\mathbf{p}\right),\, T\left(\mathbf{p}\right),\, p^g\left(\mathbf{p}\right),\, D\left(\mathbf{p}\right)\right) \tag{6.20}$$

Deriving equation (5.61), one obtains the sensitivity coefficient of intrinsic permeability:

$$\begin{aligned} \frac{dk}{d\mathbf{p}} \;=\; & \frac{\partial k}{\partial \mathbf{p}} + k_0 10^{f(T)} 10^{A_D D} \left\{ \left(\frac{p^g}{p_0^g}\right)^{A_P} \ln 10 \left[\frac{df\left(T\right)}{d\mathbf{p}} \right.\right. \\ & \left.\left. + A_D \frac{dD}{d\mathbf{p}} \right] + \frac{A_P}{p_0^g} \left(\frac{p^g}{p_0^g}\right)^{A_P - 1} \frac{dp_g}{d\mathbf{p}} \right\} \end{aligned} \tag{6.21}$$

The partial derivative of k and the total derivative of $f(T)$, with respect to the parameter vector, are:

$$\begin{aligned} \frac{\partial k}{\partial \mathbf{p}} \;&=\; \begin{cases} 10^{f(T)} \left(\frac{p^g}{p_0^g}\right)^{A_P} \cdot 10^{A_D D} & \text{if } p_i = k_0 \\ 0 & \text{otherwise} \end{cases} \\ \frac{df\left(T\right)}{d\mathbf{p}} \;&=\; \frac{dT}{d\mathbf{p}} \left[2A_T^2 \left(T - T_0\right) + A_T^1 \right] \end{aligned} \tag{6.22}$$

Thermal conductivity and specific heat of the solid skeleton

The relations which define the thermal conductivity of dry concrete and the specific heat of the solid skeleton are similar to the one used for the description of porosity evolution. Thermal conductivity and specific heat, in fact, are functions only of the parameter vector (the third and the fourth component respectively), and of temperature:

$$\begin{aligned} \chi_d &= \chi_d\left(\mathbf{p},\, \mathbf{T}\left(\mathbf{p}\right)\right) \\ C_{ps} &= C_{ps}\left(\mathbf{p},\, \mathbf{T}\left(\mathbf{p}\right)\right) \end{aligned} \tag{6.23}$$

The sensitivities of χ_d and C_{ps}, with respect to $\mathbf{p}$, are given by (5.65) and (5.67):

$$\begin{aligned} \frac{d\chi_d}{d\mathbf{p}} &= \frac{\partial \chi_d}{\partial \mathbf{p}} + \chi_{d0} A_\chi \frac{d\mathbf{T}}{d\mathbf{p}} \\ \frac{dC_{ps}}{d\mathbf{p}} &= \frac{\partial C_{ps}}{\partial \mathbf{p}} + C_{ps0} A_0 \frac{d\mathbf{T}}{d\mathbf{p}} \end{aligned} \tag{6.24}$$

where

$$\begin{aligned} \frac{\partial \chi_d}{\partial \mathbf{p}} &= \begin{cases} \left[1 + A_\chi \left(T - T_0\right)\right] & \text{if } p_i = \chi_{d0} \\ 0 & \text{otherwise} \end{cases} \\ \frac{\partial C_{ps}}{\partial \mathbf{p}} &= \begin{cases} \left[1 + A_0 \left(T - T_0\right)\right] & \text{if } p_i = C_{ps0} \\ 0 & \text{otherwise} \end{cases} \end{aligned} \tag{6.25}$$

Density of the solid skeleton

The density of the solid skeleton depends only on temperature:

$$\rho_s = \rho_s\left(T\left(\mathbf{p}\right)\right) \tag{6.26}$$

and its derivatives can easily be computed from equation (5.69):

$$\frac{d\rho_s}{d\mathbf{p}} = A_S \frac{d\mathbf{T}}{d\mathbf{p}} \tag{6.27}$$

Young's modulus and strength properties

These mechanical properties of concrete are explicitly linked to the temperature field

of the material:

$$\begin{aligned} E &= E\left(\mathbf{p}, T\left(\mathbf{p}\right)\right) \\ f_c &= f_c\left(T\left(\mathbf{p}\right)\right) \\ f_t &= f_t\left(T\left(\mathbf{p}\right)\right) \end{aligned} \tag{6.28}$$

As it can be observe in (6.28) the Young's modulus of concrete is also dependent on the material parameters vector $\mathbf{p}$.

The derivatives of equations (5.70) and (5.71) with respect to $\mathbf{p}$ yield:

$$\begin{aligned} \frac{dE}{d\mathbf{p}} &= \frac{\partial E}{\partial \mathbf{p}} + \alpha \frac{d\mathbf{T}}{d\mathbf{p}} \\ \frac{df_c}{d\mathrm{p}} &= \beta_1 \frac{d\mathbf{T}}{d\mathbf{p}} \\ \frac{df_t}{d\mathrm{p}} &= \beta_2 \frac{d\mathbf{T}}{d\mathbf{p}} \end{aligned} \tag{6.29}$$

where

$$\frac{\partial E}{\partial \mathbf{p}} = \begin{cases} 1 & \text{if } p_i = E_0 \\ 0 & \text{otherwise} \end{cases} \tag{6.30}$$

6.4.5 Sensitivity coefficients of water and gas relative permeability

The relations which define water and gas permeability link these two structure parameters to transport properties and highlight the effect of water degree of saturation on relative permeability for water and gas flow. As shown in section 5.4.1, relative permeability can be expressed as a function of liquid saturation:

$$\begin{aligned} k^{rw} &= k^{rw}\left(S\left(p^c\left(\mathbf{p}\right)\right), T\left(\mathbf{p}\right)\right) \\ k^{rw} &= k^{rg}\left(S\left(p^c\left(\mathbf{p}\right)\right), T\left(\mathbf{p}\right)\right) \end{aligned} \tag{6.31}$$

By applying the chain rule of derivative calculus to equation (6.31), the sensitivity coefficients of water and gas permeability can be computed:

$$\frac{dk^{r\pi}}{d\mathbf{p}} = \frac{\partial k^{rw}}{\partial S}\left[\frac{\partial S}{\partial p^c}\frac{dp^c}{d\mathbf{p}} + \frac{\partial S}{\partial T}\frac{dT}{d\mathbf{p}}\right] \tag{6.32}$$

where the term in square brackets represent the saturation sensitivity coefficient respect to $\mathbf{p}$.

Deriving equations (5.35) and (5.37) one obtains:

$$\frac{dk^{rw}}{d\mathbf{p}} = A^w S^{A_w - 1} \frac{dS}{d\mathbf{p}} \tag{6.33}$$

$$\frac{dk^{rw}}{d\mathbf{p}} = -\frac{A^g}{S_{cr}} \left(\frac{S}{S_{cr}} \right)^{A_g - 1} \frac{dS}{d\mathbf{p}} \tag{6.34}$$

Bibliography

[1] Gawin D., Majorana C.E., Schrefler B.A., Numerical analysis of hygro-thermal behaviour and damage of concrete at high temperature, Mechanics of Cohesive and Frictional Materials, 4: 37-74, 1999.

[2] Hascoët L., Pascual V., Tapenade 2.1 User's guide, Inria Rapport technique 300, 2004.

[3] Hascoët L., Automatic differentiation by program transformation, http://www-sop.inria.fr/tropics/papers/supportCoursDA.pdf, 2007.

[4] Souhar O., Faure J.B., Paquier A., Automatic sensitivity analysis of a finite volume model for two-dimensional shallow water flows, Journal of Environ. Fluid Mech., 7: 303-315, 2007.

[5] Cusdin P., Müller J.D., Automatic Differentiation and Sensitivity Analysis Methods for Computational Fluid Dynamics, Internal Report QUB-SAE-03-01d, 2003.

[6] Gilbert J.C., Automatic differentiation and iterative processes, Optimization Methods and Software, 1: 13-21, 1992.

[7] Griewank A., Bischof C., Corliss G., Carle A., Williamson K., Derivative convergence for iterative equation solvers, Optimization Methods and Software, 2: 321-355, 1993.

Chapter 7

Numerical example

7.1 Introduction

The model introduced in chapters 3, 4 and 5 has been developed for the analysis of the behaviour of concrete structures under severe temperature and pressure conditions.

In this chapter an application of the automatic differentiation technique (see chapter 2 and 6) to this model will be presented.

The behavior of concrete, when exposed to fire, can be determined via a model characterized by a strong coupling between three different fields: the hygrometric field, the thermal filed and the mechanical field; moreover for the definition of this model a large number of material parameters are required.

In order to determine how the physical phenomena taking place in heated concrete respond to changes in the input material parameters, a sensitivity analysis of the coupled model should be performed.

Therefore, the purpose of a sensitivity analysis of the current model is the need to determine which of the various material parameters appearing in the model definition are the most significant, in terms of their impact on the output variables. This analysis is also used to reveal how changes in the material variables affect the predicted hygro-thermal-mechanical response evolution. Finally, a careful study of the sensitivity results should allows to proceed to a simplification of the mathematical model (model reduction), once that has been found which are the main control parameters of the model.

The aim of this chapter is a step in this direction, i.e. a characterization of the material parameters influence on the hygro-thermal-mechanical response of the heated concrete structures.

7.2 One side heating of a concrete wall

In the following is shown an example concerning the application of the sensitivity analysis to the fem code Comes-HTC.

As introduced in the previous chapter, we seek to compute the sensitivity coefficients of the model outputs with respect to the material parameters summarized in the vector **p**:

$$\mathbf{p} = [n_0,\, k_0,\, \chi_0,\, C_{ps0},\, E_0,\, \beta_{s0}] \tag{7.1}$$

The code Comes-HTC, modified by means of the automatic differentiation tool Tapenade, solves simultaneously the model equations together with the derived model equations; the modified code allows to obtain both the solution given by the original code (state variables and their derived quantities) and the sensitivity coefficients.

The example deals with a C-60 concrete wall, having thickness of 12 cm, initially at temperature of $298.15\,K$, gas pressure $p^g = 101325\,Pa$ (atmospheric pressure) and relative humidity of 60% RH. It is subjected to transient heating from one side according to a temperature curve (slow heating); the concrete wall is heated for 360 minutes. On the heated surface convective BCs are assumed with heat exchange coefficient $\alpha_c = 18\,W/M^2K$. For mass exchange convective BCs, with $p^{gw} = 1300\,Pa$ and mass exchange coefficient $\beta_c = 0.018\,m/s$, are considered. Vertical displacements u_y are constrained on the sides B, whereas horizontal displacements u_x are constrained on the side C (figure 7.1). The main characteristic parameters of the material employed in the calculation are shown in table 7.1.

Parameter	Symbol	Unit	Value
Porosity	n_0	[-]	0.082
Intrinsic permeability	k_0	[m^2]	$2 \cdot 10^{-18}$
Solid density	ρ_s	[kg/m^3]	2564
Specific heat	C^s_{p0}	[J/kgK]	855
Thermal conductivity	χ_0	[W/mK]	1.92
Young's modulus	E_0	[GPa]	34.52
Thermal expansion coefficient	β_s	[K^{-1}]	$3 \cdot 10^{-5}$
Poisson's ratio	ν	[-]	0.18
Compressive strength	f_c	[MPa]	60
Tensile strength	f_t	[MPa]	6.0

Table 7.1: Characteristic properties of a C-60 concrete at ambient temperature. Bold parameters are the ones used in the sensitivity analysis.

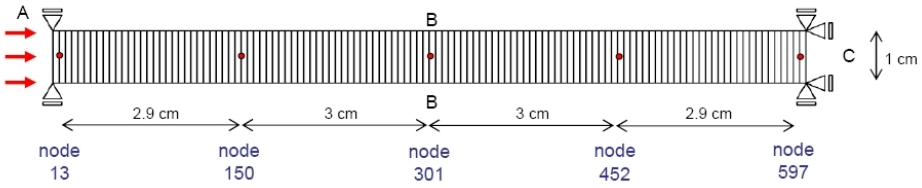

Figure 7.1: Schematization of concrete wall

Since the sensitivity coefficients s_{ij} (i^{th} model output, j^{th} material parameter) takes values spanning a wide range of magnitudes, they are normalized to make them adimensional:

$$(s_{ij})_{norm} = \left(\frac{\partial x_i}{\partial p_j}\right)_{norm} = \frac{\partial x_i}{\partial p_j}\frac{p_j}{x_i} \tag{7.2}$$

In this way, the normalized sensitivities reveal directly the relative importance of the material parameters considered with regards to the model outputs, because they allow to compare sensitivities respect to parameters whose values are orders of magnitude apart.

7.2.1 Validation of automatic differentiation with finite difference

The validity of the parameter sensitivities computed with automatic differentiation (AD) has been verified by means of the finite difference method (FD).

In the first stages of the validation process we used both the central and the forward difference method, and we observed that the second one gives a satisfactory estimation of the derivatives, with a lower numerical effort. Hence, since the finite difference method is one of most computationally expensive strategy, especially in case of long running programs as Comes-HTC, we used the forward method for checking the entire derived code, to not increase the computational cost of validation.

The forward finite differences approach has been used over a range of differencing step sizes. The main disadvantage of divided differences is that the accuracy of the approximated sensitivity coefficients depends crucially on a suitable step size. Unfortunately, an optimal or even near-optimal step size is often not known a priory: finding a reasonable perturbation of each parameter for the finite difference approximation has required many execution of the program Comes-HTC. Automatic differentiation, on the contrary, does not involve any truncation or rounding error; derivatives produced

by AD are exact up to machine precision. Nevertheless, the reliability of this method depends on the fact that the tool for differentiation detects properly all the dependencies between the independent variables (material parameters) and the dependent ones (state variables and their derived quantities), and applies correctly the chain rule to obtain derivatives.

The differentiated program produced by Tapenade has required extensive validation efforts.

Figures 7.2, 7.3, 7.4 and 7.5 show how the sensitivity coefficients computed with the finite difference method vary with the chosen step size.

In particular the figures refer to the sensitivities of the state variables p^g, p^c, T, u_x with respect to the material parameters

$$\mathbf{p} = [n_0,\, k_0,\, \chi_0,\, C_{ps0},\, E_0,\, \beta_{s0}]$$

Concerning the sensitivity coefficients of displacement, only the ones relative to the horizontal component are displayed, because the vertical displacements are constrained on all the wall.

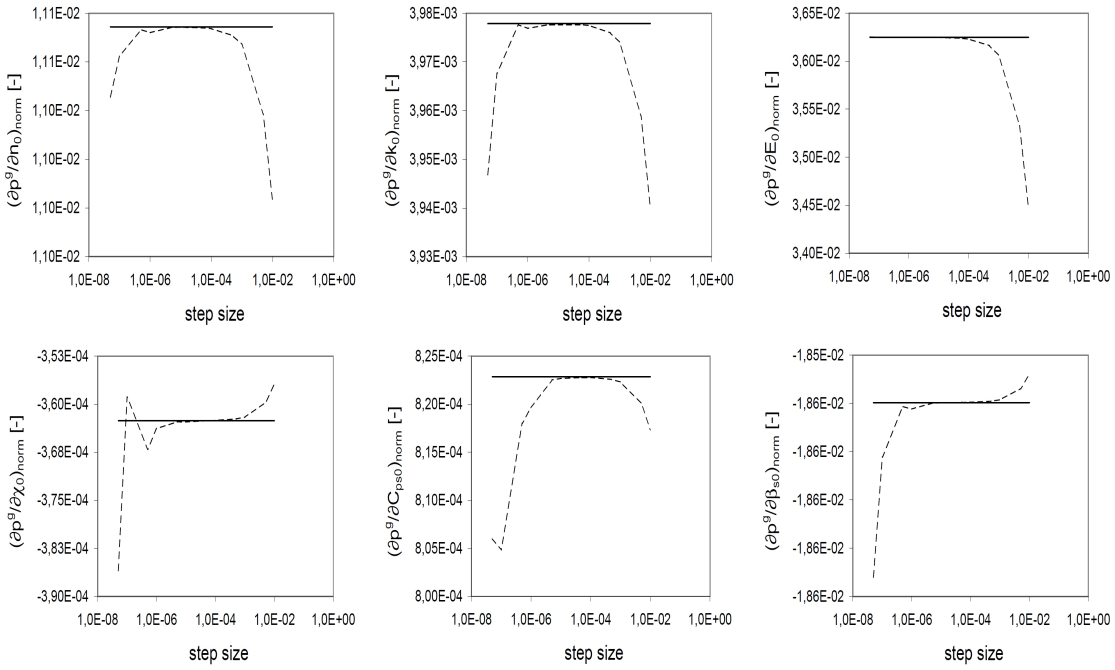

Figure 7.2: Variation with the step size of the gas pressure sensitivity coefficients computed with FD

We have found that there is a trade-off between truncation errors and round-off errors that is dependent upon the type of material parameter. Truncation errors are

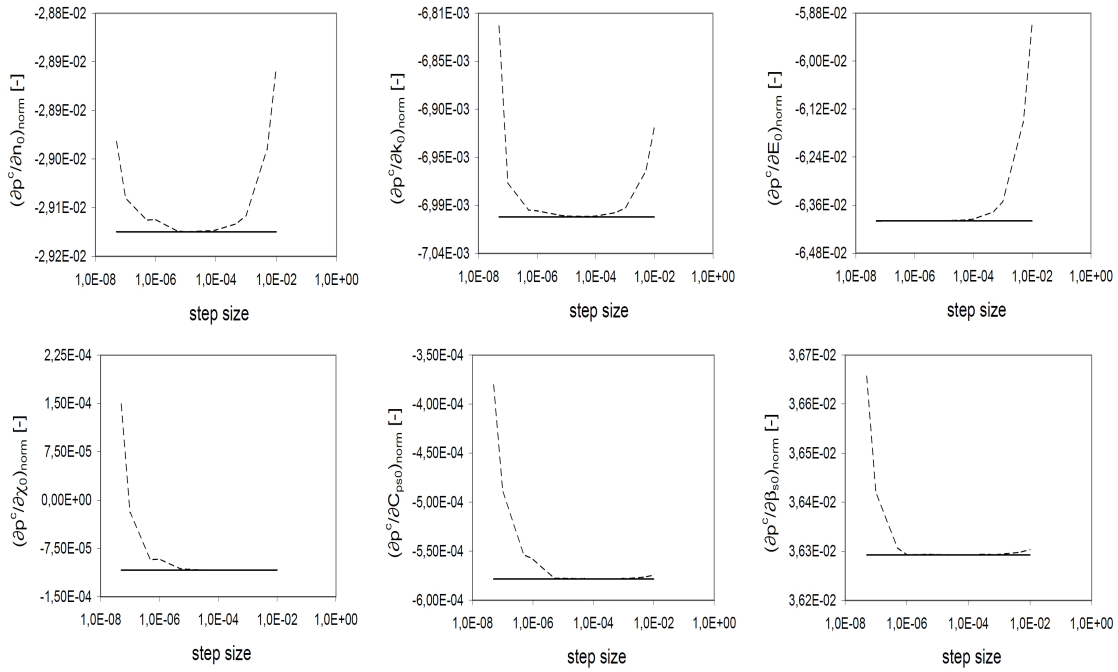

Figure 7.3: Variation with the step size of the capillary pressure sensitivity coefficients computed with FD

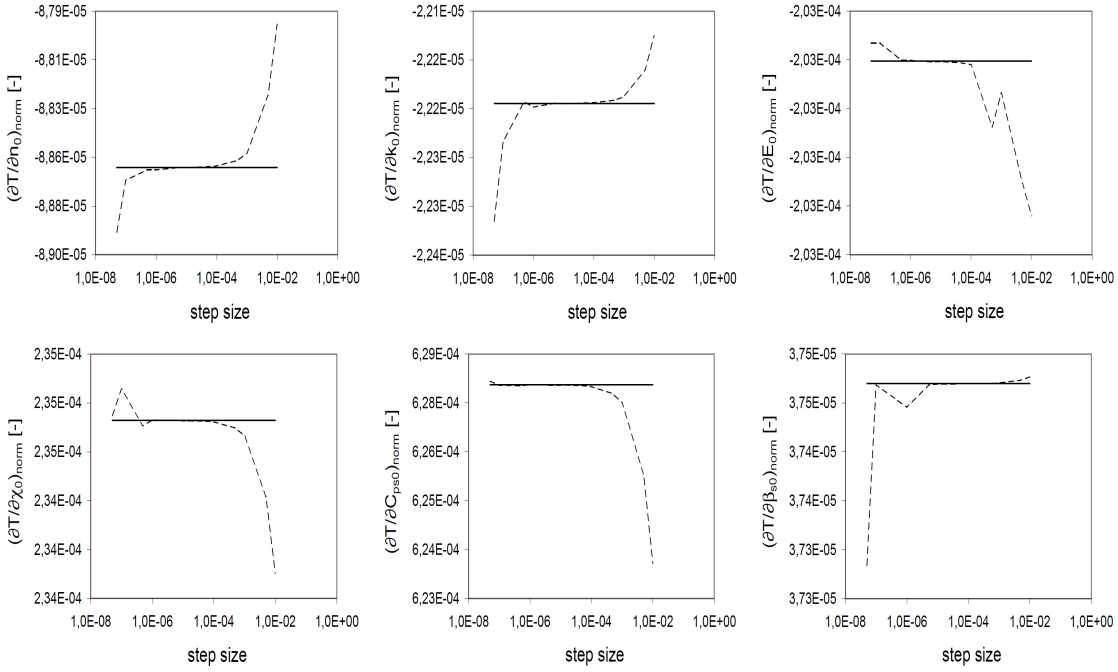

Figure 7.4: Variation with the step size of the temperature sensitivity coefficients computed with FD

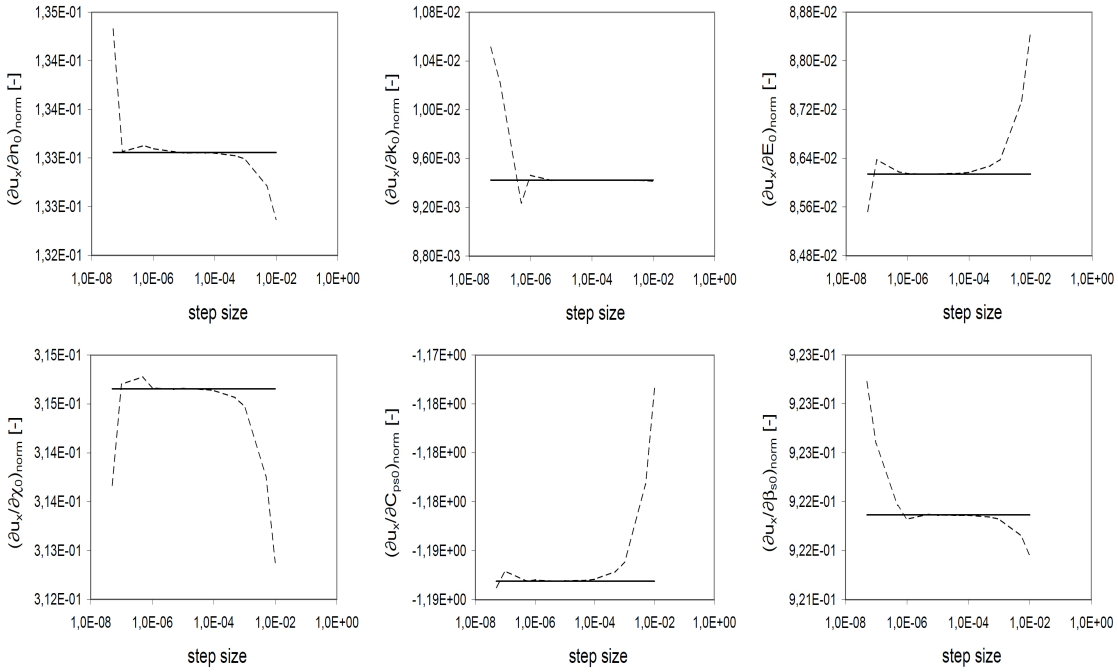

Figure 7.5: Variation with the step size of the horizontal displacement sensitivity coefficients computed with FD

larger with bigger differencing step sizes, but round-off errors are larger with smaller step sizes. As expected, using the smallest step size does not produce the best result.

To evaluate the accuracy between automatic differentiation and finite difference, we have defined, for each state variable and for each material parameter, the difference between the sensitivity coefficients computed with the two methods. This difference allows to define the error

$$error_{ij} = \frac{(s_{ij})_{norm}\big|_{AD} - (s_{ij})_{norm}\big|_{FD}}{(s_{ij})_{norm}\big|_{AD}} \tag{7.3}$$

The mean error for each material parameter, defined as

$$\overline{error}_j = \frac{\sum_{i=1}^{n} \left(\frac{(s_{ij})_{norm}\big|_{AD} - (s_{ij})_{norm}\big|_{FD}}{(s_{ij})_{norm}\big|_{AD}} \right)}{n} \tag{7.4}$$

where n is the number of state variable, has enabled to choose the best variation of the material parameters for computing the sensitivity coefficient with FD (figure 7.6). With the best perturbation, for most of the material parameters, is observed an agreement of 4–6 significant digits between the forward finite difference and the automatic differ-

entiation results, which indicates that the sensitivity coefficients are properly evaluated with the latter technique.

All the sensitivity results that will be shown in the following, have been computed using the automatic differentiation technique and validated by the forward finite difference, using the best perturbation for each material parameter.

7.2.2 Results

The sensitivity coefficients computed during the heating process are presented in normalized form. They are displayed at different time stations of the heating process and in different position of the concrete wall (see figure 7.1). For sake of clarity, the results concerning the description of physical phenomena occurring in the heated concrete wall are also shown, to better understand the link between the state variables (and the quantities from them derived) and their sensitivity coefficients.

An increase of temperature and desaturation of concrete is observed in the whole thickness of the wall; the desaturation is caused mainly by the evaporation of water. The temperature values increase progressively and, at the end of the process, the zone close to the heated surface reaches about 620 K, whereas the opposite side reaches about 420 K (fig. 7.7). Due to moisture evaporation, the relative humidity in the surface zone decreases to a very low value (fig. 7.8), and a sharp front, separating the moist and dry material, moves inwards. Close to this front an intensive evaporation takes place, resulting in formation of a zone in which vapour pressure increases considerably (fig. 7.9).

The heat flow causes water migration in the wall; because of this, the values of vapour and gas pressure initially increase up to about 0.4 MPa and the peaks move slowly toward the internal part of the wall. After about 270 min both the vapour and the gas pressure reach the peak in the zone opposite to the heated side; then they start to decrease step by step as the surface temperature moves inwards, moisture evaporates and consequently saturation decreases (figs. 7.9, 7.10 and 7.11). Gas pressure increase is caused by a growth of dry air pressure and vapour pressure due to heating; moreover, as can be observed by the comparison of figure 7.7 and 7.10, the highest values of gas pressure usually correspond to temperatures in the range of 420-500 K [1]. Vapour pressure gradients cause vapour flow from the heated surface toward the inner part of the wall. These vapour flows result in an increase of relative humidity above its initial value, as well as in condensation of vapour in the colder layers and subsequent slight increase of saturation. An additional increase of the liquid water volume in the material

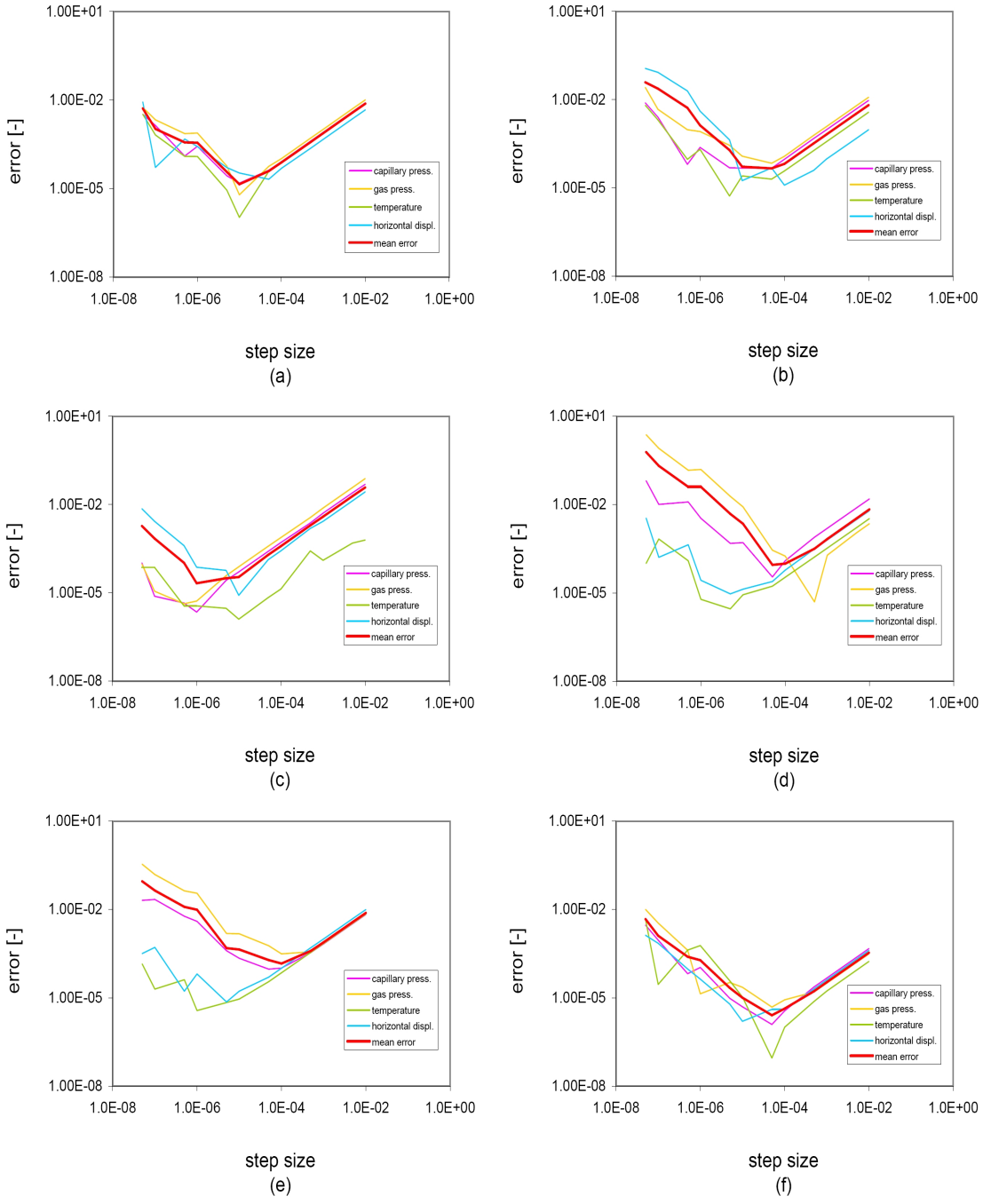

Figure 7.6: Errors in the sensitivity coefficients computed with FD, with increasing perturbation step sizes, for the different material parameters: (a) n_0; (b) k_0; (c) E_0; (d) χ_0; (e) C_{ps0}; (f) β_{s0}

pores is due to the water thermal dilatation, which is particularly important above the temperature of about 430 K [2].

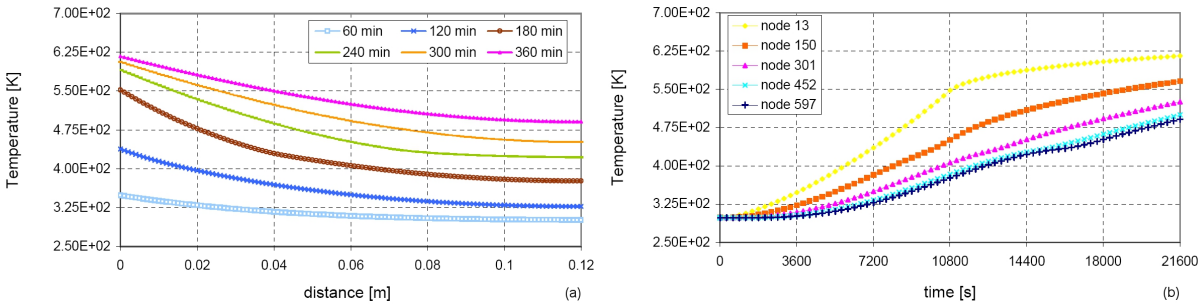

Figure 7.7: Temperature evolution in the concrete wall: (a) space distribution, (b) time distribution

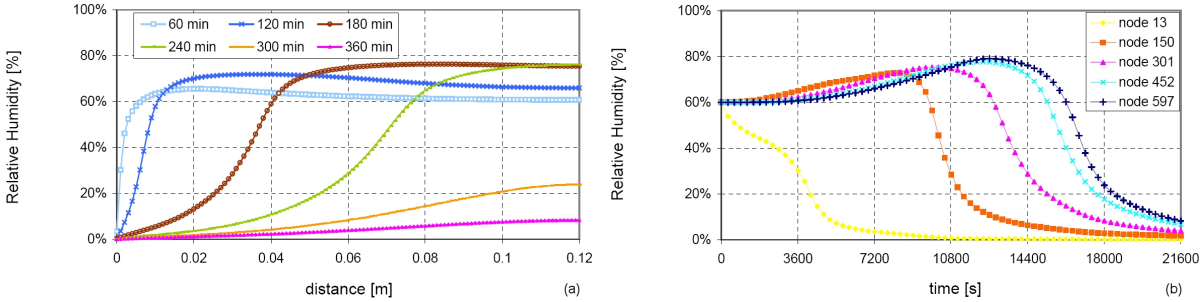

Figure 7.8: Relative humidity evolution in the concrete wall: (a) space distribution, (b) time distribution

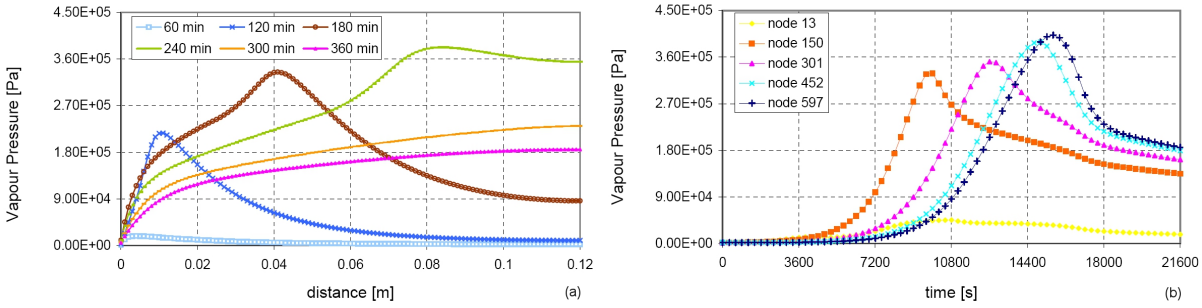

Figure 7.9: Vapour pressure evolution in the concrete wall: (a) space distribution, (b) time distribution

The combined action of hygro-thermal field results in damaging of the wall which is in part due to concrete dehydration, in part due to the material cracking and progressive crack opening, and finally due to thermal dilatation of the material skeleton [3]. Due to these cracks and chemical transformations of concrete, the concrete strength properties and Young's modulus degrade gradually, what can be expressed in terms

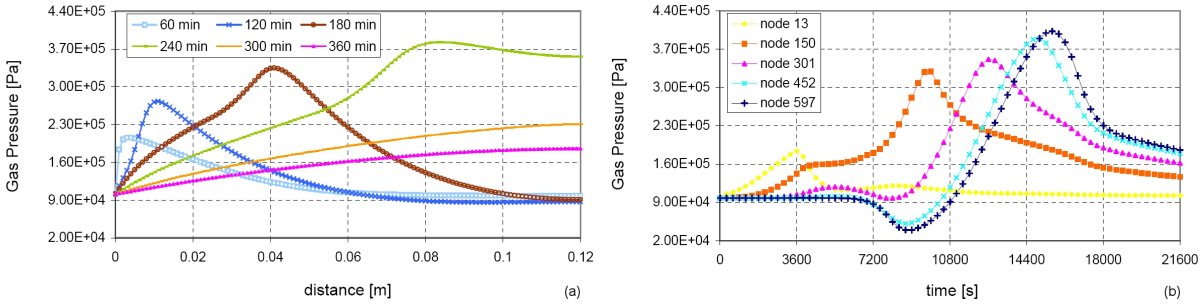

Figure 7.10: Gas pressure evolution in the concrete wall: (a) space distribution, (b) time distribution

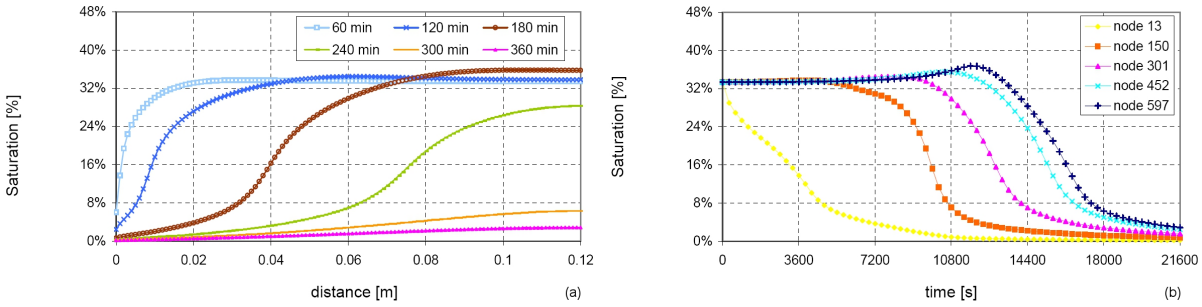

Figure 7.11: Saturation evolution in the concrete wall: (a) space distribution, (b) time distribution

of the thermo-chemical damage parameter (fig. 7.12) [4]. Thermo-chemical degradation process develops gradually, according to the temperature increase history, reaching value of about 50% on the heated surface at the end of the analysis.

The tensile stresses cause further development of cracks and fractures, parallel to the element surface, resulting in subsequent degradation of the material strength properties in the surface zone, (fig. 7.13). During the process evolution, a considerable mechanical damage can be observed. Initially it develops on the heated zone, but than it gradually expands in all the wall, reaching a value of about 65%. The combined action of mechanical and thermo-chemical damage causes that, at the end of the process, all the thickness of the wall is deteriorated with value of about 80% (fig. 7.14).

The values for the normalized sensitivities respect to the material parameters, computed for the described model outputs are shown in the following; we will write $\frac{\partial x_i}{\partial p_j}$ instead of $\left(\frac{\partial x_i}{\partial p_j}\right)_{norm}$, for sake of brevity.

First, we will present the results obtained for the hygro-thermal variables and then the ones obtained for the mechanical variables. For each material parameter, values of the sensitivity coefficients throughout the simulation are shown. For a proper interpretation of the sensitivities results, we recall that positive values of the sensitivity coefficients indicate that an increase of the material parameter value leads to an in-

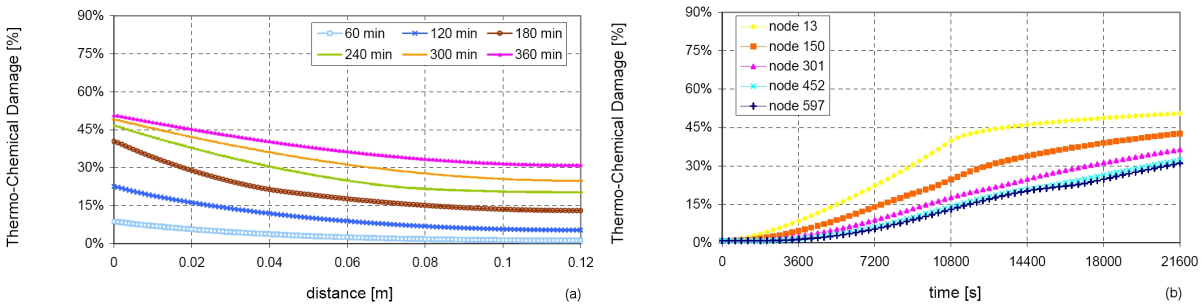

Figure 7.12: Thermo-chemical damage evolution in the concrete wall: (a) space distribution, (b) time distribution

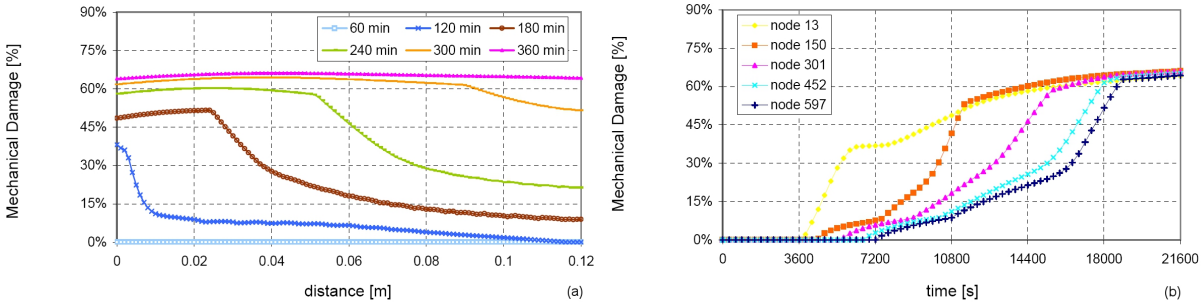

Figure 7.13: Mechanical damage evolution in the concrete wall: (a) space distribution, (b) time distribution

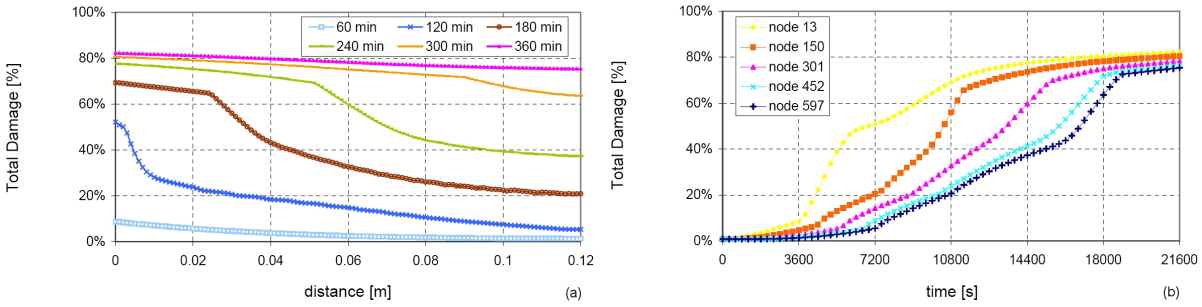

Figure 7.14: Total damage evolution in the concrete wall: (a) space distribution, (b) time distribution

crease in the output variable value, and negative values of the sensitivity coefficients indicate the opposite.

The computed response sensitivities are characterized by discontinuities more or less pronounced: they are induced by concrete transition from the undamaged to the damaged conditions. Indeed, damage (non-local damage theory) causes material instabilities that impact on the regularity of the sensitivity coefficients.

The material parameters which mainly affect temperature are those directly associated with the thermal field: in fact, both at the beginning and at the end of the heating process, the sensitivity coefficients with respect to specific heat and thermal conductivity are appreciably higher than the others (fig. 7.15). At the first heating stages, the highest sensitivity coefficients, absolute value, are in the zone near to the heated surface (both $\partial T/\partial C_{ps0}$ and $\partial T/\partial \chi_0$ have negative values) where temperature variable raises; after 360 minutes, instead, the higher values of the sensitivities are reached at the opposite side and have opposite values for $\partial T/\partial \chi_0 > 0$ and $\partial T/\partial C_{ps0} < 0$. The positive and negative values of these sensitivities are consistent with the material behaviour. A raise of the specific heat leads to a slower increase of temperature; an increase of thermal conductivity instead, leads to a faster heat conduction inside concrete: $\partial T/\partial \chi_0$ is therefore positive in all the thickness of the wall, except for the zone in contact with fire (node 13) which releases heat faster to the inner material (fig. 7.16 a).

It can also be observed that the graphs in figure 7.16 present an inflection in the range of time between 10800 and 18000 seconds. Plotting the time evolution of $\partial T/\partial \chi_0$ and $\partial T/\partial C_{ps0}$ with respect to temperature (fig. 7.17) results that this inflection, which becomes progressively more evident as we move away from the heated surface, appear between 375 and 475 K, that corresponds to the temperature range in which almost all liquid water evaporates [5]. Therefore sensitivity coefficients can capture water phase change. Variation in the trend of these sensitivity coefficients depends on the fact that, far from the surface zone, heat is not sufficient to allow both an increase of temperature and the phase change: all water must evaporate before a further temperature increase, what requires a considerable amount of energy. This behaviour is particularly evident from figure 7.18, which represents time evolution of saturation with respect to the hygrometric material parameters: a comparison between figure 7.7 b and 7.18 highlights that, for each node, the peak of the sensitivity coefficients appears just in the range 375-475 K.

The effect of the material parameters on vapour and gas pressure at the first stages of the heating process is shown in figure 7.19. Vapour pressure depends essentially on

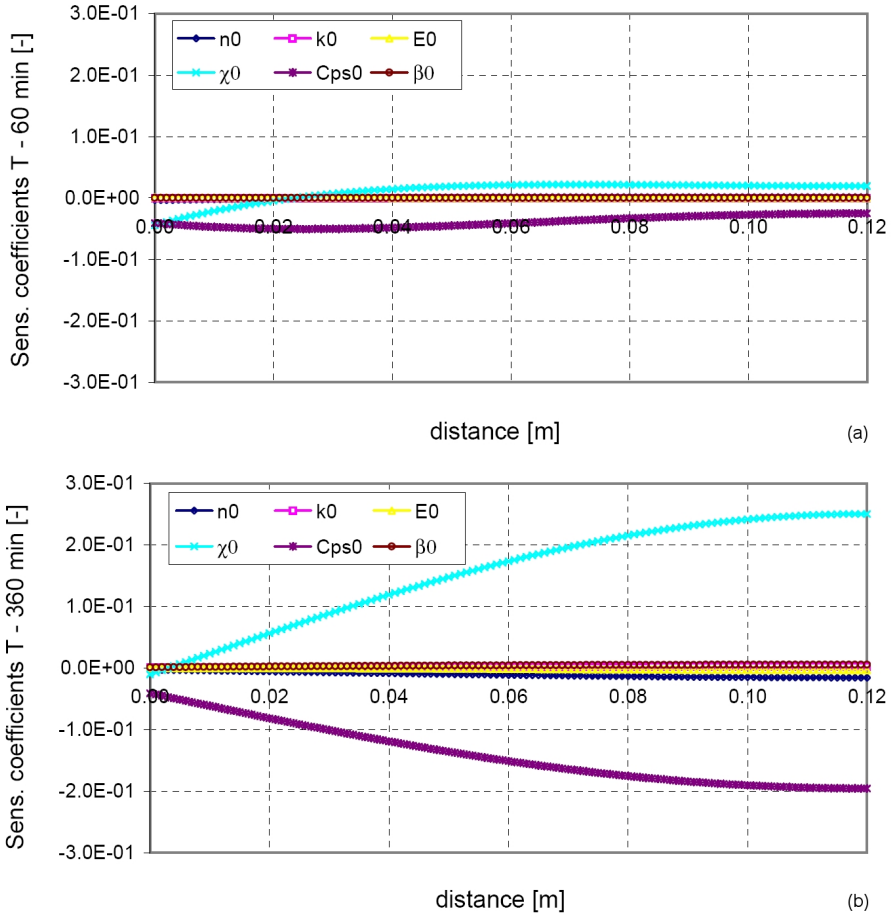

Figure 7.15: Space distribution of temperature normalized sensitivities with respect to material parameters: (a) after 60 minutes, (b) after 360 minutes

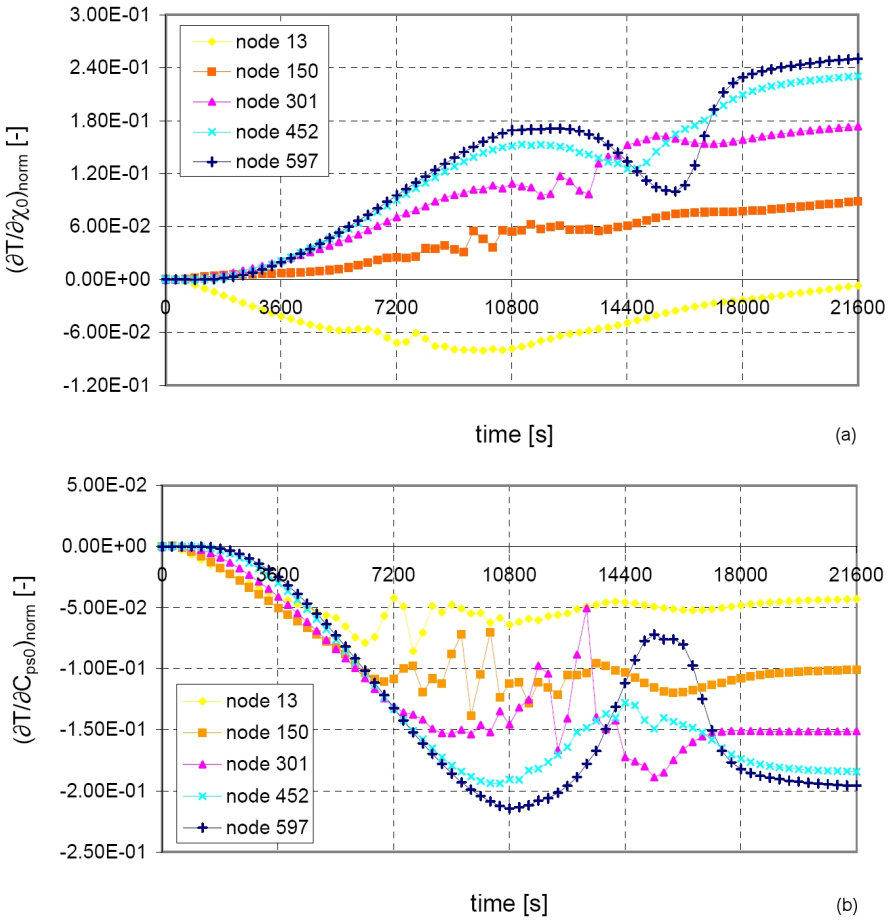

Figure 7.16: Time evolution of temperature normalized sensitivities with respect to thermal parameters: (a) solid thermal conductivity, (b) solid specific heat

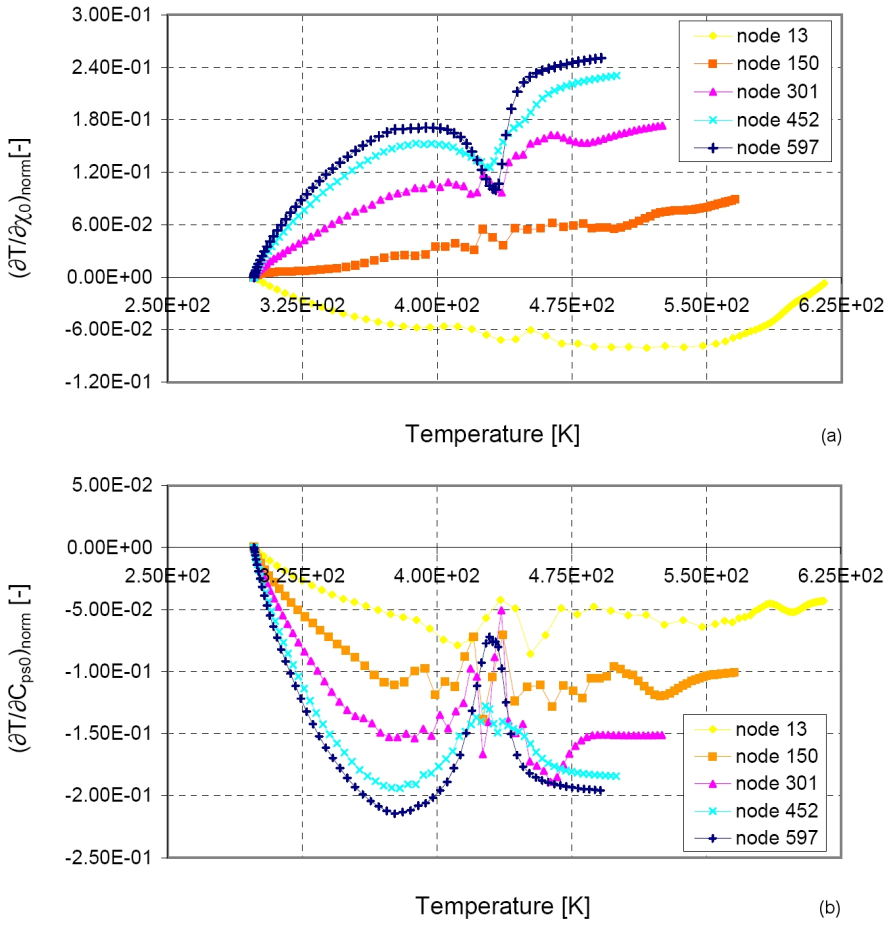

Figure 7.17: Variation with temperature of the normalized sensitivity coefficients: (a) $\partial T/\partial \chi_0$, (b) $\partial T/\partial C_{ps0}$

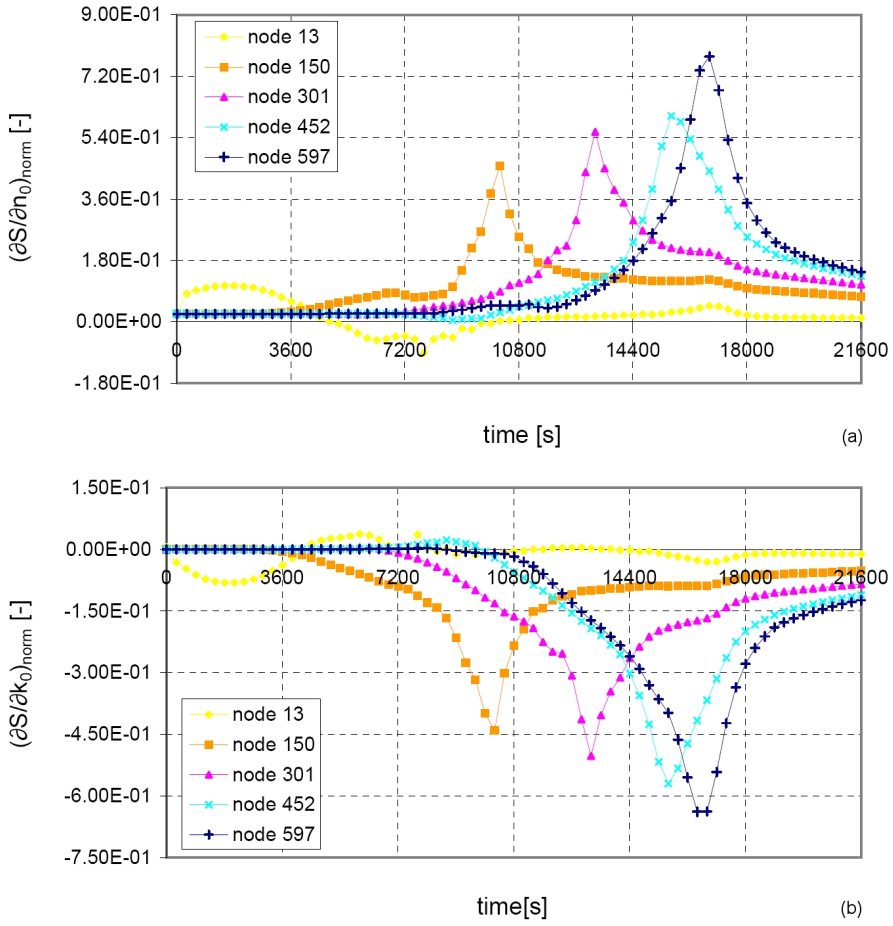

Figure 7.18: Time evolution of temperature normalized sensitivities with respect to hygrometric parameters: (a) porosity, (b) intrinsic permeability

the thermal variables, χ_0 and C_{ps0}; the values of these sensitivity coefficients are slightly higher in the first part of the concrete wall. Both $\partial p^v/\partial \chi_0$ and $\partial p^v/\partial C_{ps0}$ are negative on the heated surface, whereas at the opposite side they assume opposite values. This result is similar to the one obtained for temperature, which means that an increase of thermal conductivity leads to a decrease of vapour pressure near to the heated zone and to an increase of vapour pressure on the opposite side. An increase of specific heat, instead, leads to an increase of p^v in the entire thickness of the wall. Furthermore one can observe from figure 7.15 a and figure 7.19 a that the sensitivities of T and p^v with respect to χ_0 and C_{ps0} have different order of magnitudes, but the same trend. This correlation gives a hint to the strong link between temperature and vapour pressure at the beginning of the process (undamaged material).

An analysis of the sensitivities of gas pressure at 60 minutes (fig. 7.19 b), points out that all the material parameters has a comparable influence on this state variable. Moreover all the sensitivity coefficients take values different from zero only where there is a variation of p^g.

The sensitivities of p^v and p^g after 360 minutes reach the higher values in the further zone from fire; both the values and the trend of $\partial p^v/\partial p_j$ and $\partial p^g/\partial p_j$ are very similar in the whole thickness of the wall, except for the sensitivities with respect to n_o near to the heated surface. The mechanical material parameters E_0 and β_{so} are the ones which strongly affect these outputs, but also the influence of the thermal and hygrometric parameters is not negligible (fig. 7.20). This numerical result can be attributed to the full coupling which characterizes these three fields of the model. Slow heating in fact, causes water migration to occur in both the liquid and vapour phases, and leads to zones of increasing saturation as drying progresses. As the heating process goes on, the front of desaturation moves towards the end of the wall. Drying causes thermo-mechanical damage on the inner microstructure of the material, which in turn plays an important role on the intrinsic permeability and porosity, those are the most significant parameters representing the pore structure.

Figure 7.21 represents the sensitivities of gas pressure with respect to the material parameters for nodes 452 e 597 which are located in the last part of the wall, where the highest sensitivities values are observed. It can be seen that, for all the heating process, there is a significant correlation between the two sensitivities coefficients respect to the hygrometric variables, the two sensitivities coefficients respect to the thermal variables and the two sensitivities coefficients respect to the mechanical variables.

With regards to damage sensitivities we remind that after 60 minutes of heating only

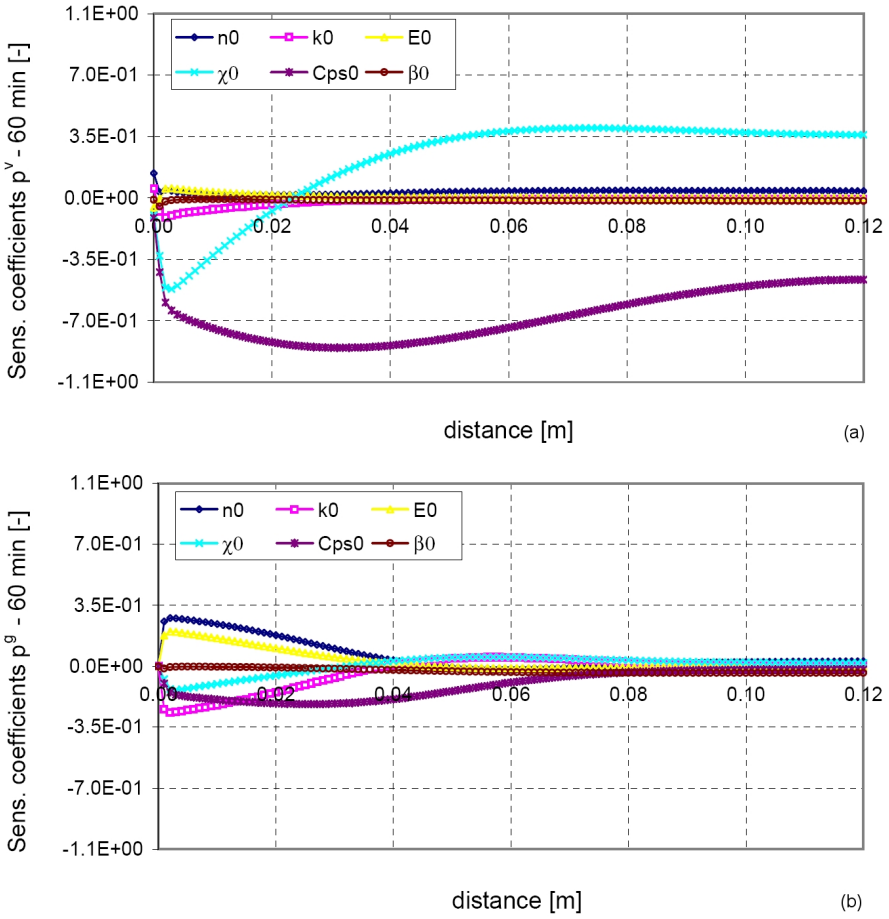

Figure 7.19: Space distribution of the normalized sensitivities with respect to material parameters after 60 minutes: (a) vapour pressure, (b) gas pressure

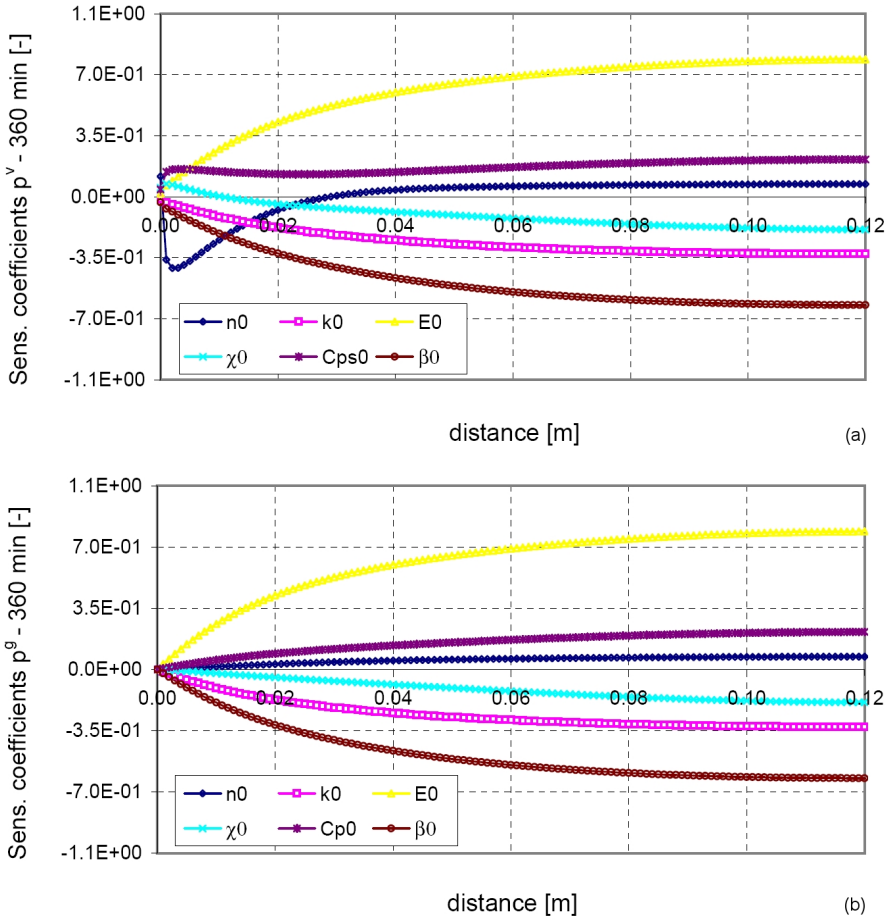

Figure 7.20: Space distribution of the normalized sensitivities with respect to material parameters after 360 minutes: (a) vapour pressure, (b) gas pressure

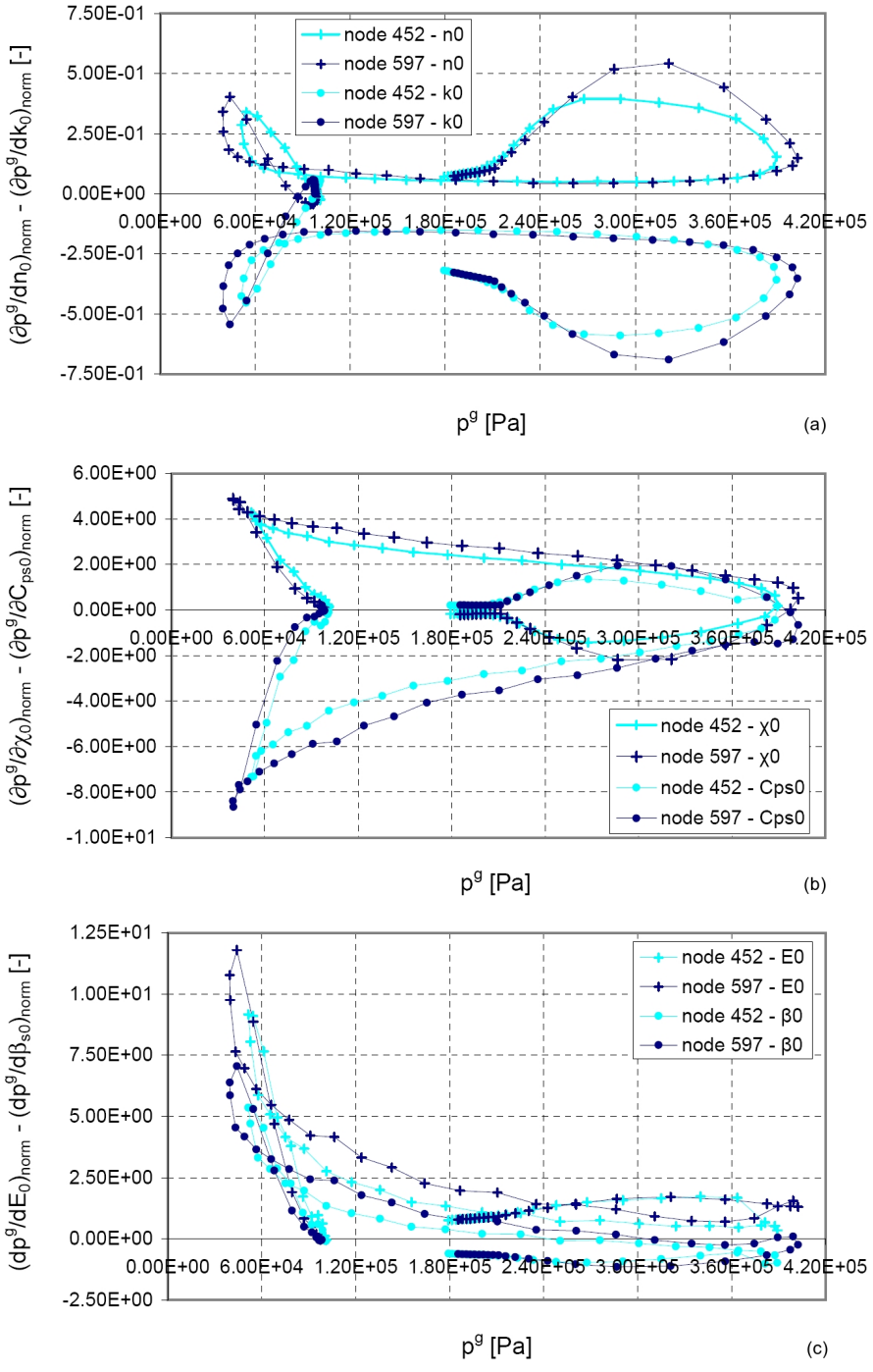

Figure 7.21: Variation with gas pressure of the normalized sensitivity coefficients: (a) $\partial p^g/\partial n_0$ and $\partial p^g/\partial n_0$, (b) $\partial p^g/\partial \chi_0$ and $\partial p^g/\partial C_{ps0}$, (c) $\partial p^g/\partial E_0$ and $\partial p^g/\partial \beta_{s0}$

thermo-chemical damage V develops inside the concrete wall, whereas the mechanical damage d is still equal to zero (figs. 7.12, 7.13 and 7.14). Therefore the sensitivity coefficients of the total damage, in the early stages of the analysis, correspond exactly to the ones of the thermo-chemical damage. The material parameters that mainly influence the thermo-chemical damage, and consequently the total damage, are the Young's modulus E_0 and the thermal parameters (figs. 7.22 a, 7.23 a and 7.24 a). This result was expected because V, which takes into account the thermally induced deterioration of the material, is defined in terms of the evolution of Young's modulus of mechanically undamaged material expressed as a function of temperature.

At the end of heating process the sensitivity coefficients of the total damage are given both by the mechanical and the thermo-chemical damage sensitivities, even if the contribution of the mechanical sensitivities is meaningful (figs. 7.22 b, 7.23 b and 7.24 b). As for total damage in fact, the total effect of the mechanical and thermo-chemical damage sensitivities is multiplicative and not just the sum of the two components. After 360 minutes, the effect of the mechanical and thermal parameters on D is found to be significantly more relevant whit respect to the one of the hygrometric parameters. We would have supposed that the role played by the hygrometric parameters, in particular by the intrinsic permeability, would have been more significant, because of the strong relationship between damage and permeability.

Figure 7.25 summarizes the foregoing results: it shows a comparison between the normalized sensitivity coefficients of the node closer to the heated surface, with respect to the material parameters. It can be observed that the different parameters have a comparable effect on the model outputs. The higher values of the sensitivities are reached for the thermal and the mechanical parameters and they are done to strong discontinuities in the sensitivities trend.

These discontinuities are caused by the material instabilities that arise during the transition between the undamaged and the damaged state of concrete [6, 7], and can be attributed above all to the mechanical component of damage. In fact, if we compute the same sensitivity coefficients presented in figure 7.25, performing an analysis in which we impose that the mechanical damage must be zero, these discontinuities totally disappear (fig. 7.26).

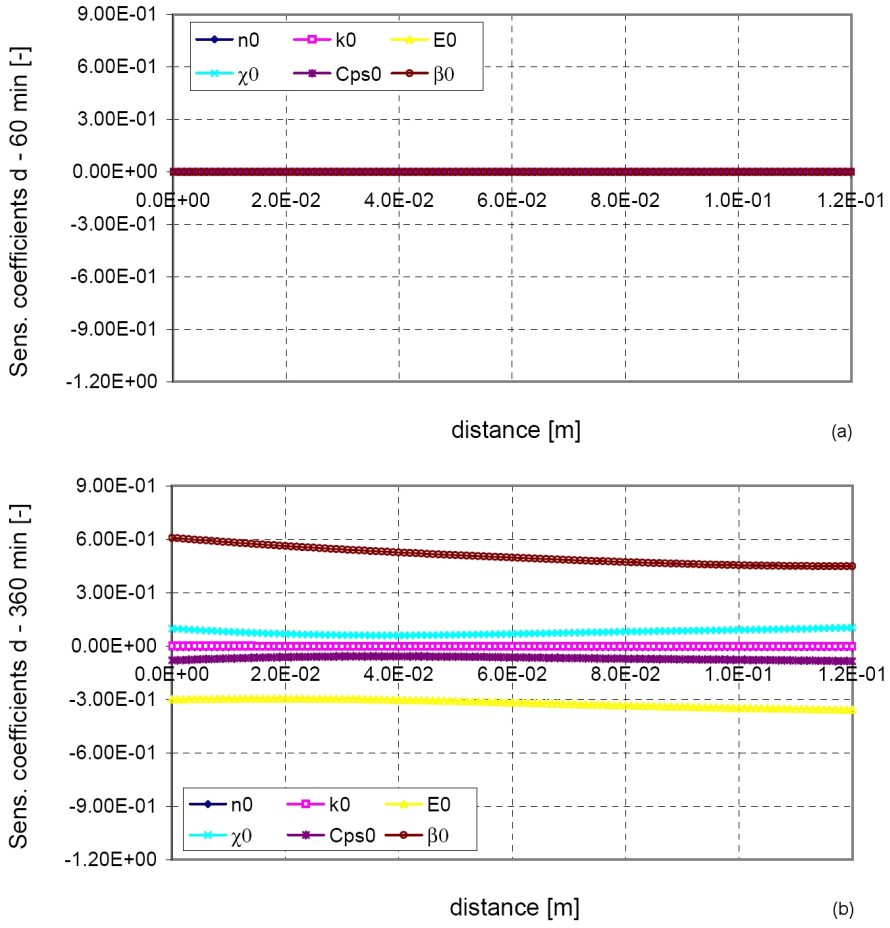

Figure 7.22: Space distribution of mechanical damage normalized sensitivities with respect to material parameters: (a) after 60 minutes, (b) after 360 minutes

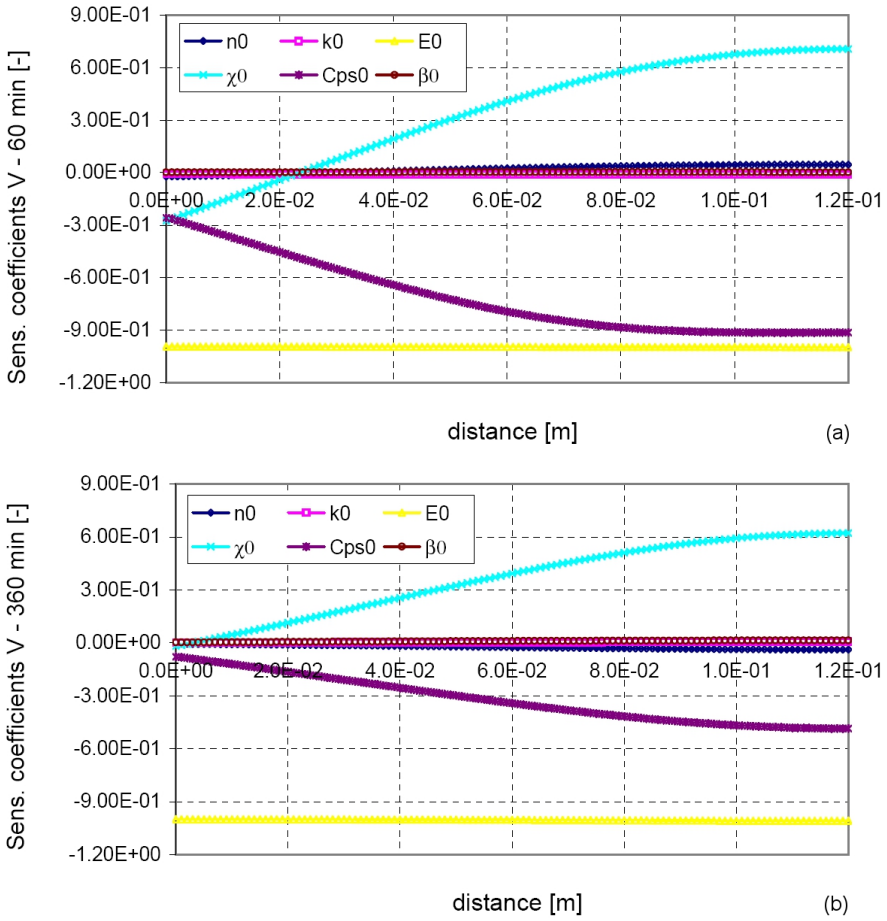

Figure 7.23: Space distribution of thermo-chemical damage normalized sensitivities with respect to material parameters: (a) after 60 minutes, (b) after 360 minutes

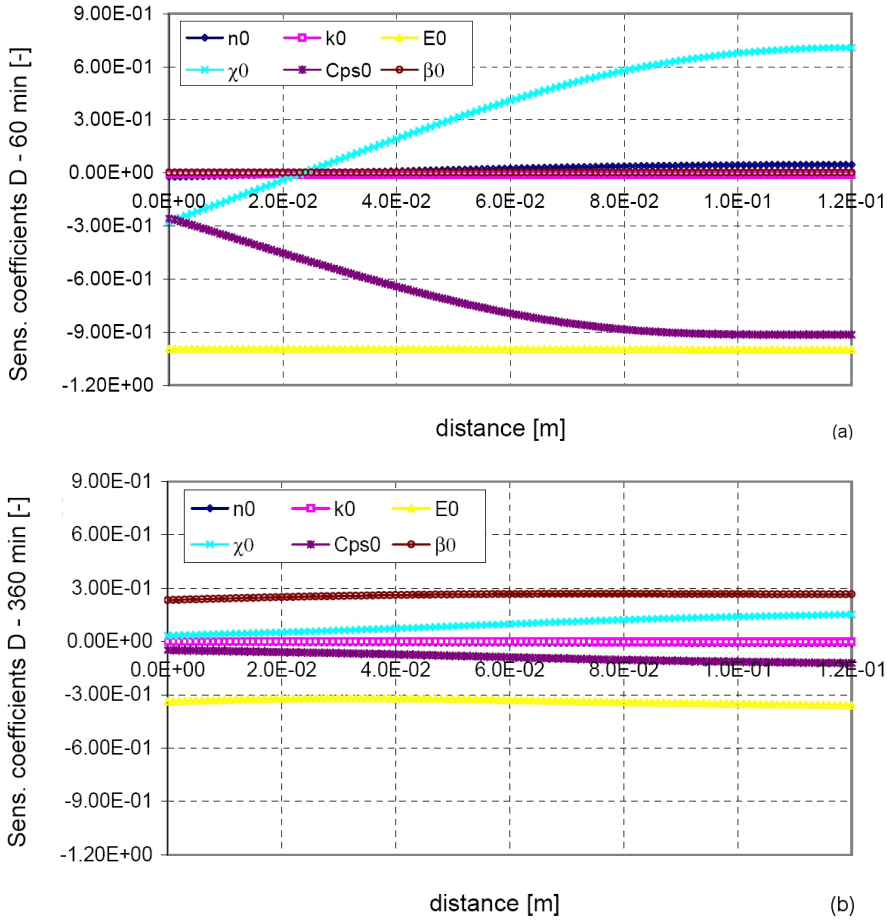

Figure 7.24: Space distribution of total damage normalized sensitivities with respect to material parameters: (a) after 60 minutes, (b) after 360 minutes

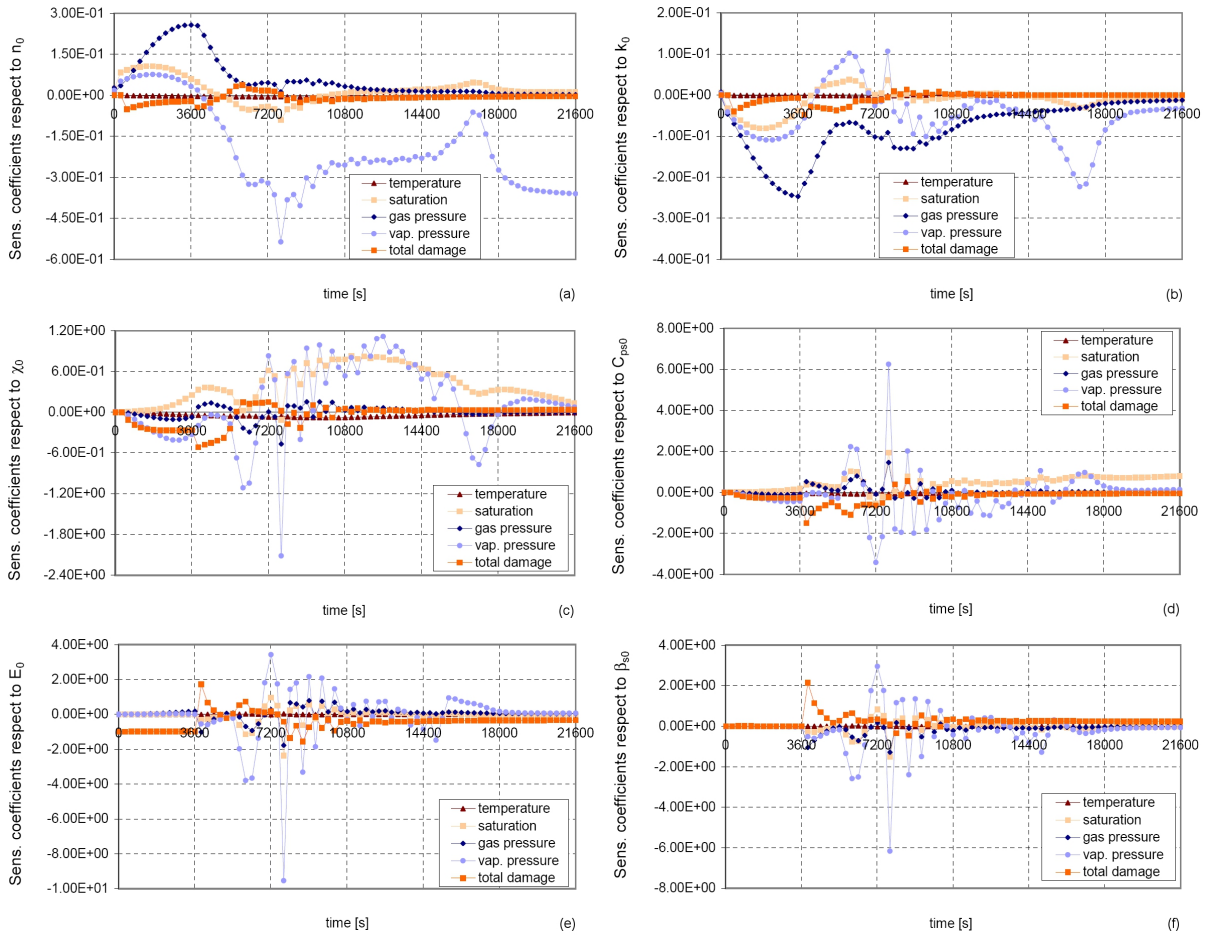

Figure 7.25: Time evolution of the normalized sensitivities of node 13 with respect to material parameters: (a) n_0, (b) k_0, (c) χ_0, (d) C_{ps0}, (e) E_0, (f) β_{s0}

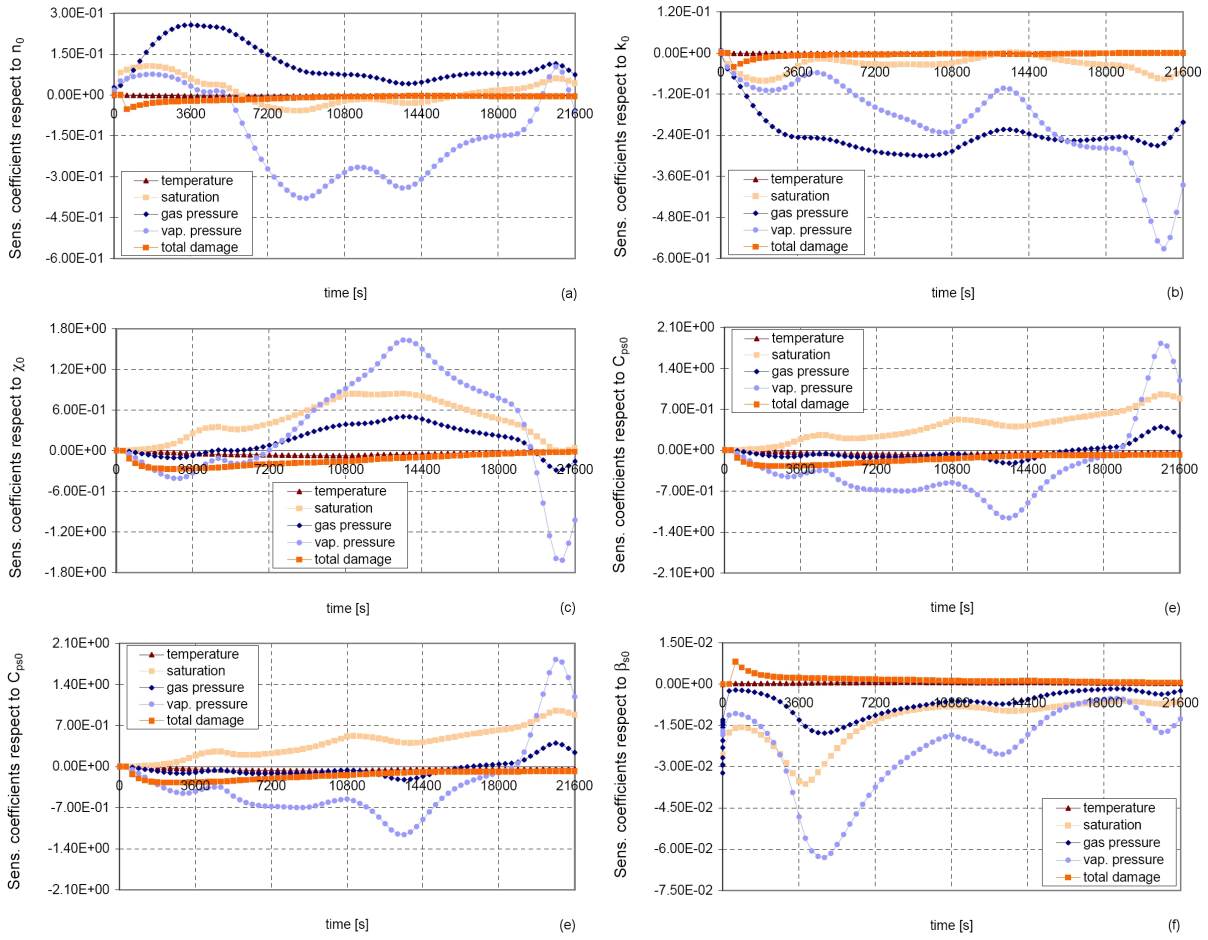

Figure 7.26: Time evolution of the normalized sensitivities of node 13 with respect to material parameters, without the contribution of mechanical damage: (a) n_0, (b) k_0, (c) χ_0, (d) C_{ps0}, (e) E_0, (f) β_{s0}

Bibliography

[1] Kalifa P., Chene G., Galle C., High-temperature behaviour of HPC with polypropylene fibers. From spalling to microstructure, Cem. Concr. Res., 31: 1487-1499, 2001.

[2] Gawin D., Pesavento F., Schrefler B.A., Modelling of hygro-thermal behaviour and damage of concrete at temperature above the critical point of water, Int. J. Numer. Anal. Methods Geomech., 26: 537-562, 2002.

[3] Schneider U., Concrete at high temperatures-a general review, Fire Safety J. The Netherlands, 55-68, 1988.

[4] Gawin D., Pesavento F., Schrefler B.A., Modelling of hygro-thermal behaviour of concrete at high temperature with thermo-chemical and mechanical material degradation, Comput. Methods Appl. Mech. Engrg., 192: 1731-1771, 2003.

[5] Gawin D., Pesavento F., Schrefler B.A., Towards prediction of the thermal spalling risk through a multi-phase porous media model of concrete, Comput. Methods Appl. Mech. Engrg., 195: 5707-5729, 2006.

[6] Kowalczyk P., Kleiber M., Shape sensitivities in elasto-plastic computations, Comput. Methods Appl. Mech. Engrg., 171: 371-986, 1999.

[7] Zona A., Barbato M., Conte J.P., Finite element response sensitivity analysis of steel-concrete composite beams with deformable shear connection, Journal of Engineering Mechanics, 131(11): 1126-1139, 2005.

Chapter 8

Conclusions

The present thesis dealt with the sensitivity analysis of a mathematical model, which describes the hygro-thermal-chemical-mechanical phenomena occurring in heated concrete; this model, which is implemented in the fem code Comes-Htc, takes into account most of the important features of the material behaviour at these conditions (chemical-physical phase changes, different physical mechanisms of liquid and gas transport, damage effects, etc.).

The sensitivities of the model outputs with respect to the material parameters have been computed via automatic differentiation (AD) through the software Tapenade, which has augmented the original version of Come-Htc by additional statements for computing derivatives.

In order to perform sensitivity analysis, two material parameters for each field considered by the model have been selected. Therefore we have considered: porosity n_0 and intrinsic permeability k_0 for the hygrometric field; solid thermal conductivity χ_0 and solid specific heat C_{ps0} for the thermal field; Young's modulus E_0 and thermal expansion coefficient β_{s0} for the mechanical field.

The application of AD to the fem code Comes-Htc has allowed to develop an efficient tool for the computation of the sensitivity coefficients. The results obtained according to AD have been validated by means of the finite difference method (FD); the latter approach is an approximation process whose reliability grounds on a suitable choice of the perturbation step size. The validation step has demonstrated that, although the difficulties intrinsic in the differentiation process of complex models, as the one which characterizes Comes-Htc, the AD method is superior to FD. In fact the sensitivity coefficients computed with this technique are exact up to machine precision; moreover, unlike the FD method, with AD is possible to obtain all the required sensitivity coefficients

in a single execution of the differentiated code.

Through sensitivity analysis it has been possible to analyze the behaviour of concrete, treated as a multiphase porous material. The results of the presented numerical example allow for a better understanding of physical phenomena described by Comes-Htc; they also highlight the full coupling between the hygral, thermal and mechanical field that impacts on the link between model variables and material parameters.

The obtained results have enabled to quantify the effect and relative importance of the material parameters with regards to the model outputs. It has been observed that the different parameters have a comparable influence on the model outputs. Moreover the sensitivity coefficients have pointed out the importance of the mechanical damage on the hygro-thermal-chemical-mechanical response of concrete and consequently on the numerical solution of the model, because of the strong influence that damage has on the stability of the sensitivities themselves.

Finally from the results stems that a drastic simplification of the model used to study concrete behaviour as a multiphase material it's not possible. Therefore it will be necessary to use different model reduction techniques to extract from the full model a simplified model to be used at industrial level.

Acknowledgements

The completion of my PhD has been possible thanks to the continued support received from people who stayed close to me in these years.

I would like to thank my supervisors Dr. Pesavento and Prof. Schrefler for giving me the opportunity to work at this research project and for their scientific support.

I am also grateful to Prof. Pironneau for the explanations about the concepts of automatic differentiation and for his useful suggestions. Moreover I thank Dr. Hascoët and Dr. Pascual of the Inria Tropics team for their fruitful responses to my requests for explanations of Tapenade.

Finally, I am extremely grateful to Piero, my family and friends for the support, encouragement and understanding they provided me throughout my PhD, when it was most required.